A CORAL ENSEMBLE RECORD OF THE EL NIÑO SOUTHERN OSCILLATION OVER THE MID-TO-LATE HOLOCENE

A Dissertation
Presented to
The Academic Faculty

by

Pamela R. Grothe

In Partial Fulfillment
of the Requirements for the Degree
Doctor of Philosophy in the
School of Earth and Atmospheric Sciences

Georgia Institute of Technology
August, 2017

A CORAL ENSEMBLE RECORD OF THE EL NIÑO SOUTHERN OSCILLATION OVER THE MID-TO-LATE HOLOCENE

Approved by:

Dr. Kim Cobb, Advisor
School of Earth and Atmospheric Sciences
Georgia Institute of Technology

Dr. Taka Ito
School of Earth and Atmospheric Sciences
Georgia Institute of Technology

Dr. Jean Lynch-Stieglitz
School of Earth and Atmospheric Sciences
Georgia Institute of Technology

Dr. Antonietta Capotondi
Physical Sciences Division
National Oceanographic and Atmospheric Sciences

Dr. Emanuele Di Lorenzo
School of Earth and Atmospheric Sciences
Georgia Institute of Technology

Date Approved: [July 27, 2017]

To the people of Christmas Island, especially Tiito Taebi

ACKNOWLEDGEMENTS

I would first like to especially thank my advisor, Kim Cobb, for her intellectual, moral, and financial support through these last five years. I specifically choose to work with Kim Cobb for my graduate work because I could see how electrifying her energy was for science and communication and how supportive and encouraging she was in helping young women scientists achieve their dreams. She did not let me down. She pushed me to think critically on topics I felt were out of my expertise, she taught me what tough means working in the field, and she gave me the freedom to explore my own scientific interests, which ultimately led to this dissertation. Additionally, she was extremely supportive of my career goal in becoming an educator first and researcher second. Lastly, I cannot thank Kim enough for her 100% support of me becoming a mother during the last year of my Ph.D. tenure. I did not initially plan to start a family during my Ph.D. and certainly did not expect to be covered financially though it as a graduate student. But Kim, a strong advocate for women and mothers in science, believed in paid maternity leave and provided me with a semester of support while I slowly wrote the final chapter of this dissertation.

I would next like to thank those in the Cobb lab for their help and support throughout the years, especially Hussein Sayani. Hussein was my sounding block through these last five years. He was always there whenever I needed moral support to make it through a tough day, technical support on repairing the mass spec, or intellectual support in working through a scientific problem. I would also like to especially thank undergraduates Shellby Miller, Gemma O'Connor, and Melat Hagos, all who of which

contributed of some magnitude to the science of this dissertation. And lastly, I would like to thank Jessica Moerman, who although not a “coral person”, was a great resource and mentor when navigating graduate student life.

I would also like to thank all the collaborators I have worked with throughout the last five years and them opening up their labs and offices to me. First, to Guaciara Santos and John Southon at the University of California Irvine for providing me support to run as many rapid screen radiocarbon analyses as I can in a week. Next, to Larry Edwards, Hai Cheng and Yanbin Yu at the University of Minnesota for training me in U/Th chemistry and unleashing me in their clean room, and ultimately running my samples on the ICP-MS. And lastly, to Antonietta Capotondi, for being the most generous host during my time at NOAA, opening up her office and home to me while helping me with the Linear Inverse Model.

I would also like you thank my undergraduate advisor, Neil Tibert, who passed away suddenly from cancer in December 2015. His support through my undergraduate years at the University of Mary Washington is what ultimately motivated me to pursue my Ph.D. so that I too could one day inspire undergraduate students to obtain that curiosity in science. I am only sorry that I will not be able to collaborate with him but am extremely grateful for the chance to follow in his footsteps as a tenure-track professor at the University of Mary Washington. I can only hope that I can be the mentor to others that he was for me.

Lastly and mostly, I would like to thank my husband William Grothe. He sacrificed so much so that I could follow my dreams and he continues to do so to this day. Without his love and support, I never would have been able to do this.

Pamela Grothe

May 2017

TABLE OF CONTENTS

LIST OF TABLES

LIST OF FIGURES

LIST OF SYMBOLS AND ABBREVIATIONS

AD	Anno Domini
AMS	Accelerator mass spectrometry
BP	Band pass
BP	Before present
C	Carbon
^{14}C	Radiocarbon
$CaCO_3$	Calcium carbonate
CMIP	Coupled Model Intercomparison Project
CP	Central Pacific
ENSO	El Niño Southern Oscillation
EOF	Empirical orthogonal function
EP	Eastern Pacific
ERSST	Extended reconstruction sea surface temperature
Fe	Iron
FS	Fossil site
GCM	Global climate model
GFDL	Geophysical Fluid Dynamics Laboratory
GPS	Global Positioning System
GSU	Georgia State University
HF	Hydrogen fluoride
HNO_3	Nitric acid
HP	High pass

ICP-QMS	Inductively coupled plasma quadruple mass spectrometry
IGOSS	Integrated Global Ocean Services System
ITCZ	Inter Tropical Convergence Zone
KCCAMS	Keck Carbon Cycle Accelerator Mass Spectrometry
ky	Thousand years
LA	Laser ablation
LGM	Last glacial maximum
LIM	Linear Inverse Model
LME	Last Millennium Ensemble
LP	Low pass
MC-ICPMS	Multi-collector Inductively coupled plasma mass spectrometer
N	Nitrogen
NCAR	National Center for Atmospheric Research
NSF	National Science Foundation
P	Palmyra
RM	Running mean
SEM	Scanning electron microscope
SSS	Sea surface salinity
SST	Sea surface temperature
Th	Thorium
^{xxx}Th	Thorium isotopes
U	Uranium
^{xxx}U	Uranium isotopes
V	Fanning
VPDB	Vienna Pee Dee Belemnite

X	Christmas
XRD	X-Ray diffraction
$\delta^{18}O$	Oxygen isotopic composition
$\delta^{18}O_{sw}$	Oxygen isotopic composition of seawater
$\delta^{13}C$	Carbon isotopic composition
ΔR	Marine reservoir correction
λ_{xxx}	Decay constant
σ	Standard deviation

SUMMARY

The El Niño-Southern Oscillation (ENSO) represents the largest source of year-to-year global climate extremes. However, its sensitivity to external climate forcing, whether natural or anthropogenic, is difficult to assess with available records. Paleoclimate reconstructions from the central tropical Pacific provide much-needed targets for climate models that are used to simulate future projections of ENSO variability under enhanced greenhouse emissions. Coral oxygen isotopes track variations in sea surface temperature and sea surface salinity, which is largely driven by ENSO. To date, paleo records rely on rare but decades-long fossil coral sequences that date to the last 7,000 years [*Cobb et al.,* 2013]. This study turns to using abundant but shorter sequences (7-20yrs-long) of fossil coral rubble samples to produce a more statistically robust reconstruction of ENSO from the central tropical Pacific through the last 7,000 years.

In Chapter 1, I provide relevant background information on ENSO in order to place this dissertation into broader scientific context. This includes the basics on ENSO dynamics and the different spatial patterns of El Niño events. I also explain the different proxies that have evolved our understanding of ENSO throughout the Holocene. Lastly, I mention where we currently are in understanding future projections of ENSO behavior under greenhouse gas emissions.

In Chapter 2, I address one of the largest challenges in using a large number of fossil corals for paleoclimate reconstruction, which involves dating hundreds of coral samples cheaply and quickly. I compared the coral dating results from a rapid

radiocarbon (^{14}C) dating method, developed at the University of California Irvine, to high precision uranium-thorium (U/Th) dates, considered the gold standard of coral dating. The rapid ^{14}C dating method allows for ~300 samples to be analyzed per week at $40/sample versus ~30 samples per week at $500/sample for U/Th dating. My results demonstrate the utility of employing ^{14}C dating to screen large numbers of corals, followed by more limited U/Th dating on samples chosen for paleoclimate reconstruction. In addition, my extensive fossil coral dating has provided a map of fossil coral age distributions across Christmas Island in the central tropical Pacific.

In Chapter 3, we extend the paleo-ENSO record through the generation of 16 new fossil coral $\delta^{18}O$ timeseries, averaging 15yrs each, for a total of 233 years of data that greatly augment the available paleo-ENSO archive. Combining this new dataset with published data, we quantify the differences in natural variations in ENSO from the early mid-Holocene to present. In this study, we document a significant increase in recent ENSO variance as compared to the last 7,000 years, implying a role for greenhouse gases in driving an intensification of ENSO. We also find a significant reduction in ENSO variance of roughly 20% from 3,000-5,000yr before present, relative to the preceding and subsequent intervals of data. The causes of the late mid-Holocene reduction in ENSO variance may be linked to the influence of fall and/or spring equatorial insolation forcing, which perturbs the seasonal cycle at the critical growth and decay phases of ENSO extremes, respectively. In distinguishing between natural variability and forced changes in ENSO, we assess the significance of our results using a variety of different null hypotheses that includes output from both a statistical and dynamical model of ENSO variability. Our findings imply that ENSO is sensitive to external forcing, both natural

and anthropogenic, although the precise mechanisms for such responses require further study. Our results imply that anthropogenic climate change likely contributed to the record-breaking 2015/2016 El Niño event, and that future ENSO variance is unlikely to decrease under continued greenhouse forcing.

In Chapter 4, I conclude the major work presented in this study and highlight the next steps in this research towards understanding how mean climate has changed throughout the Holocene and how it affects ENSO variability. Appendix A and Appendix B are supplemental information for Chapters 2 and 3, respectively. All references are presented together at the very end of this document.

CHAPTER 1. INTRODUCTION

Future projections of the strength of the El Niño-Southern Oscillation (ENSO), the largest source of year-to-year global climate variability, are highly uncertain. As ENSO extremes affect temperature and rainfall patterns around the globe, including the United States, better constraints on the frequency and amplitude of its future variations translate into improved regional climate forecasts. Such regional projections are critical to developing robust adaptation plans in the face of continued anthropogenic climate change.

Current model projections of ENSO properties over the next century vary widely, with some models showing large increases in overall variability, some showing decreases, and some no change at all [*Collins et al.,* 2010]. Such models are poorly constrained by available instrumental climate data from the tropical Pacific, which are too sparse to detect potential trends in ENSO properties. Indeed, uncovering robust trends in ENSO frequency and/or amplitude is difficult, given the large natural variations that occur from decade to decade.

Long, high-resolution paleoclimate reconstructions of ENSO activity effectively extend the instrumental record of ENSO, and provide a centuries-long baseline for assessing potential anthropogenic trends in ENSO. In particular, long-lived corals provide monthly-resolved, decades-long windows of ENSO variability over the last century and beyond, recorded as changes in the oxygen isotopic composition ($\delta^{18}O$) of the coral skeleton [*Correge*, 2006 and references therein]. Coral $\delta^{18}O$ records from the Line

Islands (4°N, 160°W), in the central equatorial Pacific, track ENSO variations over the 20th century with exceptionally high fidelity, and have been used to reconstruct ENSO over the last century [*Evans et al.,* 1999; *Cobb et al.,* 2001; *Nurhati et al.,* 2009], the last millennium [*Cobb et al.,* 2003], and the last 7,000 years [*Cobb et al.,* 2013].

To place the research of this dissertation into broader scientific context, this chapter summarizes the dynamics of ENSO, the diversity of ENSO spatial patterns, paleo-ENSO reconstructions from the Holocene, and our current future projections of ENSO under anthropogenic climate change.

1.1 The History of ENSO

In the 1600's, Peru fishermen noticed that every few years, fish harvests were low, associated with noticeably warm ocean water temperature. They called these events El Niño, meaning the Christ Child, because this phenomenon always occurred in December. Then in 1899, a severe drought in India from a failed monsoon led Gilbert Walker to identify a surface pressure oscillation across the Indo-Pacific region, where he found that high pressure over Indonesia and the Galapagos was associated with low pressure over India and Tahiti. He named this the Southern Oscillation. It was not until 1969 that Jacob Bjerknes first recognized that El Niño and the Southern Oscillation were manifestations of the same physical phenomena of unstable interactions between the ocean and atmosphere, and hence was called the El Niño Southern Oscillation, or ENSO. However, it was not until the 1982-83 strong El Niño event that scientists and the public gained significant interest in ENSO, which at this time was poorly understood.

1.2 ENSO Dynamics

Normal conditions in the equatorial Pacific consist of strong easterly trade winds and convection over the western equatorial Pacific. The trade winds cause Ekman upwelling in the eastern equatorial Pacific, causing cool surface waters and a shallow thermocline. At the same time, the trade winds pile up water in the western Pacific, causing warm surface waters and a deep thermocline. El Niño, or the warming of the tropical Pacific every 2-7years, occurs when the easterly trade winds weaken resulting in less upwelling of cold water in the eastern Pacific and the flow back of the warm water from the western Pacific to the central and eastern Pacific. Convection shifts to the central and eastern Pacific where high pressure and subsidence occurs in the western Pacific. La Niña events, which typically follow El Niño events, are amplified normal conditions.

Bjerknes [1969] first described ENSO through positive feedbacks. His theory states that the stronger the SST gradient between the east and the west, the stronger the easterly winds are, thus creating an even stronger SST gradient, a positive feedback. During El Niño conditions, the trade winds weaken, suppressing the upwelling and warming the SSTs in the west, thus forming another positive feedback where a weaker SST gradient leads to weaker winds, and thus an even weaker SST gradient. The problem is that Bjerknes could not explain how the phase could reverse, a negative feedback. Several theories have since been proposed to account for a phase reversal as well as the long period of 2-7 years associated with the cycle. Below, I summarize the delayed oscillation theory, the recharge/discharge oscillation theory, the western Pacific oscillation theory and the advective/reflective oscillation theory.

1.2.1 Delayed Oscillator

The delayed oscillator theory explains ENSO's behavior through ocean memory, which is carried in the thermocline depth through the reflection and propagation of ocean waves. *Suarez and Schopf* [1988] originally discuss the idea of a delayed oscillation to explain ENSO behavior. They propose a simple nonlinear model that includes a negative feedback through ocean waves as well as explains a 2-4-year oscillation. Their model assumes that the strongest ocean-atmosphere coupling occurs in the central Pacific where a growing perturbation from this region results in westward propagating ocean waves that reflect off the western boundary and return to the more coupled ocean-atmosphere central and eastern basin. For example, wind bursts from SST perturbations would drive westward propagating Rossby waves along the ocean thermocline, reach the western boundary and then reflect eastward as an equatorial Kelvin wave. As the Kelvin wave continues to move east it will begin to influence SST as the thermocline is shallow here – this is the delay term in their model. Analyses from their work suggest that the oscillation is several times the delay, which could explain a 2-4-year oscillation.

Battisti and Hirst [1989] use a simple coupled ocean-atmosphere model from *Cane and Zebiak* [1985], which is similar to the *Suarez and Schopf* [1988] model. Here, they explain the onset through positive SST anomalies in the eastern Pacific basin, which produce westerly wind anomalies in the central Pacific basin generating downwelling Kelvin waves to the east as well as equatorially trapped Rossby waves to the west. The downwelling Kelvin waves suppress the thermocline, pushing it deeper and thus enhancing the SST anomalies in the eastern basin. The Rossby waves reflect off the western boundary and return as upwelling Kelvin waves terminating the growth. However, *Battisti and Hirst* [1989] find that the delayed oscillator can be explained

through fundamental linear equations, compared to *Suarez and Schopf* [1988] nonlinear approach.

1.2.2 Recharge/Discharge Oscillator

The recharge/discharge oscillation theory similarly explains ENSO behavior through ocean memory that is carried by the ocean thermocline depth but where the ocean thermocline depth is constantly in non-equilibrium with equatorial wind stress on ENSO timescales. *Wyrtki* [1975, 1985] first suggested the recharge/discharge theory, where western Pacific warm water builds up gradually prior to an El Niño event – the charge – and then during El Niño the warm water flows toward higher latitudes – the discharge. The resulting state then becomes cold La Niña conditions where warm water slowly builds up again, or recharges, before the next El Niño occurs. *Wyrtki* [1985] defines the duration of the El Niño cycle by the time that is required for the accumulation of warm water in the western Pacific.

Jin [1997a,b] developed the quantitative model of the recharge discharge oscillator using the *Zebiak and Cane* [1987] model. During an El Niño event, equatorial heat is discharged by the divergence of Sverdrup transport from central Pacific westerly wind anomalies and eastern Pacific warm sea surface temperature (SST) anomalies. This heat removal causes the thermocline depth across the equatorial Pacific to be anomalously shallow, allowing cold waters to be pumped in through Ekman upwelling. During La Niña events, just the opposite occurs, where this recharge-discharge process between the two events oscillates on interannual time scales.

1.2.3 Western Pacific Oscillator

Weisberg and Wang [1997] and *Wang et al.* [1999] develop a western Pacific oscillator model that produces ENSO-like oscillations, but unlike the delayed oscillator model, this model does not require wave reflection for the coupled ocean-atmosphere system to oscillate. The model particularly emphasizes the role the western Pacific plays in the delayed oscillator model, explaining key ENSO observations where both the eastern and western Pacific displays interannual anomaly patterns [e.g. *Rasmusson and Carpenter,* 1982; *Wang et al.*, 1999; *Wang and Weisberg,* 2000]. Here, they start with condensation heating from convection in the west-central Pacific [e.g. *Deser and Wallace,* 1990; *Zebiak,* 1990] causing a pair of off-equator cyclones with westerly wind anomalies on the equator. These wind anomalies deepen the thermocline and increase SST in the equatorial central Pacific, giving rise to a positive feedback. However, these off equatorial cyclones raise the thermocline in the western Pacific by Ekman pumping, leading to a decrease in SST and an increase in sea level pressure in the off-equatorial western Pacific. This would initiate easterly wind anomalies in the western Pacific causing upwelling and cooling providing a negative feedback, allowing the system to oscillate.

1.2.4 Advective-Reflective Oscillator

The advective-reflective oscillator model, proposed by *Picaut et al.* [1997], emphasizes the positive feedback of zonal currents that advect the western Pacific warm pool toward the east during El Niño events. Interestingly, the model includes three different negative feedbacks to push the warm pool back to the western Pacific – anomalous zonal current from wave reflection at the western boundary, anomalous zonal current from wave reflection at the eastern boundary, and mean zonal current converging

at the eastern edge of the warm pool. Similarly to the other models, during El Niño, equatorial westerly wind anomalies in the central Pacific produce upwelling Rossby waves and downwelling Kelvin waves that propagate westward and eastward, respectively. Again, the westward propagating upwelling Rossby waves reflect as upwelling Kelvin waves after they reach the western boundary whereas the eastward propagating downwelling Kelvin waves reflect as downwelling Rossby waves at the eastern boundary. Their associated zonal currents push the warm pool back to its original position in the western Pacific.

1.3 ENSO spatial patterns

Although the field site of this research, located in the central tropical Pacific, is ideal for studying ENSO, it is limited in scale to understanding conditions in the central tropical Pacific only and not the equatorial Pacific as a whole. This is particularly important when interpreting paleo-ENSO variability as El Niño events have recently been categorized by their spatial footprint: the canonical eastern Pacific events (EP) and the central Pacific events (CP). Records from the central tropical Pacific will record both "flavors" of El Niño events. However, when comparing records from the central tropical Pacific with both the eastern and western tropical Pacific, we must consider changes in the spatial footprint of ENSO. In this section, I summarize our current understanding on the two different types of El Niño events.

1.3.1 Eastern verse Central Pacific El Niños

In 2004, a different pattern of sea surface temperature anomalies developed in the tropical Pacific, as compared to "typical" El Niño events observed during the 1982-83

and 1997-98 events. *Larkin and Harrison* [2005] and *Ashok et al.* [2007] initially described this event, highlighting that the anomalous warming occurs in the central equatorial Pacific. This is in comparison to the canonical El Niño, as described in *Rasmusson and Carpenter* [1982], where the anomalous warming is in the eastern equatorial Pacific. Others had earlier noticed different type of SST anomaly patterns as well [i.e. *Weare et al.,* 1976; *Donguy and Dessier,* 1983; *Fu et al.*, 1996; *Meyers et al.,* 1999]. *Ashok et al.* [2007] called this "Modoki" meaning "similar but different" but was later termed as "Central Pacific" by *Kao and Yu* [2009].

CP events, SST anomalies are mostly associated near the NIÑO3.4 and NIÑO4 regions (160°E to 120°W) whereas EP events occur in the Nino1+2 and Nino3 regions (80°W to 160°W). Statistical techniques from standard Empirical Orthogonal Function (EOF) analysis [*Ashok et al.,* 2007], combination of EOF analysis and linear regression [*Kao and Yu,* 2009], and composite analysis [*Kug et al.,* 2009] all similarly produce spatial patterns observed in EP and CP events. Importantly, for the CP ENSO pattern, they capture the poleward extension of SST anomalies into the subtropics. They suggest that CP events are associated with the local atmospheric forcing causing subsurface ocean temperature anomalies in the central Pacific, opposed to the EP ENSO events that are characterized by the subsurface temperature anomalies propagating across the Pacific basin (see references within Section 1.2). *Kao and Yu* [2009] and *Kug et al.* [2009] suggest that the dynamics behind CP ENSO events are less dependent on thermocline variations.

Convection and wind stress are also different between CP and EP ENSO events. With EP events, westerly winds extend over much of the equatorial Pacific whereas CP

events westerly winds are only centered on the central/western Pacific [*Kao and Yu,* 2009; *Kug et al.,* 2009]. At the same time, the eastern Pacific still experiences easterly winds. Convection for EP events moves to the central and eastern Pacific but for CP events, positive anomalies occur in the western Pacific and negative anomalies in the eastern Pacific [*Kao and Yu,* 2009; *Kug et al.,* 2009].

An interesting observation is that four of the five El Niño events in the 21st century were CP events, including 2014/15. This has led some to question whether this is a consequence of anthropogenic forcing. In CMIP3 model scenarios, the ratio of CP to EP events does increase, possibly due to the weakening of the Walker circulation and flattening of the thermocline [*Yeh et al.,* 2009]. But the 21st century could also be natural multidecadal variability [*McPhaden et al.,* 2011; *Newman et al.,* 2011].

1.4 Holocene ENSO variability

The instrumental record in the tropical Pacific is relatively short, limiting our ability to robustly test models of the response to ENSO variability to greenhouse forcing compared to the large natural variations observed in the system. Proxy records allow us to view ENSO variability over longer time frames in the past, which can be used to compare with model simulations. Reconstructions are created from tree rings, lake sediments, planktic foraminifera, mollusc shells, and corals.

The mid-Holocene, typically defined at 6,000 years ago, is most commonly targeted for ENSO reconstruction. During this time period precessional insolation was different from today, providing a period in time to test the sensitivity of ENSO to external forcing. When models are forced with insolation changes corresponding to 6,000 years

ago, they exhibit marked reductions in ENSO strength [*Clement et al.,* 2000; *Otto-Bliesner et al.,* 2003; *Liu et al.,* 2003; *Timmerman et al.,* 2007]. However, paleoclimate data from this time period provide conflicting accounts of ENSO strength. Some coral reconstructions support robust ENSO activity [*McGregor and Gagan*, 2004; *Cobb et al.,* 2013], while others record significant reductions in ENSO activity [*Tudhope et al.,* 2001; *McGregor et al.,* 2013]. Sedimentary archives from the eastern Pacific also provide conflicting information about ENSO strength over the last 7,000 years [*Moy et al.,* 2002; *Koutavas and Joanides,* 2012]. A new single foramifera ENSO record in the Eastern Pacific by *Koutavas and Joanides* [2012] record a mid-Holocene dampening from 4-6kyr BP by ~50% from modern, slightly later than what previous studies have shown [*Tudhope et al.,* 2001; *McGregor and Gagan*, 2004]. Even more recently, *Carré et al.* [2014], using oxygen isotopes from mollusk shells, find that ENSO was severely dampened in the Eastern Pacific between ~4-5kyr BP. In this section, I explore the different types of archives for Holocene ENSO reconstruction, outlining their strengths and weaknesses and summarizing their results. As corals are of the focus of this research, I devote more emphases in this section for using them as a paleo-ENSO recorder.

1.4.1 Lake Records

Lake sediment cores from the tropical Pacific have been used to reconstruct ENSO variability. The long continuous nature of this proxy makes it an excellent recorder for ENSO variability, however generally the resolution is too low to observe one such event. Additionally, other factors may influence the hydrology of a region, such as shifts in the ITCZ or changes in the monsoons. More recently, lake sediments from

ENSO-affected regions in the Andes have been interpreted as a result mountain glacier activity rather than ENSO variability [*Rodbell et al.,* 2008].

Rodbell [1999] and *Moy et al.* [2002] look at sedimentation from a lake cores from southern Ecuador to reconstruct ENSO over the past 15,000 and 12,000 years, respectively. Here, both studies interpret light-colored laminae as ENSO-caused alluvial deposition where increased precipitation during El Niño events causes increased debris flow deposits into the lake. *Rodbell* [1999] find low ENSO periodicity until 7,000 year ago with an increase of frequency to modern periodicities starting at ~5,000 years ago. *Moy et al.* [2002] find a gradual increase in ENSO events until 1,200 years ago followed by a decline to present. They also see millennial variability with alternating 2,000-yr periods of high and low ENSO variability. They suggest that ENSO dynamics may cause the millennial variability but that the long-term trend is due to changes in precessional insolation.

Conroy et al. [2008] look at sediment cores from a lake in the Galapagos, using grain size and C/N ratios as a proxy for changes in lake level, which is correlated with precipitation. They also find reduce ENSO variability in the early-to-mid Holocene with precipitation increasing after 4,200 BP and then a two-step increase again at 3,200 BP and 2,000 BP. However, they note that the observed increase in rainfall could be due to a southward shift in the ITCZ, which is tied to ENSO itself where El Niño events result in a southward shift of the ITCZ.

1.4.2 Foraminifera

Recently, single foraminfera have been used infer changes in ENSO variability over the Holocene and Last Glacial Maximum (LGM) [*Koutavas et al.,* 2006; *Koutavas and Joanides,* 2012]. They use the oxygen isotopic composition from many individual foraminifera from deep-sea sediments. The foraminifera record monthly changes in SST and salinity and by using a large number, they authors remove the need for annual resolution from marine sediments. Although this is a novel approach, it is limited by the short life span of each foraminifera. Additionally, the variance in the data may record more of an annual cycle than ENSO itself. *Koutavas et al.* [2006] first employ this approach to a marine sediment core near the Galapagos Islands. They find a 50% reduction of ENSO variance during the mid-Holocene (~5,900 – 6,300 years ago), too large to be from just the seasonal variance. *Koutavas and Joanides* [2012], following the same approach, analyze a core also near the Galapagos Islands, but extend the record back to the LGM. They find that ENSO was amplified during the LGM and damped during the mid-Holocene. However, their results show that between ~4,000 and 6,000 years ago ENSO was the weakest. This is consistent with the lake sediments *from Conroy et al.* [2008] but not with *Moy et al.* [2002]. They also suggest that precessional insolation is the main mechanism between these two different ENSO states. During the mid-Holocene, heating is reduced in March when the tropical Pacific is uniformly warm, reducing the heat input to the ocean and thus causing cooling. In September, upwelling intensifies keeping the eastern Pacific cool while the western Pacific warms up from solar insolation. This increases the zonal gradient and reinforces the Walker circulation, thus opposing El Niño development.

1.4.3 Mollusk shells

Reconstructing ENSO from mollusk shells is also a novel technique. Mollusk shells provide seasonal variability, much like corals, but on much shorter timescales. These archives are beneficial as they provide seasonal variability from the eastern Pacific where to date only lower-resolution marine and lake sediment records exist. In a sense, the approach is similar to the single foraminifera as the variance is estimated by statistics but provides the fidelity of high-resolution reconstructions such as corals [*Carré et al.*, 2013]. *Carré et al.* [2013] illustrate the application of this approach by comparing the geochemical record from 13 modern mollusk shells from Peru with the NIÑO1+2 index and finding they faithfully record ENSO variability except for strong El Niño events because of high mortality. *Carré et al.* [2014] then apply this approach with samples dating through the Holocene. They find that ENSO variability was similar to modern during the early Holocene, opposing the lake sediment records. They find reduced variance from 4,000 to 5,000 years ago, similar to *Koutavas and Joanides* [2012]. Interestingly, they address the spatial characteristics of ENSO events by looking at the skewness values. EP events are skewed positively with large El Niño events and small La Niña events whereas CP events are skewed negatively with moderate El Niño events and strong La Niña events. They use this skewness factor in the fossil mollusk shells and find a tendency of more CP events between 6,700 and 7,500 years ago and EP events before 8,000 years ago and after 4,000 years ago.

1.4.4 Corals

Corals, which are of particular relevance to the research of this dissertation, provide decades- to centuries-long monthly resolved ENSO reconstruction. Long-lived corals provide monthly resolved, decades-long windows of ENSO variability over the last

century and beyond, recorded as changes in the oxygen isotopic composition ($\delta^{18}O$) of the coral skeleton [*Correge,* 2006 and references therein]. Coral $\delta^{18}O$ records from the Line Islands (4°N, 160°W), in the central equatorial Pacific, track ENSO variations over the 20th century with exceptionally high fidelity, and have been used to reconstruct ENSO over the last century [*Evans et al.,* 1999; *Cobb et al.,* 2001; *Nurhati et al.,* 2009], the last millennium [*Cobb et al.,* 2003], and the last 7,000 years [*Cobb et al.,* 2013]. However, a trade-off with such high-resolution records when going back to the Holocene is that corals do not provide a continuous paleo-ENSO record.

Coral polyps secrete an aragonitic skeleton, an orthorhombic form of calcium carbonate ($CaCO_3$). During secretion, they incorporate the geochemistry of the seawater into their skeleton, recording several different geochemical ocean tracers [*Weber and Woodhead,* 1972; *Smith et al.,* 1979; *Beck et al.,* 1992]. Oxygen isotopes are the most widely used tracer of sea surface temperature (SST) and sea surface salinity (SSS). Oxygen isotopes are expressed as the ratio of the heavy isotope (^{18}O) divided by the abundance of the light isotope (^{16}O). This mass differentiation allows one isotope to be preferentially incorporated into a given phase during a physical change, resulting in a mass-dependent isotopic fractionation. Values may be positive, negative, or zero, such that a negative $\delta^{18}O$ value indicates that the sample has a lower $^{18}O/^{16}O$ ratio than the standard. For carbonate samples, the reference standard is Vienna Pee Dee Belemnite (VPDB).

Coral $\delta^{18}O$ is a function of both SST and the local $\delta^{18}O$ of seawater ($\delta^{18}O_{sw}$). On short timescales, $\delta^{18}O_{sw}$ is primarily controlled by SSS, which is a function of

precipitation and evaporation. During evaporation, the lighter oxygen isotope is preferentially removed, enriching the seawater with the heavier isotope (i.e. more positive $\delta^{18}O_{sw}$). With SST, warmer water temperatures result in a more negative coral $\delta^{18}O$, where as cooler temperatures result in more positive coral $\delta^{18}O$. This is due to the temperature dependence of fractionation where fractionation factors decrease with increasing temperature. Therefore, the $\delta^{18}O$ of the calcium carbonate is a function of both SST and SSS for any given time.

In particular relevance to this research, El Niño extremes bring warmer sea surface temperature and increased precipitation to the Line Islands (Christmas Island (2°N, 157°W), Fanning Island (4°N, 160°W), and Palmyra Atoll (6°N, 162°W)), whereas the opposite occurs during La Niña extremes. Corals record these events as $\delta^{18}O$ excursions in their aragonitic skeletons. Coral $\delta^{18}O$ decreases when temperature increases and/or when rainfall increases (resulting during El Niño events), whereas coral $\delta^{18}O$ increases when temperature decreases and/or when rainfall decreases (resulting during La Niña events). Previous studies have shown that $\delta^{18}O$ in Line Islands corals is strongly correlated to the NIÑO3.4 SST index, an SST-based indicator of ENSO phase and strength [*Reynolds et al.*, 2002]. *Cobb et al.* [2013] demonstrated that correlations between the 2-7 year bandpassed $\delta^{18}O$ records from Palmyra, Fanning, and Christmas Island modern corals and similarly filtered NIÑO3.4 SST are -0.82, -0.85, and -0.92, respectively. Coral $\delta^{18}O$ records from Christmas Island, the southern-most Line Island, provide the highest-fidelity coral reconstructions of ENSO, sharing 80% of their interannual variance with ENSO indices, as it experiences the largest warming of the

three islands during El Niño events [*Evans et al.,* 1999; *Nurhati et al.,* 2009; *Cobb et al.,* 2013].

In order to extend the coral $\delta^{18}O$ through the last several thousand years for paleo-ENSO reconstruction, we turn to "fossil" corals, or corals that lie exposed on the shoreline that were washed onshore from storms. Previous work in the Line Islands has extended the fossil coral $\delta^{18}O$ record through the last millennium [*Cobb et al.,* 2003] and into the late- to mid-Holocene [*Woodroffe et al.,* 2003; *Cobb et al.,* 2013; *McGregor et al.,* 2013]. Generally, the fossil coral records consist of monthly-resolved discontinuous sequences that range from 20- to 90-cm long, providing anywhere from 15 to 50 years of paleo-ENSO record. *Cobb et al.* [2003] produce a robust coral $\delta^{18}O$ record from Palmyra through the last millennium by splicing together overlapping U/Th dated coral records. *Cobb et al.* [2013] extend the ENSO record back to the last 7,000 years by adding fossil coral samples from Fanning and Christmas Island. In addition, *Woodroffe et al.* [2003] and *McGregor et al.* [2013] add additional coral records from Christmas Island from microatolls from the mid-Holocene. Interestingly, the different coral records suggest opposing views on mid-Holocene climate. In one sense, *Woodroffe et al.* [2003] and *McGregor et al.* [2013] suggest a mid-Holocene ENSO dampening whereas *Cobb et al.* [2013] suggest that ENSO variability, although reduced compared to the late 20th century, was still robust throughout the last 7,000 years. In addition, *Cobb et al.* [2003] find that the 20th century, although high, is not unprecedented as ENSO variability was stronger in the late 17th century.

1.4.5 Climate models

Holocene climate simulations provided early evidence for this suggestive mid-Holocene (~6,000yrs BP) ENSO dampening. *Clement et al.* [2000] use the Zebiak-Cane coupled ocean-atmosphere model [*Zebiak and Cane*, 1987] and impose changes in the solar forcing mimicking the orbital-induced insolation conditions over the last 12,000 years. They find a statistically significant weaker ENSO in the mid-Holocene (less extreme El Niño events with less frequency) with a distinct increase in both frequency and amplitude over the mid-to late Holocene, in agreement with the lake records from *Rodbell* [1999]. They suggest that it is the altered seasonal cycle from orbitally-induced changes that effect ENSO behavior where more heating in the boreal summer and less heating in the boreal winter suppresses warm events from occurring. *Otto-Bliesner et al.* [2003] extend ENSO model simulations back through the last glacial-interglacial cycle using the NCAR Climate System Model, a global, coupled ocean-atmosphere-sea ice model. For the Holocene time-period, they force the model with solar radiation changes at 3.5, 6, 8.5 and 11 kyr ago and find a statistically significant decrease in variability at 6, 8.5, and 11 kyr ago, again owing it to the changes in seasonality. *Liu et al.* [2003] similarly look at several time steps in the Holocene at 3, 6, 8, and 11 kyr ago, using two different coupled ocean-atmosphere models and both models produce weaker ENSO variability in the early to mid-Holocene. *Timmerman et al.* [2007] take a different approach by looking at the sensitivity of ENSO to different orbital parameters using a global atmosphere-ocean-sea ice model. They find that ENSO and the strength of the annual cycle are strongly correlated and are modulated by the 21,000-yr precession cycle where strong annual cycle corresponds to weaker ENSO variability.

Lastly, I think it is relevant it mention a 2,000-yr-long simulation by *Wittenberg* [2009] to simulate ENSO's natural variability. He uses the GFDL CM2.1 global GCM with all forcings fixed at 1860 AD values (solar irradiance, land cover, and atmospheric composition) and finds a strong interdecadal and intercentennial modulation of ENSO behavior. The results suggest that 500 years is needed for sampling variability to lie close to the total interannual power. *Wittenberg* [2009] hypothesizes two reasons for such large unforced ENSO modulation. One, it could arise from nonlinearities in the system between El Niño and La Niña [*Jin et al.*, 2003; *Rodgers et al.*, 2004; *Schopf and Burgman,* 2006]. Alternatively, it could occur stochastically, occurring from ENSO's interannual time scale and seasonal phase-locking [*Wittenberg*, 2009]. This study doesn't preclude that ENSO is not sensitive to changes in solar insolation, but illustrates how such large natural modulations in ENSO behavior make it challenging to detect any changes from external forcings.

1.5 Projections of ENSO under anthropogenic forcing

The large societal and economical impacts from the large 1997/98 El Niño have raised concern about the impacts of ENSO due to anthropogenic warming. Unfortunately, to date, there is no consensus on how ENSO will respond in a warming world. Some postulate that CP events will occur more frequently than EP events [*Yeh et al.*, 2009]. Others find that the Walker Circulation will weaken, weakening the zonal slope of the thermocline and thus causing more extreme El Niño events [*Vecchi et al.*, 2006; *Xie et al.*, 2010]. However, when models are forced with CO_2, they do not agree on whether ENSO variability strengthens, weakens or has no change all. Indeed, it will be

challenging to detect changes in ENSO from external forcings due to such large decadal and centennial intrinsic variability in ENSO [*Wittenberg,* 2009].

Yeh et al. [2009] run scenarios from the Coupled Model Intercomparison Project phase 3 (CMIP 3) under projected global warming scenarios and historical El Niño indexes. They find that the ratio of CP to EP El Niño events increases under greenhouse gas forcing by as much as five times. They attribute this to a change in the mean background state from global warming, causing the thermocline to flatten. Essentially, they argue that warmer SSTs will weaken the easterlies and enhance meridional transport leading to a shoaling of the thermocline depth. With this, zonal advective feedback will dominate promoting more CP El Niño events.

Most climate model projections, however, disagree on how ENSO will respond to greenhouse warming. *Collins et al.* [2010] illustrate how GCMs from CMIP3 span a range of responses of ENSO variability from a greenhouse gas forcing. Even the models, which are thought to be the best performing models, are not consistent. This work is consistent with many other previous studies [e.g. *Van Oldenborgh et al.,* 2005; *Zelle et al.,* 2005; *Park et al.,* 2009; *Yeh et al.,* 2006; *Yeh and Kirtman,* 2007; *Cherchi et al.,* 2008; *Guilyardi et al.,* 2009]. However, *Collins et al.,* [2010] do conclude that climate change will *probably* have a significant impact on ENSO. He cites changes from a weakening in the mean upwelling and zonal advection and a strengthening in the SST response to the thermocline and wind stress anomalies as a cause for larger ENSO events. However, what is unclear is how atmospheric dampening feedbacks, which reduce ENSO variability, will counterbalance the other characteristics toward a more positive ENSO response.

Recently, some have made more definitive statements about ENSO and global warming. *Cai et al.* [2014] find a doubling of occurrences of extreme El Niño events in response to greenhouse warming using an aggregate of both CMIP3 and CMIP5 models, although a decrease in the total number of El Niño events. They equate this to the fact that warming, although it occurs everywhere across the tropical Pacific, it occurs faster in the eastern tropical Pacific, thus reducing the zonal and meridional SST gradients. This means that it would require weaker changes in SST and SST gradients to causes changes in convection. *Power et al.* [2013] look at precipitation changes from El Niño in the 21st century and find more drying in the western Pacific and increased rainfall in the central and eastern Pacific due to a nonlinear response to global warming. *Kim et al.* [2014], using CMIP5 models, focus on the change in magnitude in SST. Interestingly, they find that ENSO SST amplitude increases before 2040 but then decreases afterwards. They attribute this time-varying behavior as the reason why previous models did not agree.

1.6 Summary

Although some studies are beginning to provide more certainty in the response of ENSO variability to anthropogenic climate change, it is clear that there is still no consensus in the scientific community, especially as studies highlight the large intrinsic variability within the system. Much of this is due to our evolving understanding of ENSO dynamics, of which I summarize some of the main theories above. Paleoclimate records help extend the instrumental record of ENSO variability, providing a longer baseline to measure internal variability as well as testing whether ENSO is sensitive to external forcing. Additionally, they can be compared with model output, providing more skill in future model projections. This dissertation addresses some of these challenges by

providing high-resolution coral records of ENSO variability and mean climate change over the mid-to late- Holocene from the central tropical Pacific.

CHAPTER 2. A COMPARISON OF U/TH AND RAPID-SCREEN ^{14}C DATES FROM LINE ISLAND FOSSIL CORALS

This is a reprint of an article whose final and definitive form has been published in *Geosystems, Geophysics, Geochemistry*, authored by P.R. Grothe, K.M. Cobb, S.L. Bush, H. Cheng, G.M. Santos, J.R. Southon, R.L. Edwards, D.M. Deocampo, and H.R. Sayani entitled "A comparison of U/TH and rapid-screen 14C dates from Line Island Fossil Corals".

2.1 Abstract

Time-consuming and expensive radiometric dating techniques limit the number of dates available to construct absolute chronologies for high-resolution paleoclimate reconstructions. A recently developed rapid-screen ^{14}C dating technique reduces sample preparation time and per sample costs by 90%, but its accuracy has not yet been tested on shallow-water corals. In this study, we test the rapid-screen ^{14}C dating technique on shallow-water corals by comparing 44 rapid-screen ^{14}C dates to both high-precision ^{14}C dates and U/Th dates from mid- to late-Holocene fossil corals collected from the central tropical Pacific (2-4°N, 157-160°W). Our results show that 42 rapid-screen ^{14}C and U/Th dates agree within uncertainties, confirming closed-system behavior and ensuring chronological accuracy. However, two samples that grew ~6500yrs ago have calibrated ^{14}C ages ~1000yrs younger than the corresponding U/Th ages, consistent with diagenetic alteration as indicated by the presence of 15-23% calcite. Mass balance calculations

confirm that the observed dating discrepancies are consistent with ^{14}C addition and U removal, both of which occur during diagenetic calcite recrystallization. Under the assumption that aragonite-to-calcite replacement is linear through time, we estimate the samples' true ages using the measured ^{14}C and U/Th dates and percent calcite values. Results illustrate that the rapid-screen ^{14}C dates of Holocene-aged fossil corals are accurate for samples with less than 2% calcite. Application of this rapid-screen ^{14}C method to the fossil coral rubble fields from Kiritimati Island reveal significant chronological clustering of fossil coral across the landscape, with older ages farther from the water's edge.

2.2 Introduction

Absolutely-dated, high-resolution paleoclimate records provide a detailed account of past climate variability. Precise radiometric dating of Holocene-aged carbonate proxies, such as speleothems [e.g. *Wang et al.*, 2005], bivalves [e.g. *Mangerud*, 1972], foraminifera [e.g. *Broecker et al.*, 1984], and corals [e.g. *Edwards et al.*, 1987], is necessary for accurate chronological control of paleoclimate records. Most carbonate proxies are dated using high-precision ^{14}C-accelerator mass spectrometry (AMS) and U/Th methods, whose expensive and time-consuming analyses limit the number of samples used to constrain the chronologies of paleoclimate records. In most cases, limits on the time and/or funding that can be dedicated to radiometric dating dictate the number of paleoclimate reconstructions and potentially the resolution thereof that can be pursued.

High-precision U/Th disequilibrium dating is the most precise method for dating late Pleistocene- and Holocene-aged corals [e.g. *Edwards et al.*, 1987; *Cobb et al.*, 2003a;

Potter et al., 2005; *Zhao et al.*, 2009]. High-precision measurements of ^{238}U, ^{234}U and ^{230}Th using multi-collector inductively coupled plasma mass spectrometry (MC-ICPMS) provide low uncertainties on the order of 0.1% (2σ) for material less than 10,000yrs [*Cheng et al.*, 2013]. However, high-precision U/Th disequilibrium dating is time-consuming and expensive, requiring the chemical separation of U and Th fractions in a clean room followed by ICPMS analyses. Recently, *Douville et al.* [2010] simplified tedious chemical separations and simultaneously measured U and Th atoms on an inductively coupled plasma-quadruple mass spectrometry (ICP-QMS), achieving 50 dates per day with precision levels of less than 2%. Additional rapid U/Th dating methods have been developed using laser ablation (LA) MC-ICPMS [*Eggins et al.*, 2005; *Potter et al.*, 2005; *McGregor et al.*, 2011] and are capable of analyzing 50 dates per day with only one day of sample preparation [*Spooner et al.*, 2016], but uncertainties of ±33% (2σ) [*McGregor et al.*, 2011] or more [*Potter et al.*, 2005] on late-Holocene corals are too large for many paleoclimate applications.

A variety of recent studies investigate techniques for expediting the ^{14}C dating process. For example, gas ion source AMS removes graphitization steps [*Ramsey et al.*, 2004] and can now measure up to 30 samples per day with precisions of >0.7% [*Wacker et al.*, 2013]. However, those setups have been both mostly dedicated to compound specific work, source apportionment and biomedical analysis, and so far do not provide any additional discount in sample processing and spectrometer measurement costs for reconnaissance work. Recently, *Bush et al.* [2013] developed a rapid-screen ^{14}C dating method using a standard source AMS for application to Holocene-aged marine carbonates. The rapid-screen ^{14}C method bypasses the time-consuming leaching,

hydrolysis and graphitization steps required for the preparation of carbonate samples for high-precision ^{14}C-AMS dating [*Santos et al.*, 2004]. Rather, the new technique involves direct AMS analysis of powdered calcium carbonate samples mixed with powdered iron catalyst. Analytical precisions of ±1.8% (1σ) can be achieved on carbonate samples younger than 10ky BP [*Bush et al.*, 2013]. This work improves upon more complex but fast ^{14}C dating methods by *Burke et al.* [2010] and *McIntyre et al.* [2011], which requires >10mg of $CaCO_3$ powder for measurement, and is similar to the method developed by *Longworth et al.* [2013] who use titanium instead of iron as a catalyst. The rapid-screen ^{14}C method has been applied to date dozens of deep-sea corals [*Bush et al.*, 2013], but has never been tested on shallow-water corals.

A major caveat of any dating method for shallow-water corals is the fact that diagenesis can cause the gain or loss of radiogenic parents or daughters through open system behavior [e.g. *Lazar et al.*, 2004; *Scholz et al.*, 2004]. Diagenesis in corals typically manifests itself in two forms: 1) as secondary aragonite needles precipitated in a submarine environment [e.g. *Enmar et al., 2000*; *Hendy et al.*, 2007; *Nothdurft and Webb*, 2009; *Sayani et al.*, 2011], or 2) as secondary calcites derived from dissolution of the primary aragonite skeleton and subsequent recrystallization in subaerial environments [e.g. *Rabier et al.*, 2008; *McGregor and Gagan*, 2003; *Sayani et al.*, 2011]. For the latter, ^{14}C is incorporated into the newly formed crystals, resulting in a measured ^{14}C age that is younger than the true age [*Burr et al.*, 1992]. The recrystallization process results in U loss to the coral sample [e.g. *Henderson et al.*, 1993; *Shen and Dunbar*, 1995; *Scholz et al.*, 2004; *Scholz and Mangini*, 2007], given that U is soluble in natural water [*James*,

1974; *Bathurst*, 1974; *Pingitore*, 1976; *Maliva and Dickson*, 1992; *Rabier et al.*, 2008] and has lower concentrations in the more compact calcite lattice [*Reeder et al.*, 2001].

Many studies documenting the effects of diagenesis on coral U/Th dates focus on fossil corals from the late Pleistocene [e.g. *Broecker et al.*, 1968; *Edwards et al.*, 1988; *Gallup et al.*, 1994; *Cutler et al.*, 2003]. Open system behavior is characterized by elevated initial $^{234}U/^{238}U$ activity ratios caused by the post-depositional formation of secondary carbonates with seawater $^{234}U/^{238}U$ ratios [e.g. *Bender et al.*, 1979; *Gallup et al.*, 1994; *Henderson*, 2002; *Thompson et al.*, 2003; *Scholz et al.*, 2004; *Robinson et al.*, 2006]. Marine carbonates incorporate the $^{234}U/^{238}U$ activity ratio from seawater [e.g. *Chen et al.*, 1986; *Cheng et al.*, 2000; *Robinson et al.*, 2004], which is thought to be constant to within 1% over the last glacial interglacial cycle [*Henderson*, 2002; *Esat and Yokoyama*, 2006]. If decay occurs in a closed system then age-corrected $^{234}U/^{238}U$ ratios (reported as $\delta^{234}U_{initial}$ values) should be the same as modern day [*Edwards et al.*, 1987]. However, corals with $(^{234}U/^{238}U)_{initial}$ activity ratios within the range of modern seawater may still have experienced open system behavior during diagenesis [*Gallup et al.*, 2002; *Cutler et al.*, 2003]. Additional screening criteria for corals (i.e U concentrations should be in the range of modern analogues and calcite percentages should be <2% [*Scholz and Mangini*, 2007]) help guide sample selection and ensure closed-system U/Th dates. Given the importance of obtaining accurate age constraints from fossil corals used for sea level reconstruction, recent efforts have established models for correcting U/Th dates from corals characterized by open system behavior [*Thompson et al.*, 2003; *Villemant and Feuillet*, 2003; *Scholz et al.*; 2004], which are fully explored in *Scholz and Mangini* [2007].

Very young corals (<1000yrs) with intact $^{234}U/^{238}U$ initial values can exhibit elevated $\Delta^{14}C$ values associated with secondary carbonate precipitation [*Zaunbrecher et al.*, 2010], illustrating the limitations of $^{234}U/^{238}U$ as a screening tool in young corals. Given that atmospheric exchange during the precipitation process adds appreciable ^{14}C to the sample, ^{14}C ages are much more sensitive to diagenesis than U/Th ages [*Burr et al.*, 1992; *Yokoyama and Esat*, 2004]. Techniques such as X-ray diffraction (XRD) and scanning electron microscope (SEM) imaging that enable the identification of diagenetic phases have become common screening tools prior to dating samples for paleoclimate reconstruction. However, the diagenetic condition of a given sample is heterogeneous on the mm scale, as evidenced by poor replication of duplicate U-series measurements from the same sample [*Scholz and Mangini*, 2007], which makes it challenging to establish whether the specific sample used for radiometric dating is pristine or not.

In this study, we assess the rapid-screen ^{14}C dating method from *Bush et al.* [2013] as a tool for dating Holocene-aged fossil corals by comparing rapid-screen ^{14}C dates with high-precision U/Th dates from a large collection of fossil corals from the Line Islands. We investigate the effects of calcite recrystallization observed in two older samples on both ^{14}C and U/Th dates by modeling a continuous replacement of aragonite to calcite. Lastly, we apply the rapid-screen ^{14}C dating method to a large number of fossil coral samples collected around Kiritimati Island and provide a preliminary map of fossil coral age distributions at this site.

2.3 Methods

2.3.1 Sample selection

We selected 44 samples for paired ^{14}C and U/Th dating, including three samples from *Cobb et al.* [2003b] and thirteen samples from *Cobb et al.* [2013]. The bulk of the remaining 28 samples represent newly-collected fossil *Porites* coral samples collected from Kiritimati Island in May 2012. These samples, averaging 10cm in length, were collected from fossil coral deposits lining ocean-facing beaches. Using the new and previously published dates, we achieved an approximately even temporal distribution of samples across the last 7000 years.

We sub-sampled each fossil coral sample for dating by cutting a roughly $1cm^3$-sized piece from the sample using a Dremel® Rotary tool. This sub-sample size equates to less than 1 year of skeletal accretion for the fast growing *Porites* corals. In most cases, dating subsamples were >10cm away from the exposed surface. However, some subsamples were taken within ~2cm of the exposed surface using a hammer and chisel in the field. To test whether this difference affected the dating, we compared dating results for subsamples taken from the exterior as well as the interior of select fossil coral cores.

2.3.2 Screening by X-Ray Diffraction

Select samples were screened for calcite using a Panalytical XPERT PRO X-ray diffractometer (XRD) at Georgia State University (GSU) using CuK_α radiation, 1˚ fixed incident and diffracted beam slits, 0.04rad incident and diffracted beam Soller slits, a 2˚ incident beam anti-scatter slit, a Ni diffracted beam filter, and a Panalytical PIXcel-1D fast detector. Finely powdered samples (~300 mg) were analyzed on low background mounts in the XRD operating at 45 kV and 40 mA. All samples were initially analyzed in the range 25.5-30.0 ˚2θ, and examined for the presence of the [111] and [102] aragonite

peaks (3.40Å and 3.27Å, respectively), and the [104] calcite peak (3.04Å). Based on analysis of synthetic standards, the limit of detection of calcite by this method is below 0.5 weight % calcite. This limit of detection was selected to provide a high rate of sample throughput to rapidly screen samples. Those samples with detectable calcite were subsequently analyzed by slow scans in the range 5-70˚2θ to obtain high quality diffraction data to allow Rietveld refinements for precise quantification [*Bish and Post*, 1993] using Panalytical HighScore+ vers. 3.0 with reference to the PDF-2-2011 and ICSD-2011 crystal structure databases.

2.3.3 Rapid-screen ^{14}C dating

Radiocarbon measurements were performed at the W.M. Keck Carbon Cycle Accelerator Mass Spectrometry Laboratory (KCCAMS) at the University of California Irvine, following methods outlined in *Bush et al.* [2013]. Small chunks of ~1g were chipped from the larger coral samples and ultrasonically cleaned in deionized water three times for 5 minutes, or until water was clear after sonication. Using a mortar and pestle, the cleaned coral chunks were ground to a fine powder, and 0.3mg of the powder was mixed with ~5.0mg of Fe powder (Sigma-Aldrich -400 mesh, 99.9% pure) and pressed directly into a target for AMS analysis.

Three primary standards of oxalic acid (OX-I) >0.7 mg C graphite were used per wheel to tune the AMS and to normalize the $^{14}C/^{12}C$ ratios [*Santos et al.*, 2007a; *Bush et al.*, 2013]. For background corrections from modern contamination and quality control, two calcite blanks and one secondary standard (IAEA-C2 - chalk, Fm = 0.411; ~7135 yr BP) were also measured in each wheel. Both the calcite blanks and the IAEA-C2

standard were powdered and processed using the same methodology as the coral samples. As a coral-based ^{14}C blank sample was unavailable, we used a calcite ^{14}C blank derived from a ~250kyr old stalagmite from Borneo [pers. comm. Cobb, K.M.]. We recognize that calcite blanks are cleaner than biogenic carbonates [*Eltgroth et al.*, 2006], however, since our coral samples are less than 7,000 years old, underestimating the blank correction by a few micrograms is not significant enough to skew the ages [*Wood*, 2015]. For the ^{14}C rapid-screen method, the AMS measurement time for each sample is limited to ~4 runs of 150 seconds each, as opposed to ~10-15 runs each required for a high-precision ^{14}C date. Under these conditions, the analytical precision on a ^{14}C date for a young (<10,000 years old) carbonate is approximately ±1.8% (1σ), versus the high-precision ^{14}C-AMS analytical precision of ±0.2-0.3% (1σ) [*Beverly et al.*, 2010]. We performed replicate analyses on several samples to test the reproducibility of the rapid-screen ^{14}C method in our fossil coral material. Five samples were replicated six times and 15 samples were run in duplicate. Replicate values all fell within the 1σ analytical precision limits.

Measured $^{14}C/^{12}C$ ratios were fractionation-corrected using the AMS $\delta^{13}C$ values and normalized to a $\delta^{13}C$ value of -25‰. A mass balance background correction was also applied following *Santos et al*. [2007b]. Radiocarbon ages (yrs BP = years before 1950 AD) were converted to calibrated calendar ages (yrs AD for <1000 years old and cal yrs BP for samples >1000 years old) using the Calib 7.1 software [*Stuiver et al.*, 2005] and MARINE13 calibration datasets [*Reimer et al.*, 2013]. Additionally, we used a local radiocarbon marine reservoir correction (ΔR) of 39 ±56yrs (1σ) [*McGregor et al.*, 2011]. Final calibrated ages are reported as the 2σ age ranges about the median probability. It is

important to note that significant analytical uncertainties associated with the rapid-screen ^{14}C analysis protocol translate to relatively large age uncertainties once propagated through the ^{14}C calibration curve, especially for younger samples dating to the last millennium [*Taylor and Bar-Yosef*, 2014].

For high-precision ^{14}C-AMS dates (N=3), coral samples were prepared and analyzed following protocols outlined in *Santos et al.* [2004]. Coral powder was initially leached to remove surface adsorptions (~10% by mass), acidified to CO_2 and converted to graphite using an Fe catalyst and the hydrogen reduction method. Analytical uncertainties for high-precision ^{14}C dates range from 0.2-0.3%.

2.3.4 U/Th dating

The fossil coral U/Th chemistry and isotopic analyses were performed at the Minnesota Isotope Lab at the University of Minnesota using a ThermoFinnigan Neptune multi-collector Inductively Coupled Plasma Mass Spectrometer (MC-ICPMS). Of the 56 U/Th dates discussed in this paper, 18 dates were published in *Cobb et al.* [2003b] and *Cobb et al.* [2013]. P. Grothe measured the remaining 38 fossil coral U/Th ages in June 2013.

U/Th dating was performed following procedures outlined in *Cheng et al.* [2013] following general protocols first outlined in *Edwards et al.* [1987] and subsequently revised by *Shen et al.* [2002]. Following fossil coral sampling procedures outlined in *Cobb et al.* [2003a], small pieces of ~0.05 g were broken from the coral using a stainless steel chisel and hammer. The samples were visually inspected under a microscope and any discoloring and/or debris were removed using an exacto knife. The pieces were then

ultrasonically cleaned in deionized water three times and dried overnight at 30°C. Then a ~0.05g sample was dissolved in concentrated HNO_3 and spiked with solution containing known concentrations of ^{233}U, ^{235}U, and ^{229}Th. The U and Th atoms were separated from the bulk sample by Fe precipitation, and subsequently dissolved in a dilute HNO_3 and HF solution for MC-ICPMS analyses. For each batch, a blank that was run through the same chemistry was analyzed to correct for procedural contamination. In addition, one duplicate per run was analyzed to ensure reproducibility. The age was solved iteratively using the standard age equation presented in *Edwards et al.* [1987], using decay constants of 1.55125×10^{-10} for λ_{238} [*Jaffey et al.*, 1971], 2.82206×10^{-6} for λ_{234} [*Cheng et al.*, 2013], and 9.1705×10^{-6} for λ_{230} [*Cheng et al.*, 2013]. Samples were corrected for initial non-radiogenic Th using a $^{230}Th/^{232}Th$ atomic ratio of $4.4 \pm 2.2 \times 10^{-6}$.

2.4 Results

Sample P11, whose original U/Th age was reported as 2218 ±10 cal yrs Before Present (BP) [*Cobb et al.*, 2013], yielded U/Th ages of 5075 ±16 and 5061 ±14 cal yrs BP during replicate re-analysis over the course of this study. Four different P11 samples dated via the rapid-screen ^{14}C method fall within analytical error of the revised U/Th ages, ranging from 4898 to 5437 cal yrs BP. In the absence of any evidence of diagenetic alteration, and given that P. Grothe resampled the archived core clearly labeled "P11" for this study, we use the new U/Th ages for the paired rapid-screen ^{14}C-U/Th ages.

Calibrated rapid-screen ^{14}C ages for coral samples derived from the interior (>10cm from the weathered coral surface) versus exterior (<2cm from the weathered

surface) are statistically indistinguishable from one another, and from the corresponding U/Th dates (Figure 2.1; Table 2.1).

The rapid-screen ^{14}C calibrated age ranges (±2σ) correspond well with the high-precision ^{14}C calibrated ages for the three fossil coral samples tested (Table 2.2), with an average difference of 2.4%. These differences are well within the ±2% (1σ) analytical uncertainty of the rapid-screen ^{14}C dating method, as outlined by *Bush et al.* [2013].

2.4.1 High-precision ^{14}C-U/Th comparisons

High-precision ^{14}C and U/Th ages from two unaltered samples, SB7 and V30, agree within error (2σ) (Table 2.2). We calculate the ΔR value for SB7 (U/Th date 1342 ±5 AD) and find agreement with ΔR=39 ±56yrs (1σ) used in our ^{14}C age calibrations [*McGregor et al.*, 2011]. For V30 (U/Th age 5979 ±13 cal yrs BP), we calculate a ΔR value of -77 ±33yrs. However, since the high-precision ^{14}C and U/Th ages for V30 are concordant when using ΔR= 39 ±56yrs and we do not have any additional constraints on ΔR during this time period, we continue to use ΔR= 39 ±56yrs for all of our ^{14}C age calibrations.

2.4.2 Rapid-screen ^{14}C-U/Th comparisons

Fossil coral rapid-screen ^{14}C ages match U/Th ages within combined errors (2σ) in 42 of the 44 paired analyses (Figure 2.2; Table 2.2). Concordant samples differ on average by 3.4% between the ^{14}C calibrated median probability age and U/Th age, with no systematic offsets. Such differences are well within the combined uncertainties of the analytical precision for the rapid-screen ^{14}C dating and subsequent calibration.

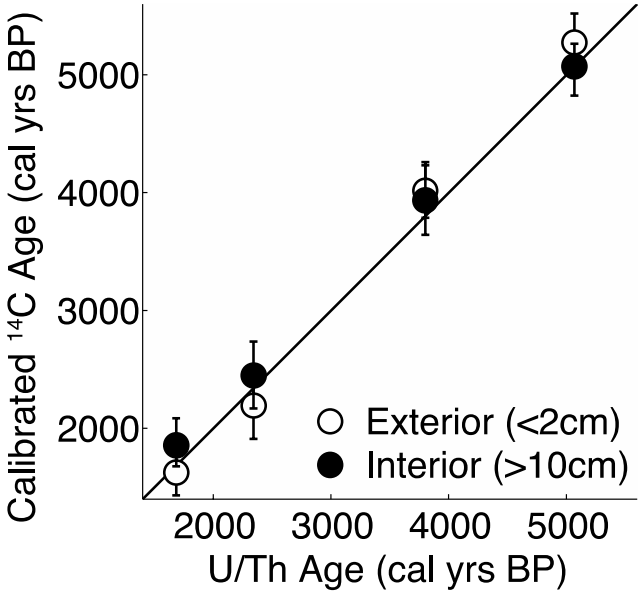

Figure 2.1 U/Th and calibrated ^{14}C dates of four fossil corals sampled near the exterior (<2cm from the weathered surface; open circles) and interior (>10cm from the weathered surface; black circles). The median probability of the calibrated rapid-screen ^{14}C date is plotted with error bars representing the 2σ age range. The 2σ error bars for U/Th dates are smaller than the symbol size.

Table 2.1 Rapid-screen ^{14}C and U/Th dates for exterior and interior samples

Sample	U/Th Age (cal yrs BP)[a,b]		Edge or Interior[c]	^{14}C Age (yrs BP)		Rapid-Screen Calibrated age (cal yrs BP)[d]	
P2	1685	±5	Exterior	2090	±60	1625	±203
			Interior	2290	±80	1858	±246
P37	2342	±7	Exterior	2570	±60	2195	±205
			Interior	2760	±60	2450	±220
P43	3802	±17	Exterior	4040	±80	4015	±283
			Interior	3980	±90	3934	±294
P11	5068	±15	Exterior	4990	±100	5275	±298
			Interior	4830	±80	5071	±237

[a] Errors quoted are 2σ.

[b] U/Th dates are published in *Cobb et al.* [2013].

[c] Exterior is defined as <2cm from the weathered surface whereas interior refers to samples taken >10cm from the weathered surface.

[d] ^{14}C ages were calibrated to calendar years using Calib7.1 software [*Stuiver et al.*, 2005] and Marine13 calibration datasets [*Reimer et al.*, 2013] and corrected for a local reservoir age using ΔR of 39 ±56 [*McGregor et al.*, 2011]. The ^{14}C calibrated age is reported as the median probability. Calibrated ^{14}C errors are 2σ.

Table 2.2 Paired ^{14}C and U/Th dates

Sample[a]	U/Th Age[b]		^{14}C Age (yrs BP)		Rapid Screen Calibrated age[c]		High-Precision ^{14}C-AMS Age (yrs BP)		High-Precision ^{14}C-AMS Calibrated Age[c]	
Last Millennium (years in AD)										
X12-3-2	2003	±4	-540	±60	post-1950					
X12-9-10	1993	±3	-725	±40	post-1950					
X12-D6-1	1986	±3	-790	±40	post-1950					
X12-4-111	1969	±3	-190	±80	post-1950					
X12-1-19	1930	±3	630	±60	1734	±199				
X12-9-6	1919	±3	590	±50	1775	±156				
X12-1-11	1910	±3	610	±60	1756	±183				
X12-1-8	1887	±4	630	±70	1733	+200				
X12-13-19	1873	±3	570	±50	1792	±193				
X12-13-8	1742	±5	590	±50	1775	±156				
X12-6-75	1733	±4	670	±60	1679	±226				
X12-D2-3	1723	±4	640	±60	1720	±208				
*SB3b**	1674	±5	710	±60	1628	±181				
X12-16-1	1622	±5	760	±60	1586	±180				
X12-16-6	1599	±5	710	±70	1633	±195				
X12-13-5	1566	±4	700	±50	1640	±173				
X12-3-23	1428	±5	950	±60	1427	±140				
*SB7**	1342	±5	1020	±70	1376	±137	1040	±15	1365	±82
X12-3-26	1229	±4	1350	±60	1099	±170				
*NB12**	945	±10	1490	±60	944	±189				
1000 - 7000 years (cal years BP)										
X12-3-47	1133	±6	1720	±60	1234	±175				
X12-3-106	1258	±6	1830	±60	1346	±169				
X12-3-107	1307	±6	1880	±50	1393	±149				
X12-16-9	1623	±7	2110	±60	1647	±204				
*P2**	1685	±5	2190	±70	1739	±212				
X12-D3-1	1979	±9	2480	±70	2088	±214				
*P37**	2342	±7	2670	±60	2321	±248				
*V10**	3066	±12	3310	±100	3097	±281				
X12-D1-6	3234	±11	3340	±70	3136	±234				
X12-D1-4	3295	±12	3380	±70	3192	±232				
*P26**	3531	±11	3690	±80	3561	±238				
X12-D2-1	3742	±13	3810	±60	3710	±218				
*P43**	3802	±17	4010	±90	3975	±299				

*P38**	4978	±14	4880	±70	5129	±261				
*P11**	5068	±15	4920	±80	5175	±270				
V39*	5951	±13	5360	±90	5694	±222				
V24*	5955	±13	5480	±80	5810	±221				
*V30**	5979	±13	5460	±90	5792	±232	5525	±20	5861	±147
V13*	6020	±12	5710	±100	6073	±252				
V2*	6051	±14	5710	±90	6074	±223				
*V8**	6073	±18	5780	±80	6145	±211				
*V28**	6350	±13	5060	±90	5369	±264				
*V33**	6593	±13	4900	±90	5151	±280	5120	±20	5439	±131
*V11**	6878	±15	6360	±90	6788	±273				

* ^{14}C age shown are averages, rounded to the nearest decade

[a] Samples italicized were originally published in *Cobb et al.* 2003b and *Cobb et al.* 2013.

[b] Errors quoted are 2σ.

[c] ^{14}C ages were calibrated to calendar years using Calib7.1 software [*Stuiver et al.*, 2005] and Marine13 calibration datasets [*Reimer et al.*, 2013] and corrected for a local reservoir age using ΔR of 39 ±56 [*McGregor et al.*, 2011]. The ^{14}C calibrated age is reported as the median probability. Calibrated ^{14}C errors are 2σ.

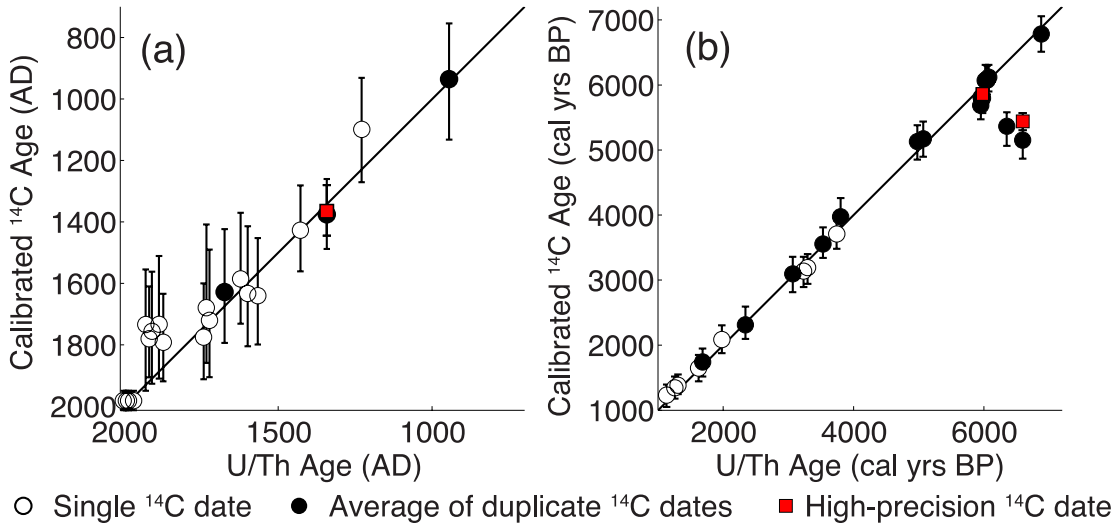

Figure 2.2 U/Th and calibrated ^{14}C fossil coral dates plotted for a) the last millennium (in years AD) and b) 1000 – 7000 cal yrs BP. Open circles represent samples with only one rapid-screen ^{14}C date; black circles represent the average of multiple rapid-screen ^{14}C dates using replicate samples from the same coral. The median probability of the calibrated rapid-screen ^{14}C date is plotted with error bars representing the 2σ age range. The 2σ error bars for U/Th dates are smaller than the symbol size. Calibrated high-precision ^{14}C-AMS dates are plotted as red squares.

Additionally, samples that dated post-bomb with the rapid-screen ^{14}C dating method were confirmed with U/Th dates to be younger than 1950 AD. All age-concordant samples contain no detectable calcite (<0.5%), as determined using XRD.

Rapid-screen ^{14}C ages from two mid-Holocene samples, V28 and V33, are 17% and 25% younger, respectively, than the corresponding U/Th ages. Published U/Th ages for V28 and V33 are 6350 ±13 and 6593 ±13 cal yrs BP, respectively [*Cobb et al.*, 2013], whereas the calibrated rapid-screen ^{14}C ages fall between 5057-5585 cal yrs BP for V28 and 4867-5427 cal yrs BP for V33. Duplicate analyses of the rapid-screen ^{14}C ages from these samples agree with our initial ^{14}C ages within error (see Table A-S1). One high-precision ^{14}C-AMS age from sample V33 also falls within error of the rapid-screen ^{14}C ages. However, duplicate U/Th ages from V28 and V33 differ by 3% and 5%, respectively, from the published results (see Table A-S2), indicative of small-scale heterogeneity in U/Th chemistries in these samples. Subsequent XRD analysis confirms that V28 and V33 contain 15% and 23% calcite, respectively, indicating substantial post-depositional alteration of the primary aragonitic skeleton and signaling open system geochemical behavior. The $\delta^{234}U_{initial}$ values for both V28 and V33 reflect seawater $\delta^{234}U$ values within error, illustrating the limitations of ^{234}U initial as a screening tool for open system behavior in young corals [*Chen et al.*, 1991; *Gallup et al.*, 2002; *Cutler et al.*, 2003; *Henderson*, 2002; *Zaunbrecher et al.*, 2010].

2.4.3 Effect of secondary calcite on ^{14}C and U/Th ages

In an effort to reconcile the discrepancies between the measured ^{14}C and U/Th ages for fossil corals V28 and V33, we use a mass balance model to estimate the effect

that continuous replacement of aragonite to calcite has on ^{14}C and U/Th ages (Figure 2.3). The model is calculated using the following mass balance equation:

$$A_m = A_T * (1 - C) + (T * C)$$

where A_m is the measured age, A_T is the true age, C is the percent calcite and T is the time at which alteration occurs. The equation is solved iteratively for true age for both ^{14}C and U/Th systems, beginning with 100% aragonite at the time of formation (true age) and ending with 15% and 23% calcite, respectively, at 1950 AD (pre-bomb). While we acknowledge that a continuous replacement of aragonite to calcite over-simplifies the diagenetic history of these samples, our approach provides a means of roughly quantifying potential diagenetic effects on the radiometric dating systematics for these two samples. For ^{14}C ages, we use the uncalibrated, rapid-screen ^{14}C ages as inputs into the model and calibrate the resulting estimates of modeled ^{14}C ages for comparison with the corals' estimates of true U/Th ages (Figure 2.4). While V33 has a high-precision ^{14}C age that would ideally provide a better input to our model, the chemical leaching performed as part of sample preparation for graphitization likely removed some of the secondary phases of interest [*Santos et al.*, 2004]. For U/Th, we only model the ages measured by P. Grothe since that is the sample for which we have XRD analyses.

The continuous replacement of aragonite to calcite has the effect of adding ^{14}C to the coral skeleton through time, making our measured ^{14}C ages 900-1500yrs younger than the estimated modeled age. Fossil coral V28's uncalibrated modeled ^{14}C age is 5950 ±90 yrs BP, or 893 years older than the measured rapid-screen ^{14}C age, while V33's corrected modeled ^{14}C age is 6360 ±100 yrs BP, or 1493 years older than the measured

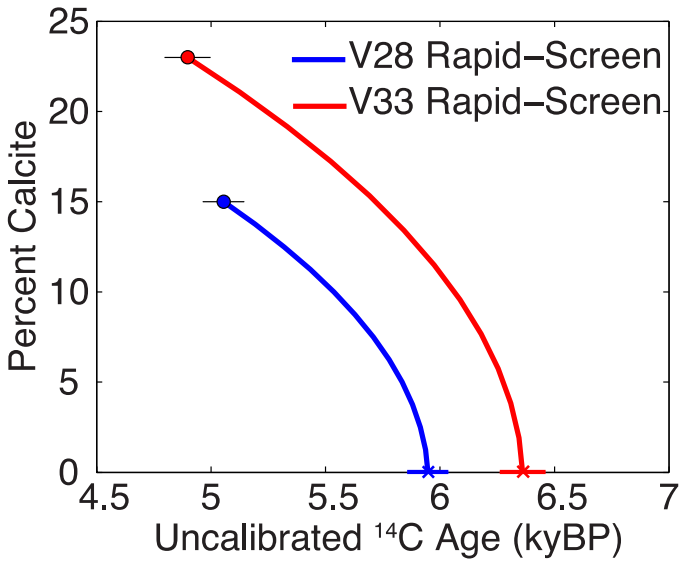

Figure 2.3 Mass balance model of coral ^{14}C ages assuming continuous replacement of aragonite to calcite, for V28 (rapid-screen ^{14}C date – blue solid line) and V33 (rapid-screen ^{14}C date – red solid line), assuming 15 and 23% calcite, respectively. Dates plotted are for uncalibrated ^{14}C dates. Note 2σ error bars on the high-precision date are smaller than the symbol size.

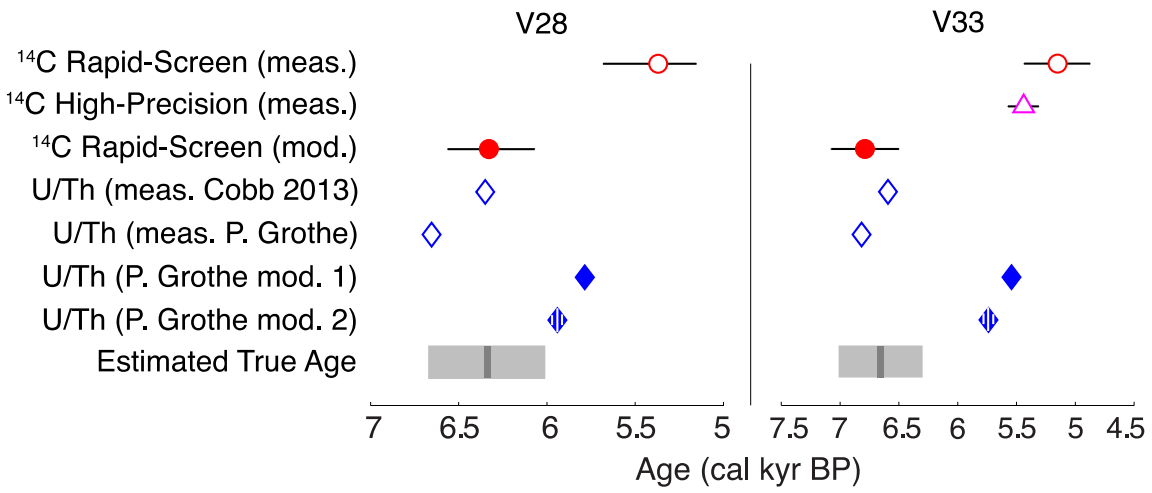

Figure 2.4 Measured and modeled ages for all coral U/Th dates and calibrated ^{14}C dates. Error bars (2σ) are shown for all calibrated ^{14}C dates but are smaller than the symbol for the U/Th dates. Measured dates are plotted as open symbols and modeled dates are plotted as closed symbols, with circles for rapid-screen ^{14}C dates, triangles for high-precision ^{14}C dates, and diamonds for U/Th dates. The modeled 1 (mod. 1) U/Th date (solid blue diamond) represents no U incorporation into the calcite whereas the modeled 2 (mod. 2) U/Th date (blue diamond with white stripes) represents 19% of the U loss being incorporated into the calcite. The dark gray vertical line represents our estimate true age with gray boxes denoting errors bars that are 50% of the original difference between the measured ^{14}C and U/Th dates.

rapid-screen ^{14}C age. Our model does not account for changes in atmospheric $\Delta^{14}C$ through time because incorporating such variations results in age differences that are smaller than the stated uncertainties on our modeled ages. When we calibrate the modeled ^{14}C ages, the dates range from 6096 – 6588 cal yrs BP (median probability 6329 cal yrs BP) for V28 and 6503 – 7087 cal yrs BP (median probability 6789 cal yrs BP) for V33. The calibrated modeled ^{14}C ages agree with one of the two measured U/Th dates for V28 and both of the measured U/Th dates for V33. One of the measured U/Th dates for V28 is older than the calibrated modeled ^{14}C age, implying that U loss may have occurred heterogeneously in the sample.

We apply the same continuous calcite replacement model to investigate potential impacts on the samples' U/Th ages, assuming that the modeled U/Th ages will be younger owing to U loss during recrystallization [e.g. *Henderson et al.*, 1993; *Shen and Dunbar*, 1995; *Scholz et al.*, 2004; *Scholz and Mangini*, 2007]. Here, we assume that 15% and 23% of V28's and V33's aragonite has dissolved and reprecipitated as calcite, respectively, mobilizing the soluble U but not the immobile Th [*Chen et al.*, 1991]. Experimental estimates for U distribution coefficients (D) in calcite range from ~$8x10^{-3}$ for biotic processes [*Russell et al.*, 1994] to 0.19 for abiotic processes [*Kitano and Oomori*, 1971; *Meece and Benninger*, 1993; *Reeder et al.*, 2001; *Heberling et al.*, 2008]. If we assume that no U is incorporated into the calcite after aragonite dissolution (i.e. equivalent to 15 and 23% U loss), then V28's modeled age estimate is 5785 cal yrs BP and V33 is 5543 cal yrs BP (Figure 4) – roughly 900 and 1300 yrs younger than the measured ages, respectively. Assuming that up to ~19% of the aragonite-derived U may be reincorporated into the calcite (i.e. equivalent to D=0.19), then the samples would

have experienced 12% and 19% U loss (modeled as 12% and 19% calcite), with modeled U/Th age estimates of 5941 cal yrs BP and 5739 cal yrs BP, respectively (Figure 2.4). Both modeled U/Th age estimates for V28 and V33 are older than the measured ^{14}C ages but younger than the corrected ^{14}C ages using the same model.

To obtain a best estimate of the true ages of our diagenetically altered samples, we take the median of the modeled ^{14}C ages, the modeled U/Th ages assuming 19% of the aragonite-derived U is reincorporated into the calcite, and both measured U/Th dates. This choice reflects the fact that there is mixed evidence for U loss during diagenesis in these samples – three of the four measured U/Th dates agree with the modeled rapid-screen ^{14}C dates. By assigning 1σ error bars that are at least 50% of the original difference between the measured ^{14}C and U/Th dates, we estimate true ages to be 6340 ±325 (1σ) cal yrs BP for V28 and 6690 ±345 (1σ) cal yrs BP for V33 (Figure 2.4; see Table A-S3).

2.4.4 Age Distribution of fossil coral rubble on Kiritimati Island

The rapid-screen ^{14}C and U/Th dating analyses of 106 undated fossil coral samples yielded a first-order chrono-map of the coral rubble fields across Kiritimati Island. Forty-four of these samples were randomly screened for XRD analysis to detect the presence of diagenetic calcite. Of these, only one sample had a detectable amount of calcite (>0.5%), with a Rietveld refinement estimate of ~15 weight %. We thus conclude that the vast majority of fossil coral samples we collected on the rubble beaches at Kiritimati Island are well preserved with respect to calcite recrystallization.

Our results show that the fossil coral dates cluster by site whereby older samples (2000-6000 cal yrs BP) originate from sites in and around the town of London and younger samples (<3000 cal yrs BP) occur along the windward sites including the Bay of Wrecks (Figure 2.5). Coral ages progressively get older farther back from the waterline (as documented at FS-1, FS-3, FS-13, FS-24, and FS-25, see Table A-S4), indicative of storm-derived deposits [*Richmond and Morton*, 2007]. At fossil coral collection site FS-1, samples collected just behind the intertidal zone date within a narrow range of 20 to 63 cal yrs BP (N=3). Along a well-defined ridgeline roughly 17m from the waterline at site FS-24, fossil corals date in a relatively narrow range between 808 to 940 cal yrs BP (N=3). Moving even farther inland at the same site to a ridge ~80m from the waterline, samples date across a wide range of 1870 and 3163 cal yrs BP (N=3).

2.5 Discussion

Concordant rapid-screen ^{14}C and U/Th dates from 42 of the 44 corals analyzed suggest the rapid-screen ^{14}C dating method, when combined with XRD, is an accurate method for dating fossil corals from the last 7000 years. However, most of our rapid-screen ^{14}C dates are associated with uncertainties on the order of several hundred years (2σ). The magnitude of this uncertainty is largely independent on the sample's age, as it derives from uncertainties in the ^{14}C blank subtraction, which is arbitrarily set at ±50% [*Bush et al.*, 2013]. These large uncertainties are prohibitive for some applications, particularly reconstructions of climate during the last millennium [e.g. *Kuhnert et al.*, 2002; *Cobb et al.*, 2003b; *Holland et al.*, 2014], but are relatively modest for samples from the early- to mid-Holocene.

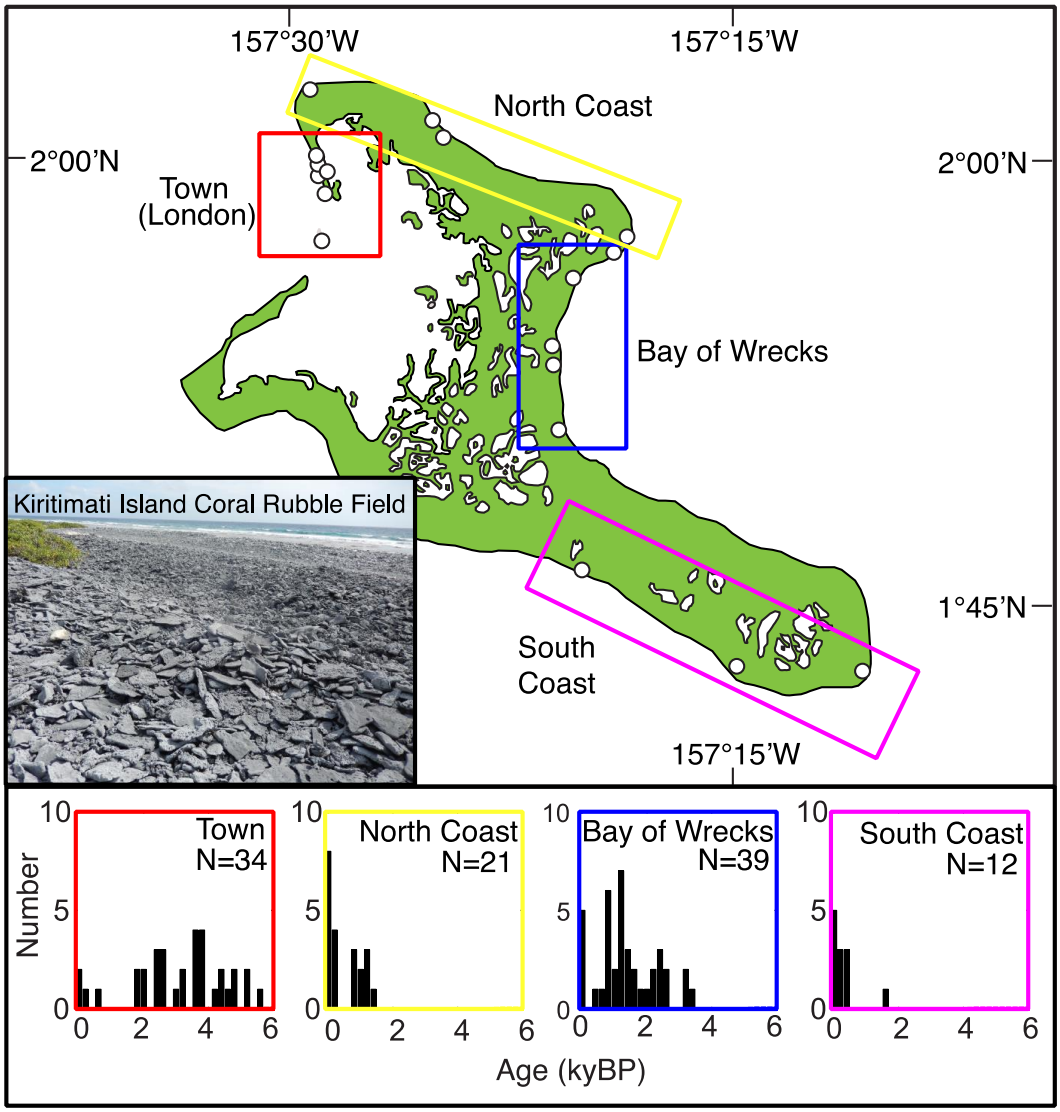

Figure 2.5 Age distributions of fossil coral samples collected on ocean-facing beaches at Kiritimati Island. Sites are grouped into four regions – the town, the north coast, the Bay of Wrecks and the south coast. Histograms were computed using bins of 200 years. For samples that have both rapid-screen ^{14}C and U/Th dates, only the U/Th date is represented as it has the lowest uncertainty. Inset is a fossil coral rubble field seen on Kiritimati Island. The ridgelines of fossil coral rubble are characteristic of the rubble fields along the windward side of the island.

Variations in ΔR on centennial to millennial timescale in the Line Islands may explain some differences in concordant ^{14}C and U/Th ages, particularly where the ^{14}C points cluster above and below the one-to-one line at 5000 and 5900 cal yrs BP. Some studies using paired ^{14}C and U/Th dates for ΔR calculations do find significant variations in ΔR during the mid-Holocene in the tropical Pacific [*Yu et al.*, 2010; *McGregor et al.*, 2008; *Hua et al.*, 2015], most likely due to changes in the ^{14}C content of upwelled water and/or variations in ocean circulation [*Hua et al.*, 2015]. However, without additional paired high-precision ^{14}C and U/Th ages and sample replication to assure against diagenetic influences on our derived ΔR estimates, we cannot provide robust new constraints on ΔR from our study. It is important to note that variations on ΔR cannot explain the large age discrepancies in V28 and V33.

Rapid-screen ^{14}C ages from five samples that grew between 1950 and ~1800 AD are consistently older than the corresponding U/Th ages, though still within 2σ errors. This consistent offset likely derives from a prolonged plateau in the ^{14}C calibration curve from ~1800-1950 AD that causes calibrated ^{14}C dates of samples that formed during this time to be slightly biased towards older ages [*Stuiver et al.,* 1998; *Taylor and Bar-Yosef,* 2014].

Two discordant ^{14}C and U/Th ages from samples with moderate calcite recrystallization (15-30%) illustrate the profound effect that diagenesis can have on the accuracy of coral radiometric ages. The measured ^{14}C ages from the altered samples have diagenetically-derived age offsets that are 3-4 times larger than analytical error. Assuming a continuous replacement of aragonite to calcite for a sample 7000 years old, as little as 2% of recrystallized calcite can change a coral's ^{14}C age by ~1.7%, with

effects increasing with greater calcite contents. Obviously, if any recrystallization occurred in the post-bomb era, then the effect on the measured ^{14}C age would be much larger.

Age biases due to diagenetic alteration can be identified a priori and independently through the application of both XRD and SEM, as we have demonstrated. SEM images of V28 and V33 reveal evidence for some trace carbonate dissolution and precipitation [*Cobb et al.*, 2013], but SEM cannot be used to quantitatively screen fossil corals for radiometric dating. XRD, however, provides a quantitative measurement of the amount of calcite in a sample, allowing us to correct for such age biases, but cannot detect secondary aragonite. Evidence of secondary aragonite crystals on Line Island corals has been observed to varying degrees on modern [*Nurhati et al.*, 2011], last millennium [*Zaunbrecher et al.*, 2010*; Sayani et al.*, 2011], and mid-Holocene corals [*Cobb et al.*, 2013] via SEM, with most containing less than ~1% by weight. We find insignificant age affects with samples containing trace amounts of secondary aragonite, in agreement with *Lazar et al.* [2004]. As a best timesaving practice for radiometric dating, we recommend a priori screening by XRD followed by SEM imaging on samples subsequently chosen for paleoclimate studies.

The convergence of modeled ^{14}C and measured U/Th ages for altered fossil corals using the continuous alteration mass balance model strongly implies that this approach yields reasonable constraints on these two samples' true ages. We assume that calcite is continuously replaced to aragonite, which oversimplifies the true diagenetic history as recrystallization may have occurred episodically [*Cheng et al.*, 1998; *Scholz et al.*, 2004]. The model also assumes an open system behavior when previous other studies suggest

the dissolution and recrystallization could occur in a closed or semi-closed system [*Bathurst*, 1974; *Pingitore*, 1976; *Maliva and Dickson*, 1992], or through simultaneous open and closed-system calcite precipitation [*Rabier et al.*, 2008]. Our assumption that diagenesis is a continuous process echoes similar assumptions made in a suite of other studies that model open-system U/Th systematics in corals [*Bender et al.*, 1979; *Gallup et al.*, 1994; *Thompson et al.*, 2003; *Villemant and Feuillet*, 2003; *Scholz et al.*, 2004]. When our mass balance model is applied to the two altered samples' measured dates, the convergence of corrected rapid-screen ^{14}C and uncorrected U/Th dates implies that only as little as 6-8% U may have been lost from the samples in the course of diagenesis, based on our estimated true ages. Nonetheless, we assign conservative error bars for our estimate of true ages for altered fossil corals, reflecting 50% of the difference between measured ^{14}C and U/Th dates, amounting to errors of roughly ±5% (1σ) for these ~6.4 cal kyr BP corals.

2.6 Conclusion

The rapid-screen ^{14}C dating method provides a quick, inexpensive, and accurate dating method for relatively young (<10,000yr old) carbonate samples with mild alteration (<2%) compared to high-precision ^{14}C and U/Th dating methods. Rapid-screen ^{14}C dating uncertainties amount to ±100-200yrs (2σ) for last millennium-aged samples and ±200-300yrs (2σ) for mid-Holocene-aged samples. However, screening for diagenesis via XRD is necessary as both U/Th and ^{14}C ages are sensitive to calcite recrystallization levels of >2%. ^{14}C ages of altered corals are more sensitive to open system behavior owing to the incorporation of atmospheric ^{14}C during the recrystallization process, and its shorter half-life. We demonstrate that fossil coral U/Th

ages are more robust for Holocene-aged samples exhibiting moderate alteration (10-20%), owing to the relatively long half-lives of U and Th isotopes. Our results show that significant diagenesis-related age discrepancies between rapid-screen ^{14}C and U/Th dates can be reconciled by modeling a continuous aragonite-to-calcite replacement, given XRD estimates of percent calcite in the sample as inputs. Lastly, application of this rapid-screen ^{14}C method to the fossil coral rubble fields from Kiritimati Island reveal significant chronological clustering of fossil corals along pronounced ridgelines, where older ages are found farther from the coastline, consistent with storm-derived origin of the fossil coral deposits.

2.7 Acknowledgements

The data for this paper are provided in Supporting Information Tables 1 and 2. This work was support by NSF grant #0752091 and NOAA grant NA11OAR4310166 to KMC as well NSF #1103403 to RLE and HC and NSF #1029020 to DMD. We would like to acknowledge Jessica L. Conroy, Elizabeth Wiggins, Diane M. Thompson and Lauren T. Toth for their assistance in the field and Lucy C. Taylor and Nathan M. Rabideaux at Georgia State University for their assistance with the XRD analyses. Lastly, we would like to acknowledge three anonymous reviewers in improving the quality of the manuscript.

CHAPTER 3. ROBUST EVIDENCE FOR FORCED CHANGES IN ENSO: FROM THE MID-HOLOCENE TO THE 21ST CENTURY

This article is in prep for *Science*, authored by P.R. Grothe, K.M. Cobb, Giovanni Liguori, Emanuele Di Lorenzo, Antonietta Capotondi, Yanbin Lu, Hai Cheng, R. Lawrence Edwards, John R. Southon, Guaciara M. Santos, Daniel M. Deocampo, Jean Lynch-Stieglitz, Tianran Chen, Hussein R. Sayani, Kayla Townsend, Melat Hagos, Gemma O'Connor, Diane M. Thompson, Lauren T. Toth, and Andrea L. Moore entitled "Robust evidence for forced changes in ENSO: from the mid-Holocene to the 21st century".

3.1 Abstract

The El Niño-Southern Oscillation (ENSO) represents the largest source of year-to-year global climate variability, yet its sensitivity to external climate forcing, whether natural or anthropogenic, is difficult to assess using available data. In this study, we reconstruct the strength of ENSO variability over the last 7,000 years with an ensemble of fossil coral oxygen isotope records from the Line Islands, located in the central equatorial Pacific. The corals document a statistically significant decrease in ENSO variance of ~20% from 3,000 to 5,000 years ago, perhaps related to the timing of spring/fall precessional insolation changes. We find that ENSO variance over the last several decades is 30% larger than pre-industrial ENSO variance, a significant increase that suggests that greenhouse gases may be altering the amplitude, frequency, and/or location of ENSO extremes.

3.2 Main Text

ENSO extremes have a profound impact on temperature and rainfall patterns around the world, driving costly floods and droughts in many regions around the world. The most recent El Niño event, in 2015/16 (Fig. 3.1), caused widespread coral bleaching and mortality across the tropical oceans [*Wake et al.*, 2016]. Improved projections of ENSO's evolution over the next decades are critical to the design of effective adaptation strategies in the face of continued climate change. Climate models project an intensification of ENSO impacts over the next century in response to greenhouse forcing [*Cai et al.*, 2014, 2015], and the recent spate of very strong El Niño events (1982/83, 1997/98, 2015/16) raises the specter that El Niño Southern Oscillation (ENSO) extremes are already changing in response to anthropogenic greenhouse warming. However, the small number of ENSO extremes captured in relatively short instrumental climate records precludes a definitive attribution of recent ENSO activity to anthropogenic climate change.

Reconstructions of past ENSO based on paleoclimate archives provide quantitative estimates of ENSO properties under a variety of natural climate forcing scenarios, serving as out-of-sample tests for climate model simulations of ENSO's response to external climate forcing. Specifically, a suite of theoretical and climate modeling studies [*Clement et al.*, 2000; *Liu et al.*, 2000, *Otter-Bliesner et al.*, 2003, *Timmerman et al.*, 2007, *Zheng et al.*, 2008, *Liu et al.*, 2014] suggest that changes in the amplitude of the seasonal cycle, related to precessional insolation forcing, have a significant effect on ENSO properties. In such studies, the amplitude of the seasonal cycle is inversely proportional to the amplitude of ENSO extremes, predicting a relative

minimum in ENSO variance ~6 thousand years ago (6kyBP), when perihelion occurred during boreal summer. However, while some of the earliest reconstructions of ENSO over the Holocene supported this framework [*Rodbell,* 1999; *Moy et al.,* 2002; *Conroy et al.,* 2008], several recent studies do not show any reduction in ENSO variance during this time [*Koutavas and Joanides,* 2012; *Cobb et al.,* 2013; *Carré et al.,* 2014]. A recent review of available Holocene paleo-ENSO reconstructions from across the tropical Pacific suggests that ENSO may have been somewhat reduced 3-5kyBP [*Emile Geay et al.,* 2016], albeit using a limited dataset. Given the high level of intrinsic variability ascribed to ENSO by both data [*Cobb et al.,* 2013] and models [*Wittenberg,* 2009], the small number of available paleo-ENSO datasets precludes a robust statistical test of potential forced changes in ENSO, whether related to natural or anthropogenic forcing.

Fossil coral records from the central tropical Pacific provide high-fidelity paleo-ENSO reconstructions owing to their location in the heart of the ENSO region, their monthly resolution, and their demonstrated sensitivity to ENSO-related changes in sea surface temperature (SST) [*Cobb et al.,* 2003; *McGregor et al.,* 2013; *Cobb et al.,* 2013]. Indeed, coral oxygen isotopic ($\delta^{18}O$) records from Palmyra (6°N, 162°W), Fanning (4°N, 160°W), and Christmas Island (2°N, 157°W) closely track variations in the NIÑO3.4 SST index (fig. B-S9), a key ENSO metric, as the warm, rainy (cold, dry) conditions that occur during El Niño (La Niña) events drive coral $\delta^{18}O$ lower (higher) [*Cobb et al.,* 2013].

In this study, we present 16 new monthly-resolved fossil coral $\delta^{18}O$ sequences from Christmas Island whose U/Th dates span from 2.5 kyBP to 5.2 kyBP. Modern coral oxygen isotopes from Christmas Island show remarked reproducibility among multiple

sequences and demonstrate high fidelity to local changes in sea surface temperature (SST) as a primary driver of coral $\delta^{18}O$ changes (Fig. 3.2). The new fossil sequences range from 7 years to 26 years in length, for a total of 233 years of new monthly-resolved data [see Supplemental Info, (fig. B-S2), (table B-S2)]. We carefully screen each coral sequence for diagenesis using scanning electron microscopy, X-Ray diffraction, and by testing for concordance between ^{14}C and U/Th dates, following procedures outlined in *Grothe et al.* [2016]. XRD analyses revealed no detectable calcite (<0.5%), while SEM photos revealed evidence of trace to minor alteration characterized by small discontinuous patches of secondary aragonite crystals (<10μm) and/or minor dissolution [see Supplemental Info, (fig. B-S6)]. The coral $\delta^{18}O$ analyses were conducted on powders drilled at 1mm increments, following standard procedures for coral core slabbing and cleaning. Long-term reproducibility for the Thermo-Finnigan Delta V-Kiel at Georgia Tech is better than ±0.07 per mil (1σ, N>1,000).

To assess relative changes in ENSO variance across the Line Islands coral reconstructions, fossil coral interannual variance changes are benchmarked against modern coral interannual variance estimates from the corresponding site. We quantify interannual variance as the standard deviation of 13-month running mean versions of the timeseries, reported as the average standard deviation in sliding 20yr-windows back through time, relative to a 1987 to 2007 reference period. The 20yr window length employed in our analyses is designed to match the length of most fossil coral sequences, though we also repeated our analyses using a range of window lengths [see Supplementary Info, (fig. B-S14)]. The 1987-2007 reference period represents the most

recent period for which modern coral $\delta^{18}O$ data exist from Christmas, Palmyra, and Fanning Islands.

The new coral archive reveals a large range of interannual variance, from –77% roughly 4,200yrs ago to +18% roughly 260yrs ago, well within the range of previously published data from the Line Islands [*Cobb et al.*, 2003]. In any given millennium, interannual variance is highly variable, confirming that a high degree of intrinsic variability is a perennial feature of late-Holocene ENSO, and providing a quantitative benchmark for data-model comparisons. By comparison, changes in ENSO variance over the last 120yrs are relatively muted, ranging from a low of –45% in 1944-1964 to +8% in 1980-2000, relative to the 1987-2007 reference period [see Supplementary Info, (fig. B-S9)].

Over the entire 7,000yr reconstruction, a multi-millennium period centered at 4,000yrs ago stands out as one marked by episodes of dramatically reduced, or perhaps absent, interannual variability (Figure 3.3). Indeed, estimates of interannual variance from 3-5kyBP averages -49% relative to the 1987-2007 benchmark, as compared to -37% in the 5-7kyBP and –30% in the 0-2kyBP intervals.

Given the sparse nature of the coral reconstruction, it is important to test whether the observed patterns of changes in interannual variance reflect real changes in the expression of ENSO, or simply result from under-sampling of a highly variable system. We employ a Monte Carlo analysis wherein we replicate the coral reconstruction as 10,000 psuedocoral reconstructions randomly drawn from two multi-millennium timeseries of simulated ENSO variability. For each psuedocoral dataset, the number and length of the actual coral timeseries is preserved. As null hypotheses of intrinsic ENSO

variability, we use the NINO3.4 timeseries from 1) a statistical model, specifically a linear inverse model (LIM) representing ENSO statistics over a 1958-1997 training period [*Capotondi and Sardeshmukh*, 2017] and 2) a dynamical model, specifically the Last Millennium Ensemble (LME) that contains 10 x 1,000-yr-long simulations of the NCAR-CESM coupled model forced with solar and volcanic radiative perturbations [*Otto-Bleisner et al.*, 2016]. While neither model likely represents the true range of ENSO variance over many millennia, the distribution of interannual variance estimates observed in the pre-industrial coral dataset is consistent with interannual variance distributions in both the LIM and LME [see Supplemental Info, (fig. B-S10)]. We infer that, by choosing two very different types of null hypotheses, we have applied the most stringent test available for identifying potentially forced changes in ENSO variability.

The Monte Carlo significance testing shows that the 3-5kyBP reduction in interannual variance is statistically significant (>99% confidence) for both choices of null hypotheses (Fig. 3.4, A-D). These results add to the growing amount of paleo-ENSO records that show the strongest ENSO reduction around 4kyBP with higher variance in amplitude both before and after the long quiescent period. These archives include both $\delta^{18}O$ records from mollusk shells [*Carré et al.*, 2014] and foraminifera [*Koutavas and Joanides*, 2012] from the eastern tropical Pacific as well as a stalagmite $\delta^{18}O$ record from Borneo [*Chen et al.*, 2016]. Taken together, these independent lines of evidence support a basin-wide reduction in ENSO variance from 3-5kyBP, whether through a decrease in the underlying SST variance and/or a reduction of ENSO-related hydrological variability, rather than a shift in the spatial footprint of ENSO (i.e. *Karamperidou et al.*, 2015].

A prolonged reduction in ENSO variance from 3-5kyBP may reflect a dynamical response to precessional forcing, although a new mechanism is required to explain the timing of the reduction, which aligns with fall/spring insolation rather than summer/winter insolation. In climate models, boreal summer insolation modulates the strength of annual cycle across the equatorial Pacific, driving a marked reduction in ENSO when the annual cycle increases [*Clement et al.*, 2000; *Liu et al.*, 2000; *Zheng et al.*, 2008; *Braconnot et al.*, 2012]. However, the existing data no longer support a 6kyBP reduction in ENSO variance as inferred from paleoclimate modeling studies. Given that El Niño growth rates are the highest in the fall, changes to equatorial insolation during this time may modulate ENSO variance over long millennial timescales [*Karamperidou et al.*, 2015] through as yet unknown dynamical feedbacks in the coupled ocean-atmosphere system. As such, the prolonged change in ENSO variance from 3-5kyBP represents a compelling target for coupled model simulations, with important implications for long-term ENSO prediction. Of course, the observed reduction in ENSO variance from 3-5kyBP may reflect unforced variability in the coupled system, whose long-term behavior, including cross-basin interactions, are poorly constrained.

One striking feature of the new reconstruction is that almost all of the sequences reflect interannual variability that is, on average, roughly 39% lower than the 1987-2007 reference period. In fact, interannual variance over the last 50 years (1966-2016) is significantly higher than the pre-industrial era (quantified using all of the fossil coral data that pre-date 1850), for both choices of null hypotheses (Figure 3.4, E-F). In fact, our analyses reveal a statistically significant increase in interannual variance from the pre-industrial to the modern period whether the latter is defined by the previous 30, 50, or 75

years before 2016 [see Supplemental Info, (fig. B-S12, A-F)]. Interannual variability is relatively high in the early 1900's [see Supplemental Info, (fig. B-S9)], but it is not significantly higher than pre-industrial levels (fig. B-S12, G-H). The modern intensification of interannual variability remains significant even if all 3-5kyBP data are removed from the pre-industrial dataset [see Supplemental Info, (fig. B-S13)]. However, with the removal of the 1997/98 El Niño event from the modern coral dataset, we find no significant increase in recent interannual activity [see Supplemental Info, (fig., B-S14)]. While there is no a priori reason to exclude this record-breaking event from our analysis, this finding does illustrate that we may have only recently exceeded the detection limit for observing an anthropogenic shift in ENSO properties, as measured against long-term ENSO variability.

A growing number of ENSO reconstructions [*Li et al.,* 2013; *Liu et al.,* 2017] and multi-proxy synthesis [*McGregor et al.,* 2013] collectively provide strong empirical support for an anthropogenic increase in ENSO extremes. However, all available ENSO reconstructions, including that presented here, rely to varying degrees on capturing ENSO-related hydrological responses. As such, it is important to keep in mind that these paleo-data may collectively reflect a recent intensification of the atmospheric response to ENSO-related SST anomalies, as projected by climate models in response to rising greenhouse gases [*Power et al.,* 2013; *Cai et al.,* 2015]. Of course, given known deficiencies in the representation of ENSO physics in the current generation of climate models [e.g. *Bellenger et al.,* 2014], such model-data agreement does not exclude the possibility that ENSO-related SST anomalies have intensified in recent decades. In that scenario, whether the SST extremes have increased basin-wide, or only in the central

equatorial Pacific, has profound implications for projections of ENSO impacts in coming decades.

The new coral data document sustained, significant changes in ENSO properties – a weakening from 3-5kyBP potentially linked to spring/fall insolation, and an intensification in the last decades associated with anthropogenic climate change. Both findings find support in a number of recent paleo-ENSO reconstructions, and as such represent high-priority targets for future investigations with numerical climate models. While the chain of dynamical feedbacks responsible for the observed changes in ENSO – past and present - remains unclear, the prospect for larger ENSO extremes under continued greenhouse forcing greatly increases the societal and ecological vulnerabilities to climate change. As such, regional assessments of climate vulnerabilities would do well to incorporate information from paleoclimate studies of climate extremes in order to accurately quantify the risks of continued anthropogenic climate change.

3.3 Acknowledgements

The authors acknowledge the Republic of Kiribati for allowing research activities on Christmas Island through permits provided by the Environment and Conservation Division. P. Grothe received funding for this research through a Sigma Delta Epsilon-Graduate Women in Science fellowship. Data availability: All data and metadata are archived at NCDC (https://www.ncdc.noaa.gov/paleo/study/22415).

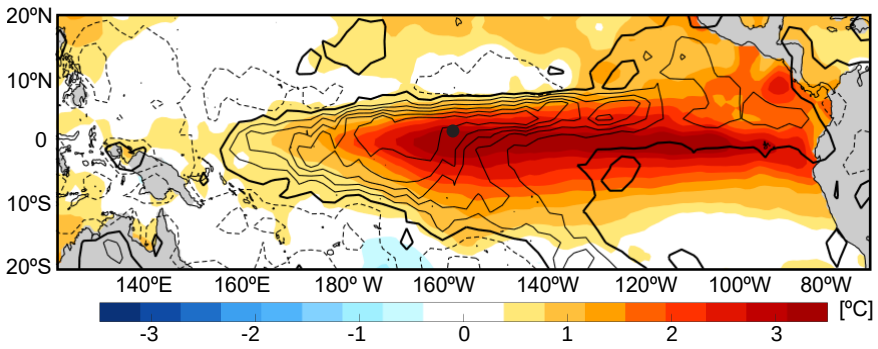

Figure 3.1 SST (color shading)[*Reynolds et al.*, 2002] and precipitation (contours)[*Xie and Arkin*, 1997] anomalies in the tropical Pacific during the peak of the 2015/2016 El Niño event, as represented by November-December-January average. Contour spacing is 2 mm/day and the thick solid line represents the 0 anomaly which separates positive [solid lines] and negative [dashed lines] anomalies. Black dote denotes Christmas Island.

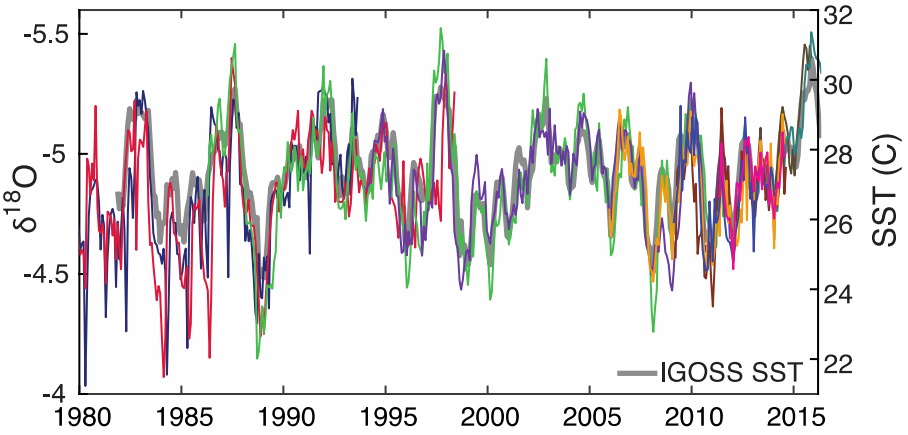

Figure 3.2 Ten monthly-resolved modern coral $\delta^{18}O$ records from Christmas Island plotted with IGOSS SST [*Reynolds et al.*, 2002] from Christmas Island (grey). Each coral record has been shifted by up to 0.15 per mil to match the mean $\delta^{18}O$ values in overlapping intervals of the records (see Supplementary Info; Figure S2). [Corals from left to right: Evans et al., 1999 (navy); Nurhati et al., 2009 (crimson); this study, X12-6 (emerald) and X12-3 (purple); T. Chen, X14-1 (sienna), X14-14 (orange), X14-7 (blue) and X14-9 (hotpink); G. O'Connor, X16-MC1 (brown) and X16-MC2 (teal)].

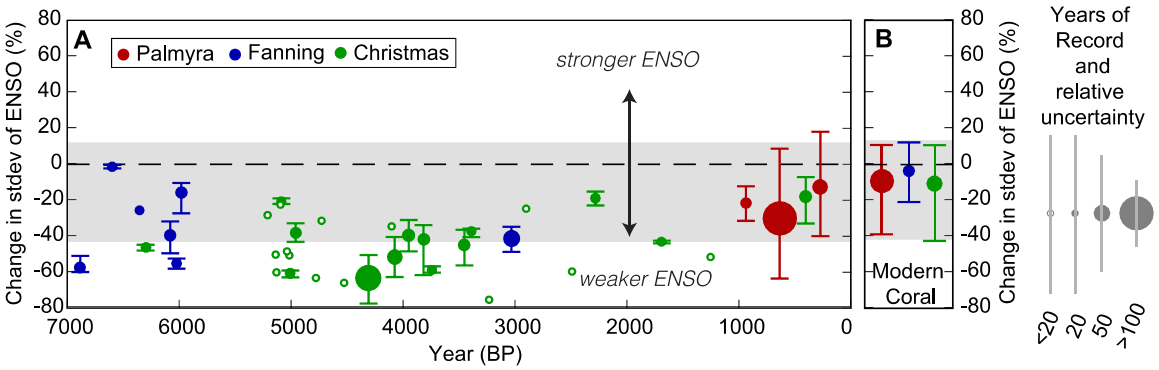

Figure 3.3 Estimates of interannual variability from new and published coral $\delta^{18}O$ records from the Line Islands. A) Relative ENSO variance changes in fossil coral $\delta^{18}O$ calculated from the standard deviation of sliding 20-year windows of monthly coral $\delta^{18}O$ data that was first 10-year high-passed, then 13-month averaged, plotted as the average standard deviation of each coral timeseries relative to the 1987-2007 C.E. intervals of corresponding modern coral $\delta^{18}O$ timeseries from each site (the dashed 'zero' line). Coral data originate from Palmyra (red; Cobb et al., 2003), Fanning (blue; Cobb et al., 2013), and Christmas (green; Cobb et al., 2013; McGregor et al., 2013; this study)]. The bars represent the full range of interannual variability in 20-yr windows of each coral sequence. Coral timeseries of <20 years are plotted with open circles. Coral timeseries from 20 years < length > 320 years are plotted linearly with size where smaller dots are shorter sequences. The gray box denotes the full range of modern ENSO variability in 20yr windows, as reflected in the modern coral variability plotted in (B). Estimates of relative uncertainty (1σ) are based solely on the record length of coral segments, as determined by Monte Carlo sampling of the LIM model [*Capotondi and Sardeshmukh*, 2017]. B) Same as in (A) but for the composite modern coral $\delta^{18}O$ timeseries for each island. Colors as in (A).

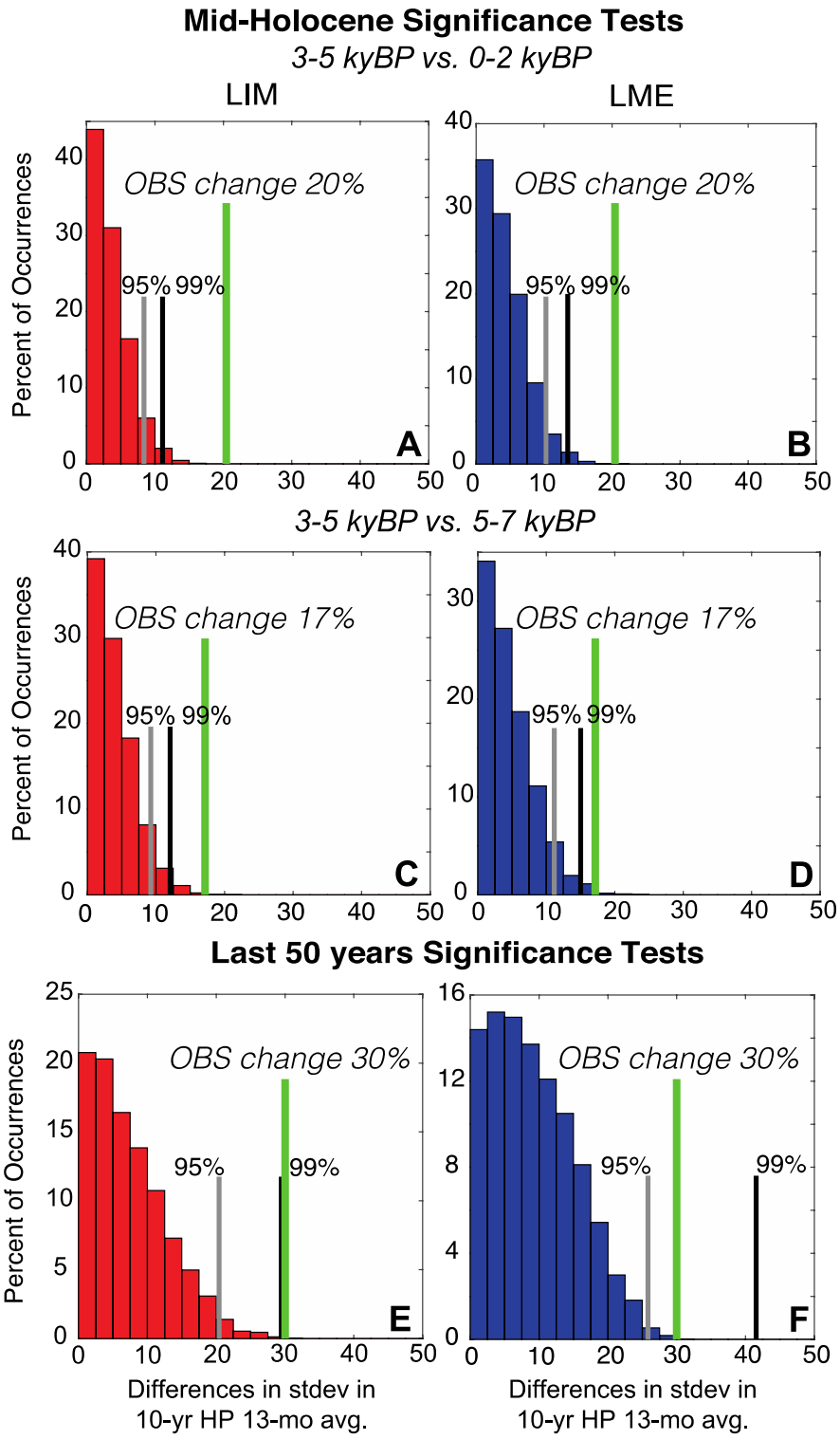

[Caption on following page]

Figure 3.4 Results of significance testing for the observed differences in interannual variability of coral $\delta^{18}O$ over last 7,000yrs. A) Probability density function and significance levels (95%, 99%; gray and black lines, respectively) of differences between interannual variance in 10,000 pseudocoral datasets designed to replicate the segment lengths of the 3-to 5-kyBP Line Islands fossil coral data and the 0- to 2-kyBP fossil coral data, generated from NIÑO3.4 time series from a linear inverse model (LIM) of ENSO [*Capotondi and Sardeshmukh*, 2017]. The observed difference in interannual variance between the 3-5kyBP and 0-2kyBP fossil coral data is denoted by the green line. B) Same as (A) but psuedocoral data are generated from NIÑO3.4 time series from the Last Millennium Ensemble (LME) [*Otto-Bliesner et al.*, 2016]. C) Same as (A) but targeted at the 3-to 5-kyBP versus 5-to 7-kyBP fossil coral data. D) Same as C but pseudocoral data are generated from the LME. E) Same as A) but targeted at the difference between the last 50-years of coral data (1966-2016) versus the entire Line Islands fossil coral dataset, with psuedocoral data generated from the LIM. F) Same as (E) but pseudocoral data generated from the LME.

CHAPTER 4. CONCLUDING REMARKS AND FUTURE RESEARCH

4.1 Concluding Remarks

The El Niño Southern Oscillation is the largest source of extreme weather patterns worldwide, yet our understanding of what drives this climate phenomenon is limited, inhibiting our ability to make more accurate predictions for community preparedness. Three recent extreme El Niño events (1982/83, 1997/98, 2015/16) have fueled much of the research in understanding the driving mechanisms, attempting to make more accurate predictions and identifying different spatial patterns. However, limited instrumental observations that only span reliably back to the 1950's have blinded these efforts since we can not put these extreme events into context of historical events. The goal of this research was to use fossil corals from the central tropical Pacific to reconstruct snapshots of ENSO behavior over the last 7,000 years so that we can place these recent events into context of its range of natural variability.

Previous work from fossil corals began to reveal that modern ENSO is intensified in comparison to the last 7,000 years [*Cobb et al.,* 2013]. However, this work failed to find any evidence for other periods of change during the Holocene that was statistically significant, whereas newer studies were starting to show a reduction in the eastern Pacific during the mid-Holocene from changes in precessional insolation [*Koutavas and Joanides,* 2012; *Carré et al.,* 2014]. One hypothesis for the mismatch between the corals from the central tropical Pacific and the proxy data from the eastern tropical Pacific is

that the spatial footprint of ENSO changed to more central Pacific events [*Karamperidou et al.,* 2015]. My hypothesis, however, was that there was not enough corals dating to the mid-Holocene to detect a change that is statistically significant. This idea is what drove my research direction in attempting to amass significantly more coral data around ~4,000-5,000 years ago.

First, I devised a new approach in using smaller but more numerous fossil coral sequences, as the long pristine sequences that *Cobb et al.* [2013] used are rare to find. In Chapter 2 I address the biggest challenge with using more numerous coral sequences – radiometric dating. I compared a rapid-screen ^{14}C dating method to high precision U/Th dating and illustrated how it allowed us to screen a large number of fossil corals quickly for a relatively inexpensively price, compared to the costly and time-consuming U/Th dating method. Samples that dated in a target time period, such as the mid-Holocene, were then followed by high precision U/Th dating. This approach also allowed screening for secondary calcite on the dating chips as the presence of calcite causes discordant dates.

After screening hundreds of fossil corals, I selected the longest and best-preserved corals that were 2,000 years and older in an attempt to determine if ENSO was reduced during the mid-Holocene, and if so when and how long. Following similar methods from *Cobb et al.* [2013], I found that 3,000-5,000 years ago was the most reduced and that the difference from both periods before and after was statistically significant. Additionally, I found that ENSO was intensified during the late 20th and early 21st century. These results strongly suggest that ENSO is sensitive to external forcing – precessional insolation during the mid-Holocene and anthropogenic greenhouse gases for the modern. This work

provides useful targets for data-model comparisons to further understand the precise mechanisms for such responses.

4.2 Future Work

The next step of this research is to understand how the mean climate state of the tropical Pacific during the Holocene has evolved and how this affects the properties of ENSO. Climate models suggest that ENSO is sensitive to the annual cycle and background climate state [*Jin et al.,* 1994; *Liu et al.,* 2000; *Clement et al.,* 2000; *Fedorov and Philander,* 2001; *Timmerman et al.,* 2007]. Sedimentary SST proxy records from the western tropical Pacific indicate a Holocene-long cooling trend [*Stott et al.,* 2004; *Linsley et al.*; 2010], but there are no Holocene SST records from the central tropical Pacific. Additionally, it's been suggested that changes in precessional insolation have caused hydrological changes throughout the Holocene by changing the position and/or strength of the Intertropical Convergence Zone (ITCZ)[e.g. *Haug et al.,* 2001; *Stott et al.,* 2004; *Dykoski et al.,* 2005]. Coral $\delta^{18}O$ and Sr/Ca measurements (Sr/Ca is an SST-only proxy in corals [*Beck et al.,* 1992]) from Christmas Island fossil corals would provide quantitative constraints on the magnitude of paleo-SST and $\delta^{18}O$ of seawater trends in the central tropical Pacific. This would allow us to assess the influence of the background climate state, both temperature and hydrology, on the properties of ENSO, as well as investigate such connections through data-model intercomparisons.

APPENDIX A. SUPPLEMENTARY MATERIALS FOR "A COMPARISON OF U/TH AND RAPID-SCREEN 14C DATES FROM LINE ISLAND FOSSIL CORALS"

A.1 Introduction

This supporting information provides tables of all the new ^{14}C and U/Th data that were performed as part of this study, the span of dates for samples V28 and V33, as well as GPS coordinates for sites on Kiritimati Island.

Table A-S1 ^{14}C dating results

Sample	Method	Date Run	Fraction Modern[a,b,c]	$\Delta^{14}C$ (‰)[d]	^{14}C age (BP)[e]
NB12	Rapid	Jan 19 2013	0.8235 ± 0.0054	-182.7 ± 3.4	1560 ± 60
NB12	Rapid	Jan 19 2013	0.8421 ± 0.0075	-164.3 ± 4.6	1380 ± 80
P11	Rapid	Jan 19 2013	0.5412 ± 0.0045	-462.9 ± 3.0	4930 ± 70
P11	Rapid	Jan 19 2013	0.5418 ± 0.0044	-462.3 ± 3.3	4920 ± 70
P26	Rapid	Jan 19 2013	0.6324 ± 0.0066	-372.4 ± 3.4	3680 ± 90
P26	Rapid	Jan 19 2013	0.6319 ± 0.0052	-372.9 ± 4.1	3690 ± 70
P38	Rapid	Jan 19 2013	0.5428 ± 0.0042	-461.3 ± 3.4	4910 ± 70
P38	Rapid	Jan 19 2013	0.5467 ± 0.0047	-457.5 ± 3.3	4850 ± 70
V8	Rapid	Jan 19 2013	0.4982 ± 0.0047	-505.6 ± 4.5	5600 ± 80
V8	Rapid	Jan 19 2013	0.4792 ± 0.0043	-524.5 ± 3.1	5910 ± 80
V11	Rapid	Jan 19 2013	0.4492 ± 0.0052	-554.2 ± 3.3	6430 ± 100
V11	Rapid	Jan 19 2013	0.4576 ± 0.0045	-545.9 ± 3.4	6280 ± 80
SB3b	Rapid	Feb 18 2013	0.9177 ± 0.0083	-89.3 ± 8.3	690 ± 80
SB3b	Rapid	Feb 18 2013	0.9176 ± 0.0059	-89.4 ± 5.9	690 ± 60
SB3b	Rapid	Feb 18 2013	0.9071 ± 0.0060	-99.8 ± 6.0	780 ± 60
SB3b	Rapid	Feb 18 2013	0.9205 ± 0.0095	-86.5 ± 9.5	670 ± 90
SB3b	Rapid	Feb 18 2013	0.9147 ± 0.0049	-92.2 ± 4.9	715 ± 45
SB3b	Rapid	Feb 18 2013	0.9126 ± 0.0052	-94.3 ± 5.2	735 ± 50
SB7	Rapid	Feb 18 2013	0.9123 ± 0.0074	-94.6 ± 7.4	740 ± 70
SB7	Rapid	Feb 18 2013	0.8773 ± 0.0053	-129.3 ± 5.3	1050 ± 50
SB7	Rapid	Feb 18 2013	0.8869 ± 0.0063	-119.9 ± 6.3	960 ± 60
SB7	Rapid	Feb 18 2013	0.8829 ± 0.0062	-123.8 ± 6.2	1000 ± 60
SB7	Rapid	Feb 18 2013	0.8787 ± 0.0049	-128.0 ± 4.9	1040 ± 45
SB7	Rapid	Feb 18 2013	0.8775 ± 0.0050	-129.2 ± 5.0	1050 ± 50
NB12	Rapid	Feb 18 2013	0.8298 ± 0.0050	-176.5 ± 5.0	1500 ± 50
NB12	Rapid	Feb 18 2013	0.8312 ± 0.0085	-175.1 ± 8.5	1490 ± 90
NB12	Rapid	Feb 18 2013	0.8332 ± 0.0069	-173.1 ± 6.9	1470 ± 70
NB12	Rapid	Feb 18 2013	0.8349 ± 0.0061	-171.4 ± 6.1	1450 ± 60
NB12	Rapid	Feb 18 2013	0.8252 ± 0.0046	-181.1 ± 4.6	1545 ± 45
NB12	Rapid	Feb 18 2013	0.8312 ± 0.0048	-175.1 ± 4.8	1485 ± 50
V30	Rapid	Feb 18 2013	0.4971 ± 0.0052	-506.7 ± 5.2	5610 ± 90
V30	Rapid	Feb 18 2013	0.5033 ± 0.0066	-500.5 ± 6.6	5510 ± 110
V30	Rapid	Feb 18 2013	0.5037 ± 0.0062	-500.1 ± 6.2	5510 ± 100
V30	Rapid	Feb 18 2013	0.5160 ± 0.0058	-487.9 ± 5.8	5310 ± 90
V30	Rapid	Feb 18 2013	0.5132 ± 0.0055	-490.7 ± 5.5	5360 ± 90
V30	Rapid	Feb 18 2013	0.5058 ± 0.0052	-498.1 ± 5.2	5480 ± 90
V33	Rapid	Feb 18 2013	0.5287 ± 0.0056	-475.3 ± 5.6	5120 ± 90
V33	Rapid	Feb 18 2013	0.5387 ± 0.0064	-465.4 ± 6.4	4970 ± 100
V33	Rapid	Feb 18 2013	0.5559 ± 0.0049	-448.3 ± 4.9	4720 ± 80
V33	Rapid	Feb 18 2013	0.5385 ± 0.0060	-465.6 ± 6.0	4970 ± 100

V33	Rapid	Feb 18 2013	0.5403	±	0.0059	-463.8	±	5.9	4950	± 90
V33	Rapid	Feb 18 2013	0.5596	±	0.0047	-444.6	±	4.7	4660	± 70
SB7	High-prec.	Mar 1 2013	0.8787	±	0.0012	-128.0	±	1.2	1040	± 15
V30	High-prec.	Mar 1 2013	0.5027	±	0.0010	-501.1	±	1.0	5525	± 20
V33	High-prec.	Mar 6 2013	0.5288	±	0.0012	-457.3	±	1.2	5120	± 20
P2 EXT	Rapid	Apr 03 2013	0.7705	±	0.0055	-235.3	±	5.5	2090	± 60
P2 INT	Rapid	Apr 03 2013	0.7519	±	0.0070	-253.8	±	7.0	2290	± 80
P11 EXT	Rapid	Apr 03 2013	0.5373	±	0.0064	-466.8	±	6.4	4990	± 100
P11 INT	Rapid	Apr 03 2013	0.5478	±	0.0049	-456.3	±	4.9	4830	± 80
P37 EXT	Rapid	Apr 03 2013	0.7262	±	0.0053	-279.3	±	5.3	2570	± 60
P37 INT	Rapid	Apr 03 2013	0.7089	±	0.0052	-296.5	±	5.2	2760	± 60
P43 EXT	Rapid	Apr 03 2013	0.6051	±	0.0055	-399.5	±	5.5	4040	± 80
P43 INT	Rapid	Apr 03 2013	0.6094	±	0.0063	-395.3	±	6.3	3980	± 90
V10	Rapid	Apr 03 2013	0.6676	±	0.0068	-337.4	±	6.8	3250	± 90
V10	Rapid	Apr 03 2013	0.6580	±	0.0074	-347.0	±	7.4	3360	± 100
V13	Rapid	Apr 03 2013	0.4883	±	0.0063	-515.4	±	6.3	5760	± 110
V13	Rapid	Apr 03 2013	0.4948	±	0.0051	-509.0	±	5.1	5650	± 90
V28	Rapid	Apr 03 2013	0.5337	±	0.0050	-470.3	±	5.0	5040	± 80
V28	Rapid	Apr 03 2013	0.5322	±	0.0057	-471.8	±	5.7	5070	± 90
V2	Rapid	Apr 03 2013	0.4924	±	0.0051	-511.3	±	5.1	5690	± 90
V2	Rapid	Apr 03 2013	0.4900	±	0.0050	-513.7	±	5.0	5730	± 90
V24	Rapid	Apr 03 2013	0.5044	±	0.0047	-499.5	±	4.7	5500	± 80
V24	Rapid	Apr 03 2013	0.5070	±	0.0047	-496.8	±	4.7	5460	± 80
V39	Rapid	Apr 03 2013	0.5140	±	0.0049	-489.9	±	4.9	5350	± 80
V39	Rapid	Apr 03 2013	0.5129	±	0.0053	-491.0	±	5.3	5360	± 90
X12-FS1-8	Rapid	Apr 03 2013	0.9246	±	0.0080	-82.4	±	8.0	630	± 70
X12-FS1-11	Rapid	Apr 03 2013	0.9274	±	0.0063	-79.6	±	6.3	610	± 60
X12-FS1-19	Rapid	Apr 03 2013	0.9241	±	0.0058	-83.0	±	5.8	630	± 60
X12-FS3-2	Rapid	Apr 03 2013	1.0709	±	0.0074	62.8	±	7.4	-540	± 60
X12-FS3-23	Rapid	Apr 03 2013	0.8884	±	0.0057	-118.3	±	5.7	950	± 60
X12-FS3-26	Rapid	Apr 03 2013	0.8455	±	0.0058	-160.9	±	5.8	1350	± 60
X12-FS3-106	Rapid	Apr 03 2013	0.7962	±	0.0054	-209.9	±	5.4	1830	± 60
X12-FS3-47	Rapid	Apr 03 2013	0.8076	±	0.0056	-198.5	±	5.6	1720	± 60
X12-FS3-107	Rapid	Apr 03 2013	0.7916	±	0.0045	-214.4	±	4.5	1875	± 50
X12-FS4-111	Rapid	Apr 03 2013	1.0254	±	0.0095	17.6	±	9.54	-190	± 80
X12-FS4-113	Rapid	Apr 03 2013	0.9606	±	0.0053	-46.7	±	5.30	325	± 45
X12-FS4-117	Rapid	Apr 03 2013	1.1095	±	0.0056	101.0	±	5.60	-830	± 45
X12-FS6-34	Rapid	Apr 03 2013	1.0651	±	0.0054	57.0	±	5.41	-500	± 45
X12-FS6-74	Rapid	Apr 03 2013	1.0823	±	0.0056	74.1	±	5.59	-630	± 45
X12-FS6-75	Rapid	Apr 03 2013	0.9200	±	0.0069	-86.9	±	6.87	670	± 60
X12-FS9-5	Rapid	Apr 03 2013	1.0760	±	0.0065	67.8	±	6.49	-585	± 50
X12-FS9-6	Rapid	Apr 03 2013	0.9299	±	0.0050	-77.1	±	5.04	585	± 45
X12-FS9-10	Rapid	Apr 03 2013	1.0954	±	0.0053	87.1	±	5.34	-725	± 40

X12-FS13-5	Rapid	Apr 03 2013	0.9165	±	0.0052	-90.5	±	5.22	700	± 50
X12-FS13-8	Rapid	Apr 03 2013	0.9289	±	0.0058	-78.1	±	5.77	590	± 50
X12-FS13-11	Rapid	Apr 03 2013	0.9426	±	0.0051	-64.6	±	5.07	475	± 45
X12-FS13-19	Rapid	Apr 03 2013	0.9317	±	0.0057	-75.4	±	5.72	570	± 50
X12-FS13-28	Rapid	Apr 03 2013	1.0978	±	0.0070	89.5	±	6.99	-740	± 60
X12-FS13-32	Rapid	Apr 03 2013	1.0943	±	0.0059	85.9	±	5.86	-720	± 45
X12-FS15-6	Rapid	Apr 03 2013	0.9425	±	0.0054	-64.7	±	5.43	475	± 50
X12-FS15-7	Rapid	Apr 03 2013	1.0928	±	0.0053	84.5	±	5.34	-710	± 40
X12-FS15-10	Rapid	Apr 03 2013	0.9199	±	0.0050	-87.0	±	5.05	670	± 45
X12-FS16-1	Rapid	Apr 03 2013	0.9093	±	0.0061	-97.6	±	6.05	760	± 60
X12-FS16-6	Rapid	Apr 03 2013	0.9153	±	0.0069	-91.6	±	6.94	710	± 70
X12-FS16-9	Rapid	Apr 03 2013	0.7693	±	0.0050	-236.5	±	5.00	2110	± 60
X12-FSD1-4	Rapid	Apr 03 2013	0.6563	±	0.0055	-348.7	±	5.53	3380	± 70
X12-FSD1-6	Rapid	Apr 03 2013	0.6599	±	0.0054	-345.1	±	5.37	3340	± 70
X12-FSD2-1	Rapid	Apr 03 2013	0.6222	±	0.0046	-382.5	±	4.57	3810	± 60
X12-FSD2-3	Rapid	Apr 03 2013	0.9239	±	0.0067	-83.1	±	6.67	640	± 60
X12-FSD3-1	Rapid	Apr 03 2013	0.7344	±	0.0055	-271.1	±	5.54	2480	± 70
X12-FSD6-1	Rapid	Apr 03 2013	1.1038	±	0.0054	95.4	±	5.38	-790	± 40
X13-FS1-8	Rapid	Nov 13 2013	0.8035	±	0.0040	-202.6	±	4.0	1755	± 45
X13-FS1-9	Rapid	Nov 13 2013	0.7864	±	0.0049	-219.5	±	4.9	1930	± 55
X13-FS1-12	Rapid	Nov 13 2013	0.7123	±	0.0058	-293.1	±	5.8	2720	± 70
X13-FS1-1	Rapid	Nov 13 2013	0.7066	±	0.0052	-298.7	±	5.2	2790	± 60
X13-FS1-38	Rapid	Nov 13 2013	0.7040	±	0.0048	-301.3	±	4.8	2820	± 60
X13-FS3-18	Rapid	Nov 13 2013	0.8281	±	0.0067	-178.1	±	6.7	1510	± 70
X13-FS3-23	Rapid	Nov 13 2013	0.8535	±	0.0063	-153.0	±	6.3	1270	± 60
X13-FS3-25	Rapid	Nov 13 2013	0.7753	±	0.0046	-230.6	±	4.6	2045	± 50
X13-FS3-41	Rapid	Nov 13 2013	0.8334	±	0.0051	-172.9	±	5.1	1465	± 50
X13-FS3-40	Rapid	Nov 13 2013	0.7681	±	0.0065	-237.7	±	6.5	2120	± 70
X13-FS3-43	Rapid	Nov 13 2013	0.8075	±	0.0057	-198.6	±	5.7	1720	± 60
X13-FS3-55	Rapid	Nov 13 2013	0.7199	±	0.0055	-285.6	±	5.5	2640	± 70
X13-FS3-59	Rapid	Nov 13 2013	0.7512	±	0.0058	-254.5	±	5.8	2300	± 70
X13-FS3-50	Rapid	Nov 13 2013	0.6581	±	0.0045	-346.9	±	4.5	3360	± 60
X13-FS3-66	Rapid	Nov 13 2013	0.6527	±	0.0065	-352.3	±	6.5	3430	± 90
X13-FS3-63	Rapid	Nov 13 2013	0.6388	±	0.0062	-366.0	±	6.2	3600	± 80
X13-FS3-65	Rapid	Nov 13 2013	0.6929	±	0.0073	-312.3	±	7.3	2950	± 90
X13-FS17-29	Rapid	Nov 13 2013	0.9208	±	0.0063	-86.2	±	6.3	660	± 60
X13-FS17-12	Rapid	Nov 13 2013	0.9224	±	0.0085	-84.6	±	8.5	650	± 80
X13-FS17-8	Rapid	Nov 13 2013	0.9223	±	0.0079	-84.7	±	7.9	650	± 70
X13-FS24-49	Rapid	Nov 13 2013	0.8374	±	0.0058	-169.0	±	5.8	1430	± 60
X13-FS24-41	Rapid	Nov 13 2013	0.8429	±	0.0060	-163.5	±	6.0	1370	± 60
X13-FS24-42	Rapid	Nov 13 2013	0.8510	±	0.0056	-155.4	±	5.6	1300	± 60
X13-FS24-64	Rapid	Nov 13 2013	0.8199	±	0.0072	-186.3	±	7.2	1590	± 80
X13-FS24-67	Rapid	Nov 13 2013	0.7962	±	0.0048	-209.9	±	4.8	1830	± 50

X13-FS24-72	Rapid	Nov 13 2013	0.8032	±	0.0060	-202.9	±	6.0	1760	± 60
X13-FS25-8	Rapid	Nov 13 2013	0.8999	±	0.0064	-106.9	±	6.4	850	± 60
X13-FS25-11	Rapid	Nov 13 2013	0.7343	±	0.0051	-271.3	±	5.1	2480	± 60
X13-FS25-12	Rapid	Nov 13 2013	0.7169	±	0.0055	-288.6	±	5.5	2670	± 70
X13-FS25-15	Rapid	Nov 13 2013	0.7302	±	0.0067	-275.4	±	6.7	2530	± 80
X13-FS20-3	Rapid	Nov 13 2013	0.8818	±	0.0056	-124.9	±	5.6	1010	± 60
X13-FS20-18	Rapid	Nov 13 2013	0.9681	±	0.0055	-39.2	±	5.5	260	± 50
X13-FS20-22	Rapid	Nov 13 2013	0.7585	±	0.0055	-247.3	±	5.5	2220	± 60
X13-FS20-14	Rapid	Nov 13 2013	0.6956	±	0.0066	-309.7	±	6.6	2920	± 80
X13-FS21-36	Rapid	Nov 13 2013	0.6695	±	0.0051	-335.6	±	5.1	3220	± 70
X13-FS21-45	Rapid	Nov 13 2013	0.5464	±	0.0064	-457.7	±	6.4	4860	± 100
X13-FS21-51	Rapid	Nov 13 2013	0.5976	±	0.0050	-406.9	±	5.0	4140	± 70
X13-FS21-12	Rapid	Nov 13 2013	0.5656	±	0.0049	-438.7	±	4.9	4580	± 70
X13-FS21-50	Rapid	Nov 13 2013	0.6151	±	0.0051	-389.5	±	5.1	3900	± 70
X13-FS21-38	Rapid	Nov 13 2013	0.5842	±	0.0048	-420.3	±	4.8	4320	± 70
X13-FS21-10	Rapid	Nov 13 2013	0.6291	±	0.0048	-375.7	±	4.8	3720	± 70
X13-FS21-28	Rapid	Nov 13 2013	0.6226	±	0.0048	-382.1	±	4.8	3810	± 70
X13-FS21-15	Rapid	Nov 13 2013	0.5421	±	0.0054	-462.0	±	5.4	4920	± 90
X13-FS21-41	Rapid	Nov 13 2013	0.6939	±	0.0050	-311.3	±	5.0	2940	± 60
X13-FS21-14	Rapid	Nov 13 2013	0.5691	±	0.0050	-435.3	±	5.0	4530	± 70
X13-FS21-32	Rapid	Nov 13 2013	0.5869	±	0.0052	-417.6	±	5.2	4280	± 80
X13-FS21-7	Rapid	Nov 13 2013	0.6321	±	0.0050	-372.7	±	5.0	3680	± 70
X13-FS22-1	Rapid	Nov 13 2013	0.7005	±	0.0054	-304.8	±	5.4	2860	± 70
X13-FS22-7	Rapid	Nov 13 2013	0.7582	±	0.0082	-247.5	±	8.2	2220	± 90
X13-FS22-14	Rapid	Nov 13 2013	0.6289	±	0.0053	-375.9	±	5.3	3730	± 70
X13-FS22-11	Rapid	Nov 13 2013	0.6282	±	0.0051	-376.6	±	5.1	3730	± 70
X13-FS22-8	Rapid	Nov 13 2013	0.5173	±	0.0049	-486.6	±	4.9	5290	± 80
X13-FS1-3	Rapid	Nov 13 2013	0.9357	±	0.0085	-71.4	±	8.5	530	± 80
X13-FS27-2	Rapid	Nov 14 2013	0.5606	±	0.0049	-439.4	±	4.9	4650	± 80
X13-FS3-28	Rapid	Nov 14 2013	0.8003	±	0.0054	-199.7	±	5.4	1790	± 60
X13-FS3-32	Rapid	Nov 14 2013	0.8047	±	0.0044	-195.3	±	4.4	1745	± 45
X13-FS3-33	Rapid	Nov 14 2013	0.8152	±	0.0051	-184.8	±	5.1	1640	± 60
X13-FS24-6	Rapid	Nov 14 2013	0.8406	±	0.0055	-159.4	±	5.5	1390	± 60
X13-FS24-7	Rapid	Nov 14 2013	0.8378	±	0.0043	-162.2	±	4.3	1420	± 45
X13-FS24-59	Rapid	Nov 14 2013	0.8184	±	0.0044	-181.6	±	4.4	1610	± 45

[a] Radiocarbon concentrations are given as fractions of the Modern standard, $\Delta^{14}C$, and conventional radiocarbon age, following the conventions of Stuiver and Polach [*Radiocarbon*, v. 19, p.355, 1977].

[b] Sample preparation backgrounds have been subtracted, based on measurements of ^{14}C-free speleothem.

[c] All results have been corrected for isotopic fractionation according to the conventions of Stuiver and Polach [1977], with $\delta^{13}C$ values measured on prepared graphite using the AMS spectrometer. These can differ from $\delta^{13}C$ of the original material, if fractionation ocurred during sample graphitization or the AMS measurement, and are not shown.

[d] $\Delta^{14}C$ follows conventions of Stuiver and Polach [*Radiocarbon*, v. 19, p.355, 1977].

[e] The errors are 1σ. B.P. stands for "Before Present" where the "Present" is defined as the year 1950 A.D

Table A-S2 U/Th dating results

Sample	^{238}U (ppb)[a]		^{232}Th (ppt)		$^{230}Th/^{232}Th$ (atomic x 10^6)		$\delta^{234}U$ (measured)		$^{230}Th/^{238}U$ (activity)[b]		^{230}Th Age (yr) (uncorrected)		^{230}Th Age (yr) (corrected)		$\delta^{234}U_{initial}$ (corrected)[c]		^{230}Th Age (yr BP) (corrected)[d,e]	
D6-1	2052	±3	3	±2	3215	±2190	148.0	±1.8	0.00029	±0.00003	28	±3	28	±3	148	±2	-35	±3
D6-1	2557	±3	9	±3	1234	±406	146.3	±1.6	0.00027	±0.00003	26	±3	26	±3	146	±2	-37	±3
9-10	3001	±4	6	±3	1940	±1126	147.9	±1.7	0.00022	±0.00003	21	±3	20	±3	148	±2	-43	±3
3-2	2038	±3	170	±4	26	±7	147.5	±1.9	0.00013	±0.00004	13	±3	10	±4	148	±2	-53	±4
4-111	2513	±4	6	±2	3148	±1124	146.5	±1.7	0.00046	±0.00003	44	±3	44	±3	147	±2	-19	±3
13-19	2546	±3	41	±2	1504	±88	144.4	±1.6	0.00147	±0.00003	140	±3	140	±3	144	±2	77	±3
9-6	2426	±3	5	±2	8102	±3503	145.0	±1.8	0.00099	±0.00003	94	±3	94	±3	145	±2	31	±3
13-8	2038	±2	4	±5	26270	±39152	145.0	±1.6	0.00284	±0.00005	271	±5	271	±5	145	±2	208	±5
1-11	2405	±4	4	±3	9805	±5935	146.9	±1.9	0.00108	±0.00003	103	±3	103	±3	147	±2	40	±3
1-19	2370	±3	26	±2	1304	±119	145.5	±1.7	0.00087	±0.00003	83	±3	83	±3	146	±2	20	±3
1-8	1818	±2	18	±2	2234	±302	146.1	±1.4	0.0013	±0.0000	127	±4	126	±4	146	±1	63	±4
D2-3	2210	±3	24	±2	4688	±432	144.0	±1.5	0.0030	±0.0000	291	±4	290	±4	144	±1	227	±4
6-75	2199	±3	2	±3	69472	±130873	144.1	±1.7	0.0029	±0.0000	280	±4	280	±4	144	±2	217	±4
13-5	2325	±3	7	±2	25176	±7505	146.0	±1.6	0.0047	±0.0000	447	±4	447	±4	146	±2	384	±4
16-6	2276	±4	44	±3	3720	±224	144.3	±1.8	0.0043	±0.0001	414	±5	414	±5	144	±2	351	±5
16-1	2354	±3	17	±18	9485	±10114	144.9	±1.8	0.0041	±0.0001	391	±5	391	±5	145	±2	328	±5
3-23	2183	±3	28	±2	7861	±645	143.7	±1.8	0.0061	±0.0001	585	±5	585	±5	144	±2	522	±5
3-26	2405	±4	11	±2	30545	±6888	145.4	±2.0	0.0082	±0.0000	784	±4	784	±4	146	±2	721	±4
W13	2251	±3	10	±2	27800	±5411	145.5	±1.6	0.0078	±0.0001	746	±5	746	±5	146	±2	683	±5
2-32	2147	±2	28	±2	17716	±1343	144.5	±1.5	0.0139	±0.0001	1329	±6	1328	±6	145	±2	1265	±6
3-47	2282	±4	40	±3	11754	±785	143.2	±2.1	0.0125	±0.0001	1197	±6	1196	±6	144	±2	1133	±6
3-106	2125	±3	5	±3	91232	±58086	144.5	±1.9	0.0138	±0.0001	1321	±7	1321	±7	145	±2	1258	±7
3-107	2153	±3	8	±2	64527	±19046	142.7	±1.9	0.0143	±0.0001	1370	±6	1370	±6	143	±2	1307	±6
3-107	2178	±3	3	±3	190273	±223710	145.9	±1.7	0.0143	±0.0001	1369	±6	1369	±6	146	±2	1306	±6

16-9	2471	±3	6	±5	130016	±127034	144.2	±1.6	0.0176	±0.0001	1686	±7	1686	±7	145	±2	1623	±7
3-32	2537	±4	3	±2	3764	±3220	145.6	±1.8	0.00023	±0.00002	22	±2	22	±2	146	±2	-41	±2
3-27	2346	±3	44	±3	8308	±492	145.2	±1.5	0.0094	±0.0001	896	±5	895	±5	146	±2	832	±5
3-34	2218	±3	30	±2	11270	±768	144.7	±1.8	0.0093	±0.0000	888	±4	887	±4	145	±2	824	±4
3-39	2321	±3	75	±3	5016	±172	142.3	±1.5	0.0098	±0.0000	936	±4	936	±4	143	±2	873	±4
3-42	2098	±3	28	±2	11245	±906	144.8	±1.5	0.0090	±0.0000	864	±5	864	±5	145	±2	801	±5
D3-1	2334	±3	3	±3	275450	±285646	144.8	±1.7	0.0212	±0.0001	2042	±9	2042	±9	146	±2	1979	±9
D1-6	2244	±3	3	±2	431730	±335552	144.5	±1.7	0.0341	±0.0001	3297	±11	3297	±11	146	±2	3234	±11
D1-4	2728	±5	28	±3	55124	±4995	143.9	±1.9	0.0347	±0.0001	3358	±12	3358	±12	145	±2	3295	±12
D2-1	2384	±4	7	±2	208139	±57507	141.3	±1.8	0.0392	±0.0001	3805	±13	3805	±13	143	±2	3742	±13
D2-2	254	±0	0	±0	360355	±210502	144.6	±1.7	0.0404	±0.0001	3917	±13	3917	±13	146	±2	3854	±13
D2-5	2306	±3	16	±2	61919	±8689	144.1	±1.5	0.0265	±0.0001	2554	±8	2554	±8	145	±2	2491	±8
D4-3	2497	±4	9	±2	117912	±30210	143.4	±1.8	0.0257	±0.0001	2475	±8	2475	±8	144	±2	2412	±8
D2-7	1072	±1	19	±122	21106	±138972	144.6	±1.6	0.0221	±0.0001	2129	±9	2129	±10	146	±2	2066	±10
D2-6	2380	±4	2	±2	446265	±471471	143.5	±1.7	0.0256	±0.0001	2464	±8	2464	±8	145	±2	2401	±8
P11	2472	±4	17	±3	126352	±21847	142.6	±1.8	0.0526	±0.0001	5138	±16	5138	±16	145	±2	5075	±16
P11	2737	±4	10	±2	234586	±54052	141.7	±1.6	0.0524	±0.0001	5124	±14	5124	±14	144	±2	5061	±14
V33	1959	±3	97	±3	23353	±771	143.2	±1.7	0.0700	±0.0002	6882	±21	6881	±21	146	±2	6818	±21
V28	1981	±3	13	±2	176645	±28384	143.7	±1.6	0.0684	±0.0001	6717	±18	6717	±18	146	±2	6654	±18

[a] The errors reported in this table are quoted as 2σ. B.P. stands for "Before Present" where the "Present" is defined as the year 1950 A.D. For [^{238}U] error is for last significant figure.

[b] The measured, uncorrected (^{230}Th/^{238}U)activity ratio; 2σ error is for last significant figure.

[c] δ^{234}Uinitial was calculated based on ^{230}Th age (T), i.e., δ^{234}Uinitial = δ^{234}Umeasured x $e^{\lambda 234}$xT.δ^{234}U was calculated from the following formula: $\delta^{234}U = ([^{234}U/^{238}U]\text{activity} - 1)\text{x}1000$.

[d] Calculations were used with the following U and Th decay constants: $\lambda^{238} = 1.55125\text{x}10^{-10}$ [*Jaffey et al.*, 1971], $\lambda^{234} = 2.82206\text{x}10^{-6}$ [*Cheng et al.*, 2013], and $\lambda^{230} = 9.1705\text{x}10^{-6}$ [*Cheng et al.*, 2013].

[e] Corrected ^{230}Th ages assume the initial ^{230}Th/^{232}Th atomic ratio of 4.4 ±2.2 x10^{-6}. Those are the values for a material at secular equilibrium, with the bulk earth ^{232}Th/^{238}U value of 3.8.

Table A-S3 Measured and modeled dates for samples V28 and V33[a]

	V28		V33	
^{14}C measured - rapid-screen	5369	+216/-312	5151	+276/-284
^{14}C measured - high-precision	-	-	5439	+127/-134
^{14}C corrected	6329	+259/-233	6789	+289/-286
U/Th measured - Cobb et al., 2013	6350	±13	6593	±13
U/Th measured - P. Grothe	6654	±18	6818	±21
U/Th corrected - 15 and 23% U loss	5785	±18	5543	±21
U/Th corrected - 12 and 18.4% U loss	5941	±18	5739	±21
Estimated Age	6330	±325	6600	±345

[a] All ages reported as 'cal yrs BP'

Table A-S4 GPS coordinates for sample collection sites on Kiritimati Island

Site Number	Latitude	Longitude
FS-1	01.8640500°	157.3447500°
FS-3	01.9352833°	157.3331500°
FS-4	01.9660667°	157.3020667°
FS-6	02.0393500°	157.4252167°
FS-9	02.0439500°	157.4921333°
FS-13	01.7676500°	157.3377500°
FS-15	01.7229333°	157.2607667°
FS-16	1.6978167°	157.1733833°
FS-17	1.963898°	157.30321°
FS-20	2.0079833°	157.4846500°
FS-21	2.00079°	157.48595°
FS-22	2.01171°	157.48595°
FS-24	2.0362°	157.42416°
FS-25	1.89891°	157.34573°
FS-27	2.0116167°	157.4845667°
FS-D1	1.9991000°	157.4807667°
FS-D2	1.9876667°	157.4778833°
FS-D3	1.9943167°	157.4801000°
FS-D4	2.0026833°	157.4832333°
FS-D6	1.9892500°	157.4706000°

APPENDIX B. SUPPLEMENTARY MATERIALS FOR "ROBUST EVIDENCE FOR FORCED CHANGE IN ENSO: FROM THE MID-HOLOCNE TO THE 21ST CENTURY"

B.1 Materials and Methods

B.1.1 Modern coral processing and construction of composite records

Two cores from living *Porites* corals on Christmas Island were drilled via SCUBA using an underwater compressed air drill in May 2012. One core was collected off the leeward side of the island (X12-3) and the other off the southern shoreline (X12-6)(Fig. B-S1; Table B-S1). Cores were cut into slabs of 1 cm thickness and X-Rayed to view banding and any visual signs of alteration (Fig. B-S2, Plate 1). Transect lines were placed down the primary growth axis and samples were drilled every 1mm to obtain sub-monthly sampling resolution (growth rates 18-19mm/year). Relative chronologies were carefully constructed by tying maximum and minimum $\delta^{18}O$ points to maximum and minimum SST values (from IGOSS SST dataset centered on Christmas Island) within a given year and linearly interpolating in between these tie points. The Christmas Island composite record was constructed by tying end points from several published and unpublished coral sequences together (Fig. B-S3). The final record combines data from *Evans et al.* [1999], *Nurhati et al.* [2009], X12-6 [this study], X14-14 [data provided by T. Chen], and X16-MC1 [data provided by G. O'Connor], providing a continuous record from 1939 to 2016. We accounted for offsets in $\delta^{18}O$ by taking the average from the first

two records where they overlap and adding or subtracting that difference to each of those records. All subsequent records were offset similarly to these two records.

The Palmyra Island composite record utilizes two new cores that were previously drilled by others to extend the *Cobb et al.* [2003] record to 2007 (Fig. B-S4). R. Dunbar provided monthly $\delta^{18}O$ data from a modern Palmyra *Porites* core, which spans 1994-2003. E. Druffel provided core P13 and H. Sayani measured the monthly $\delta^{18}O$ data, providing a record from 1998-2007 [*Sayani et al.,* in prep]. The Palmyra Island composite was similarly constructed as the Christmas Island modern composite but the two new records were adjusted for offsets based on the *Cobb et al.* [2003] record.

B.1.2 Fossil coral processing and chronologies

Fifteen new fossil coral sequences were collected off ocean facing beaches on the leeward side of Christmas Island (GPS coordinates for sites published in *Grothe et al.*, 2016) (Fig. B-S1; Table B-S2). Smaller samples were collected by hand and larger samples were drilled using a Tech2000 hydraulic drilling rig. Samples are labeled 'X' followed by the year collected, then the site location, and then sample number. Samples were similarly processed as the modern cores. They were cut into 1cm thick slabs and sampled at 1mm resolution down the main growth axis as determined by X-Ray imaging (Fig. B-S2, Plates 2-8). Fossil corals were first screened using a low-precision rapid-screen ^{14}C dating method and subsequently dated using high-precision ^{238}U-^{234}U-^{230}Th, with errors of ±0.5-1% 2σ (Table S3), following procedures outlined in *Grothe et al.*, 2016. Relative chronologies were constructed by assigning the maximum $\delta^{18}O$ point for a given year to January 15th and linearly interpolating in between the tie points. Where

maximum $\delta^{18}O$ points were ambiguous, we used the $\delta^{13}C$ timeseries as an additional measure to determine the annual cycle. Consistent growth rates within each coral were maintained for the construction of the chronologies. Relative chronology error within a given sample is approximately two to three months.

B.1.3 Coral Isotopic Analysis

Approximately 100μm of coral powder were drilled every one millimeter down the primary growth axis (see transect lines on Fig. B-S2, plates 1-8) and analyzed for $\delta^{18}O$ and $\delta^{13}C$ using a Thermo Finnigan Finnegan Delta V+ with a Kiel IV Carbonate device located at Georgia Institute of Technology with a precision of 0.07‰. In places where the geochemistry was altered by diagenesis, a secondary transect line was run alongside the original transect line (labeled T2 in Fig. B-S2). Plots of the raw $\delta^{18}O$ are presented in Fig. B-S5.

B.1.4 Screening for diagenesis

Corals were screened for diagenesis using Scanning Electron Microscopy (SEM), X-Ray Diffraction (XRD) and paired ^{14}C and U/Th dates [*Grothe et al., 2016*]. Initial chips taken for dating were first screened using XRD to detect calcite in the sample. All samples chosen for this study had no detectable calcite. In fact, less than 10% of all the samples collected and dated from Christmas Island (n>300) showed no significant calcite (>1%), most likely due to excellent preservation from the dry climate on the island. Samples chosen for this study were subsequently dated using U/Th dating and all dates were concordant with their respective ^{14}C dates, providing confidence that our dates are reliable [*Grothe et al., 2016*]. Small chips of ~5mm by 5mm were taken from multiple

places along each coral for SEM screening (Fig. B-S6). Samples were chosen from top, middle and bottom of each sequence (or top and bottom from smaller sequences) to characterize diagenetic alteration changes throughout the coral. Additionally, chips were taken from locations where the geochemistry suggested diagenetic alteration as well as from spots were large El Niño events were recorded.

B.1.5 Filtering ENSO variance

Since the new coral sequences average 15-years long with the shortest only 7 years, the standard 2-7-year bandpass filter fails as a robust metric for filtering ENSO variability in these short sequences. We compare different methods of filtering ENSO variability using the monthly ERSST v3b NIÑO3.4 time series by comparing it to the 2-7 year bandpass filter. We find that using a 10-year high pass followed by a 13-month moving average captures most of the variance seen in the 2-7-year bandpass filter (correlation coefficient of 0.92) (Fig. B-S7). We apply a 10-year high pass and then 13-month moving average to both the modern and fossil coral records. In Fig. B-S8, we plot both the 2-7-year bandpass filter and the 10-year high pass 13-month moving average on the longest fossil coral sequence (13^{th} century splice from Palmyra) as well as a 5-yr moving average and 9-year low pass to illustrate the strong decadal variability that is removed by using our chosen filter.

In order to compare the data from across the three islands, we apply similar techniques from *Cobb et al.* [2013] where each of the fossil corals are benchmarked to their modern equivalent from a reference period of 1987-2007 and plotted as the percent difference from this period (fig. B-S9). Because many of the fossil coral sequences are less than 20 years long, we chose a 20-yr window to benchmark the fossil corals to, as

this is the shortest interval we can achieve for capturing robust ENSO variance. Coral samples that are less than 20 years long are reflected as open circles in Fig. 3 to denote where we compute the differences in two different length sequences. Our choice of 1987-2007 reflects the most recent 20-yr time period for which we have modern data from all three islands.

B.1.6 Monte Carlo statistical testing of ENSO variance changes

We constructed 'psuedocoral' timeseries from one statistical (LIM) and one dynamical (LME) model in order to assess the statistical significance of the observed ENSO variance difference between the Line Islands fossil and modern corals. The Linear Inverse Model (LIM) is a 20,000-yr long time series of NIÑO3.4 SST constructed using statistics from SST and thermocline depth from 1967-1997 and assumes tropical Pacific climate evolves as a linear, stochastically-forced system [*Capotondi and Sardeshmukh,* 2017]. The LME uses output of the NIÑO3.4 time series from the state-of-the-art Last Millennium Ensemble to construct the LME dataset [*Otto-Bliesner et al.,* 2016]. We string together ten fully forced runs of the NIÑO3.4 time series from 850 to 1850 C.E. for a 10,000-year long timeseries. The runs include transient forcings of solar intensity, volcanic emissions, preindustrial greenhouse gases, aerosols, land-use conditions and orbital conditions.

First, we determine how appropriate our choices of models are and if they are fair substitutions for the fossil coral timeseries. To test this, we generate 10,000 different realizations of the Line Island fossil coral database (N=1,631yrs of data in 38 sequences, ranging in length from 7-318 years each, see Table B-S3), replicating each fossil coral sequence with random segments from model-derived NIÑO3.4 timeseries from the LIM

and LME. The model psuedocoral segments were processed in the same way as the actual fossil coral segments. In Figure S10, we plot the envelope of distributions of the 10-yr high pass and 13-month running mean variance changes for each of the 10,000 psuedocoral databases for both the LIM and LME with the distribution changes for all the fossil coral and find that the fossil coral distribution is consistent with the ENSO variance distribution in both models. We also compare the power spectrum for the 10,000 psuedocoral databases of both the LIM and LME with modern observations from the NINO3.4 SST index, the modern Line Islands coral timeseries and the longest fossil coral sequence, the 320-yr long 13th century splice from Palmyra Island (Figure B-S11).

In order to test whether the observed changes in ENSO variance in the mid-Holocene or the last 50 years are significant or not, we sampled 10,000 sequences of both the LIM and LME data to build psuedocoral subsets that match the actual Line Islands coral data in number and length. We processed the pseudocoral data in the same way as the actual coral data, using a 10-yr high pass and 13-mo running average, and then took the difference between the subsets from the varying time periods in question. We plot the distribution of these psuedocoral differences and denote both the 95% and 99% confidence threshold for significant variance differences. For the mid-Holocene, we chose 3-5kyBP as that is the time period of maximum difference from other millennia.

B.1.7 Sensitivity Testing of the Recent ENSO Intensification

We compute the differences in the last 30, 75 and 100 years of modern coral data with all the fossil coral data (Fig. B-S12, A-F) and find that the significance stays above 95% for both the LIM and LME for all time periods. Though we have no reason to

exclude the data from the mid-Holocene, we also compute the differences for the last 30, 50, 75 and 100 with all the fossil coral data except the sequences that lie within 3-5kyBP in order to test how much of the anthropogenic intensification we see may be driven by the high number of reduced coral sequences during the mid-Holocene (Fig. B-S13). The significance does not decline to less than 95% for both the LIM and LME until the last 100 years of modern coral data are used. As an additional measure, we test the first 50 years of modern coral data [1886-1936] with the entire fossil coral dataset as well as the sequences from 3-5kyBP removed dataset (Fig. B-S14). The observed change is 14% for the former and 8% for the latter, which are not significant.

We also check the significance of the last 50 years of intensification in ENSO variability against our fossil coral data from the last millennium, assuming that climatological conditions during this time were more similar to present than the data in the mid- to late Holocene. The results are similarly significant, with the observed change of 25%, and significance of 99% and 96% for the LIM and LME, respectively (Fig. B-S15).

We perform an additional sensitivity test to see how the extreme 1997/98 event influences the significance in the recent intensification over the last 50 years. We remove the 1997/98 event from the modern coral record and replace it with the climatological average for each month from the last 50 years (Fig. B-S16, A). The observed change is 20%, which drops the significance to 94% using the LIM and 89% using the LME (Fig. B-S14, B-C). If we repeat the analyses with the coral sequences from 3-5kyBP removed, the observed change is 15%, and the significance drops to 86% and 77% for the LIM and LME, respectively (Fig. B-S14, D-E).

To test the influence of our chosen window size on our results, we repeat our analyses using a 50-yr window (Fig. B-S17). The observed change remains the same at 30% with greater than 99% and 95% using the LIM and LME, respectively.

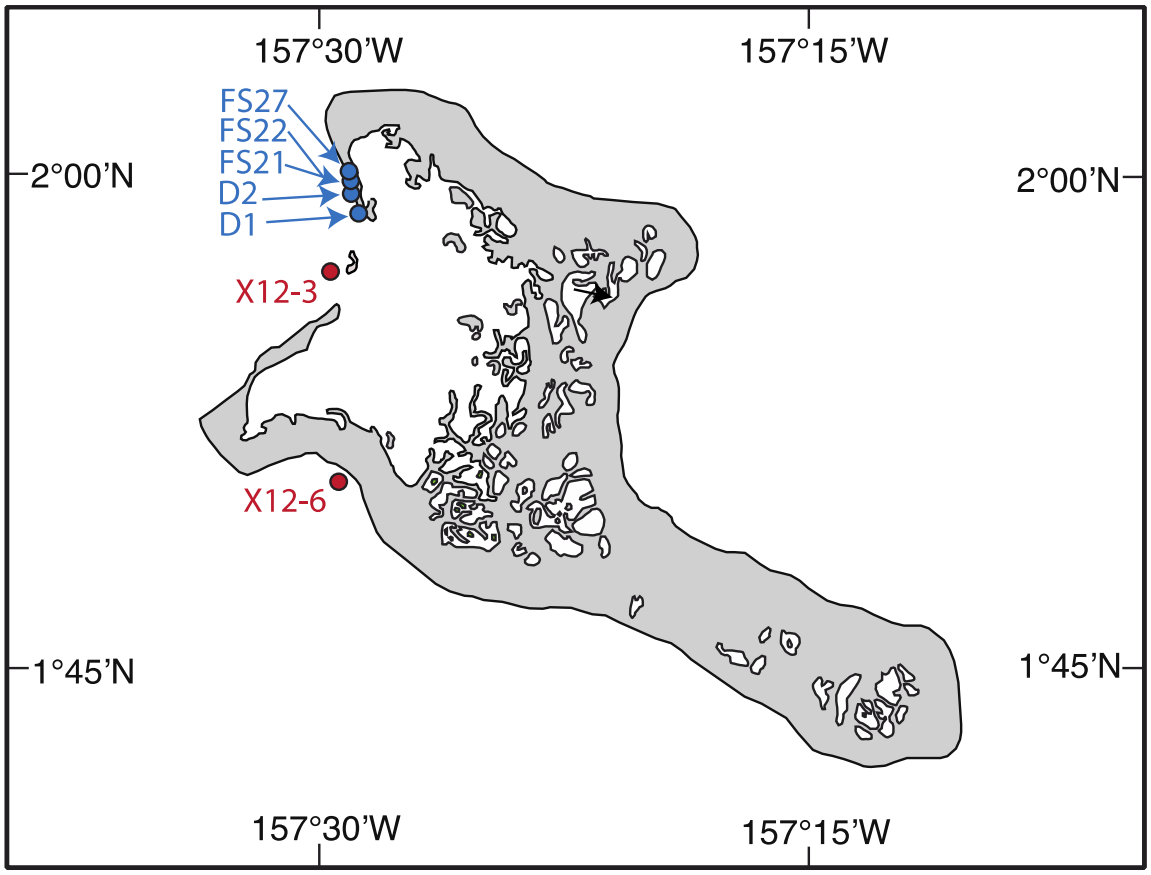

Figure B-S1 Map of Christmas Island with location of the new fossil and modern corals that are presented in this study. Fossil corals are denoted with a blue circle and modern corals with a red circle. GPS coordinates for fossil corals are presented in Grothe et al. [2016]. GPS coordinates for the modern corals are listed in Table B-S1.

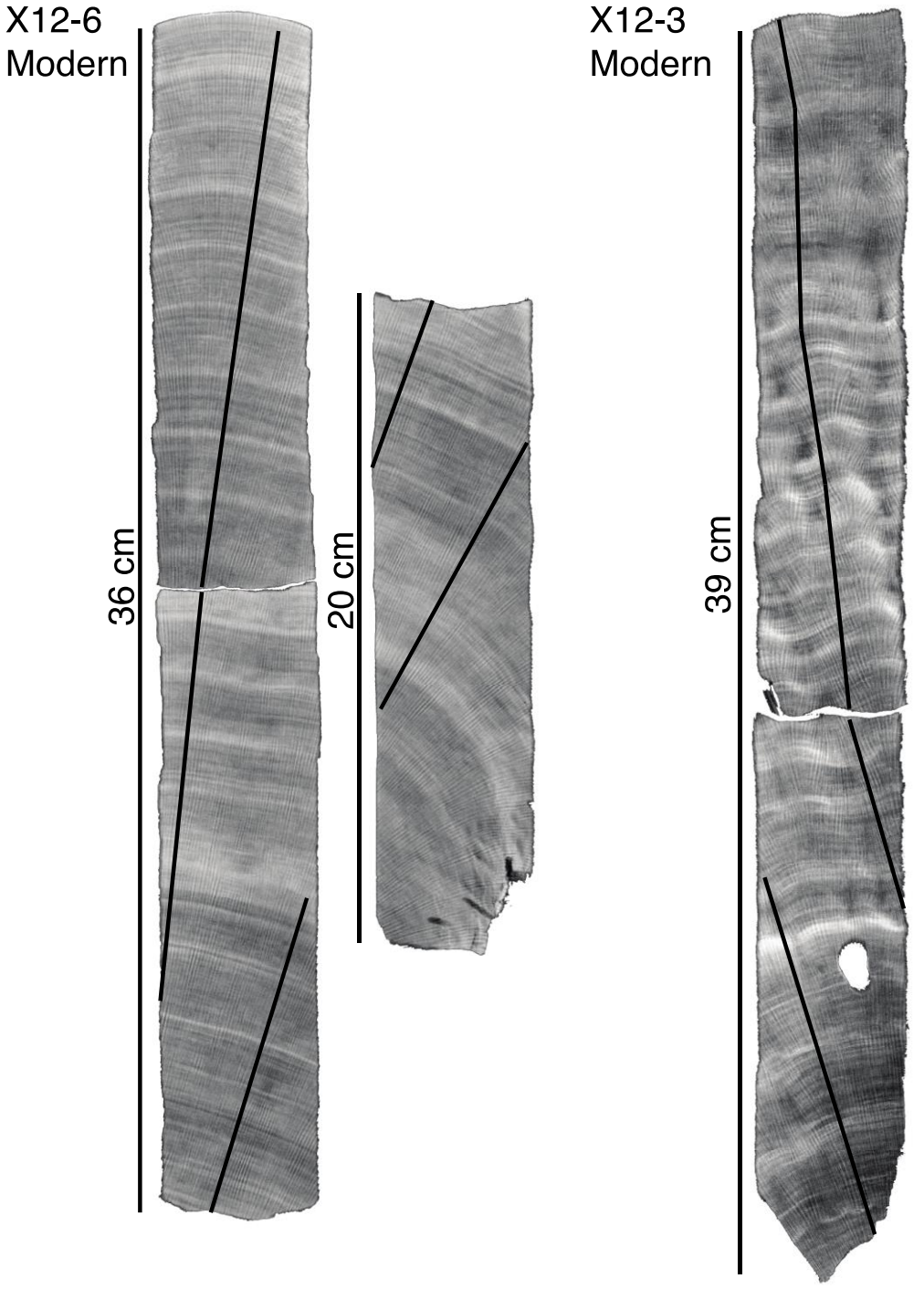

Figure B-S2, Plate 1 X-Ray images with sampling transects of Christmas Island coral. [Full caption under Plate 5.]

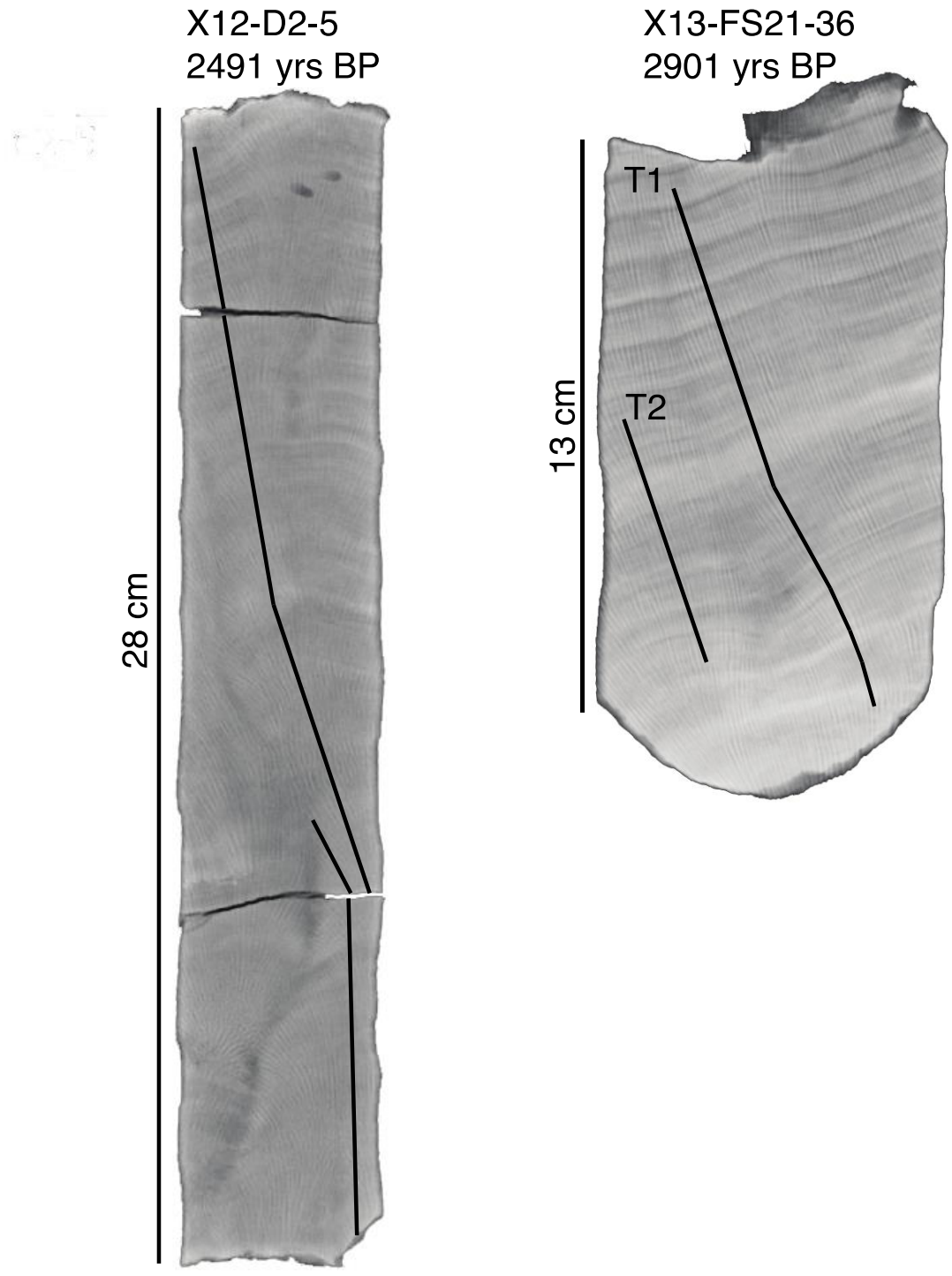

Figure B-S2, **Plate 2** X-Ray images with sampling transects of Christmas Island coral. [Full caption under Plate 5.]

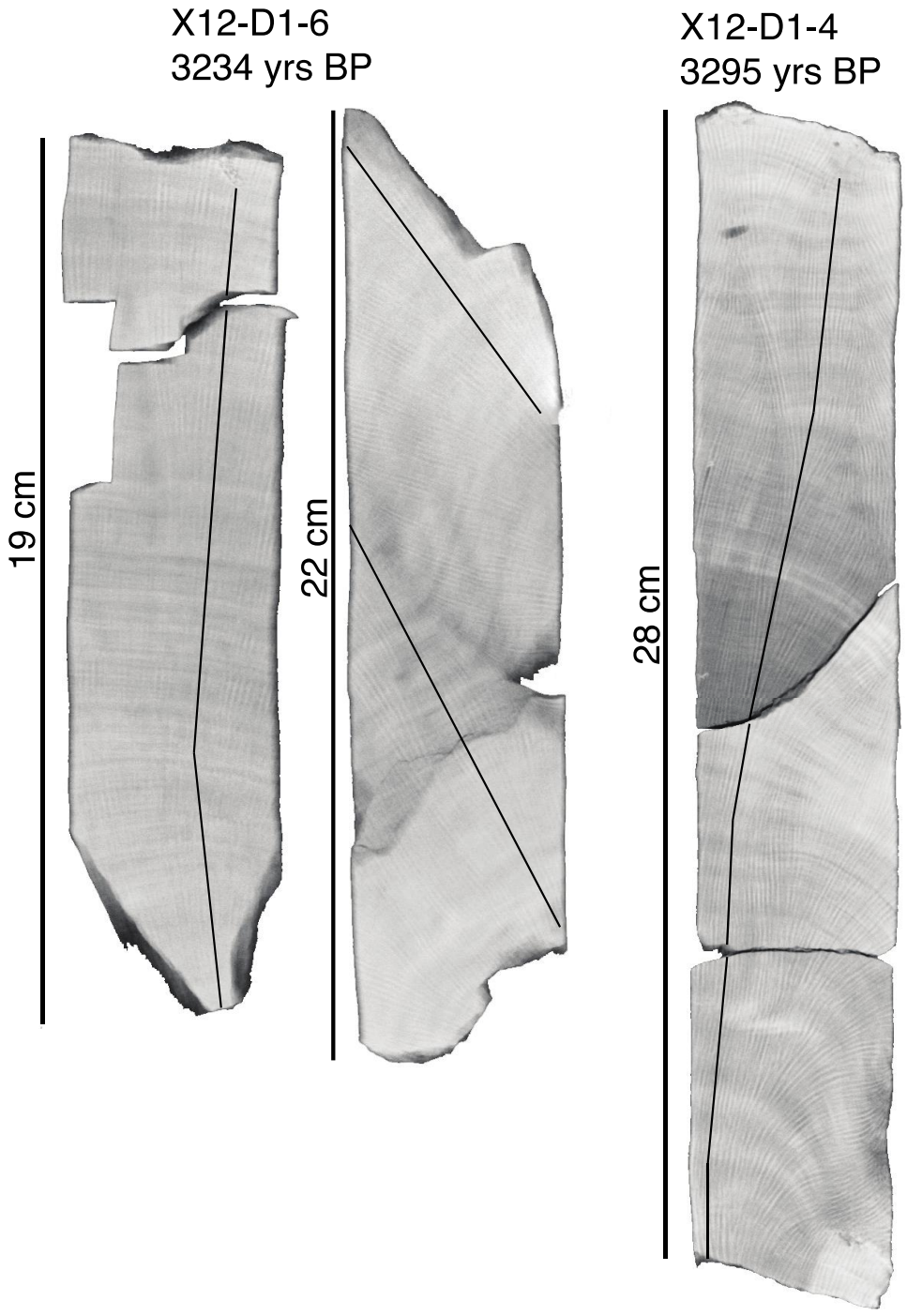

Figure B-S2, Plate 3 X-Ray images with sampling transects of Christmas Island coral. [Full caption under Plate 5.]

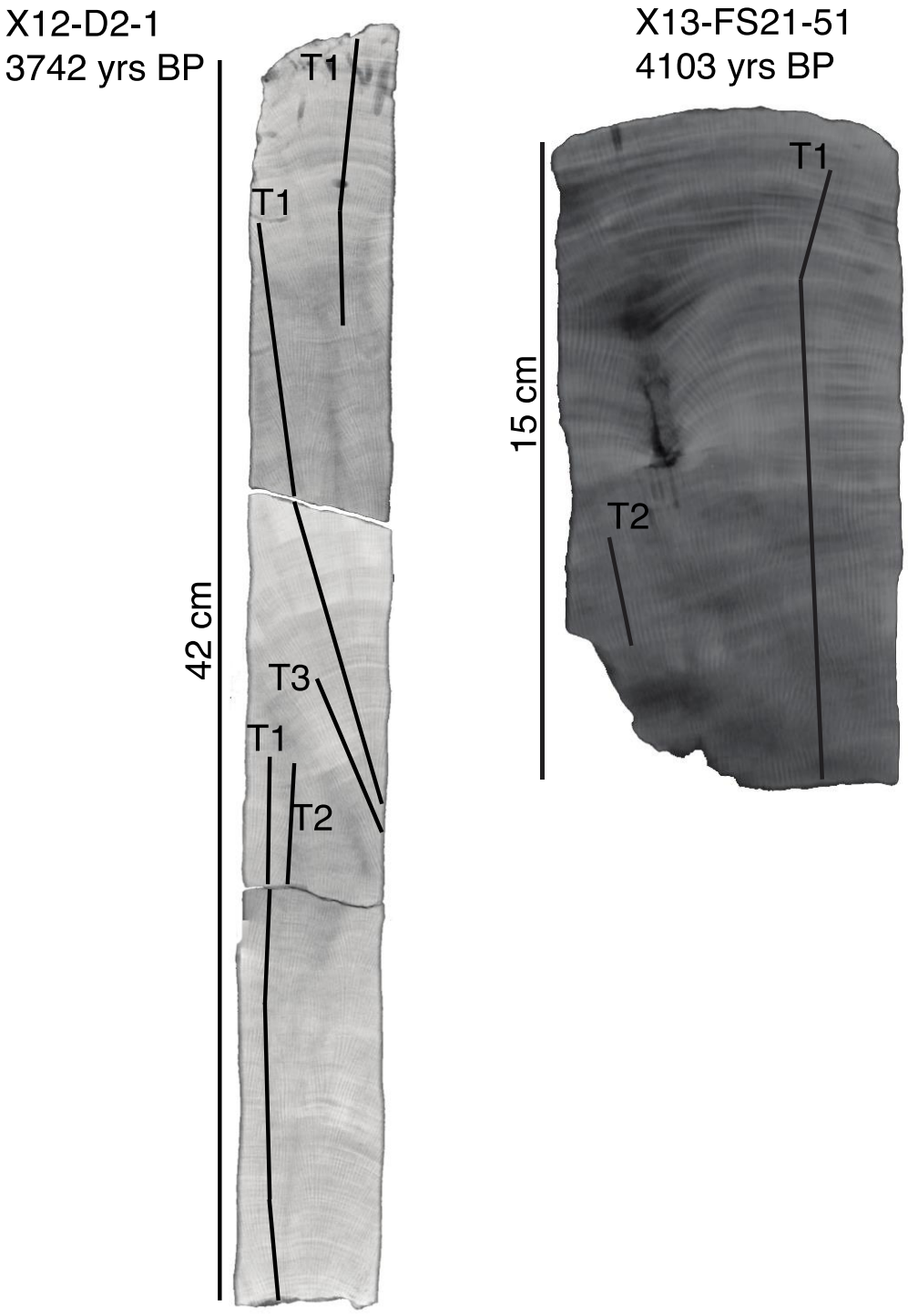

Figure B-S2, Plate 4 X-Ray images with sampling transects of Christmas Island coral. [Full caption under Plate 5.]

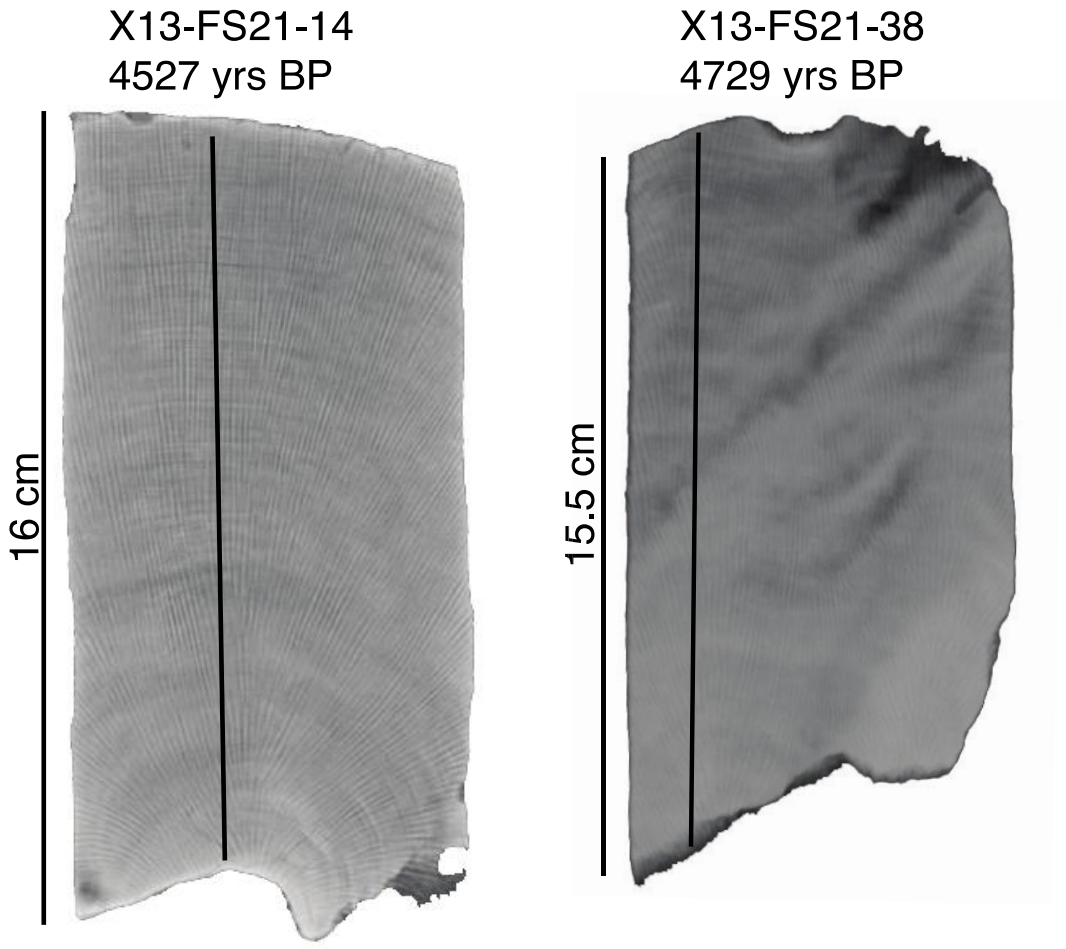

Figure B-S2 Plate 5 X-Ray images with sampling transects of Christmas Island coral.
Plate 1. X12-6 and X12-3 Moderns
Plate 2. X12-D2-5 and X12-FS21-36
Plate 3. X12-D2-1 A and X12-D1-4
Plate 4. X12-D2-1 and X13-FS21-51
Plate 5. X13-FS21-14 and X13-FS21-38
Plate 6. X13-FS27-2 and X13-FS21-15
Plate 7. X13-FS21-40, X13-FS21-22 and X13-FS21-38
Plate 8. X13-FS21-16 and X13-FS22-8

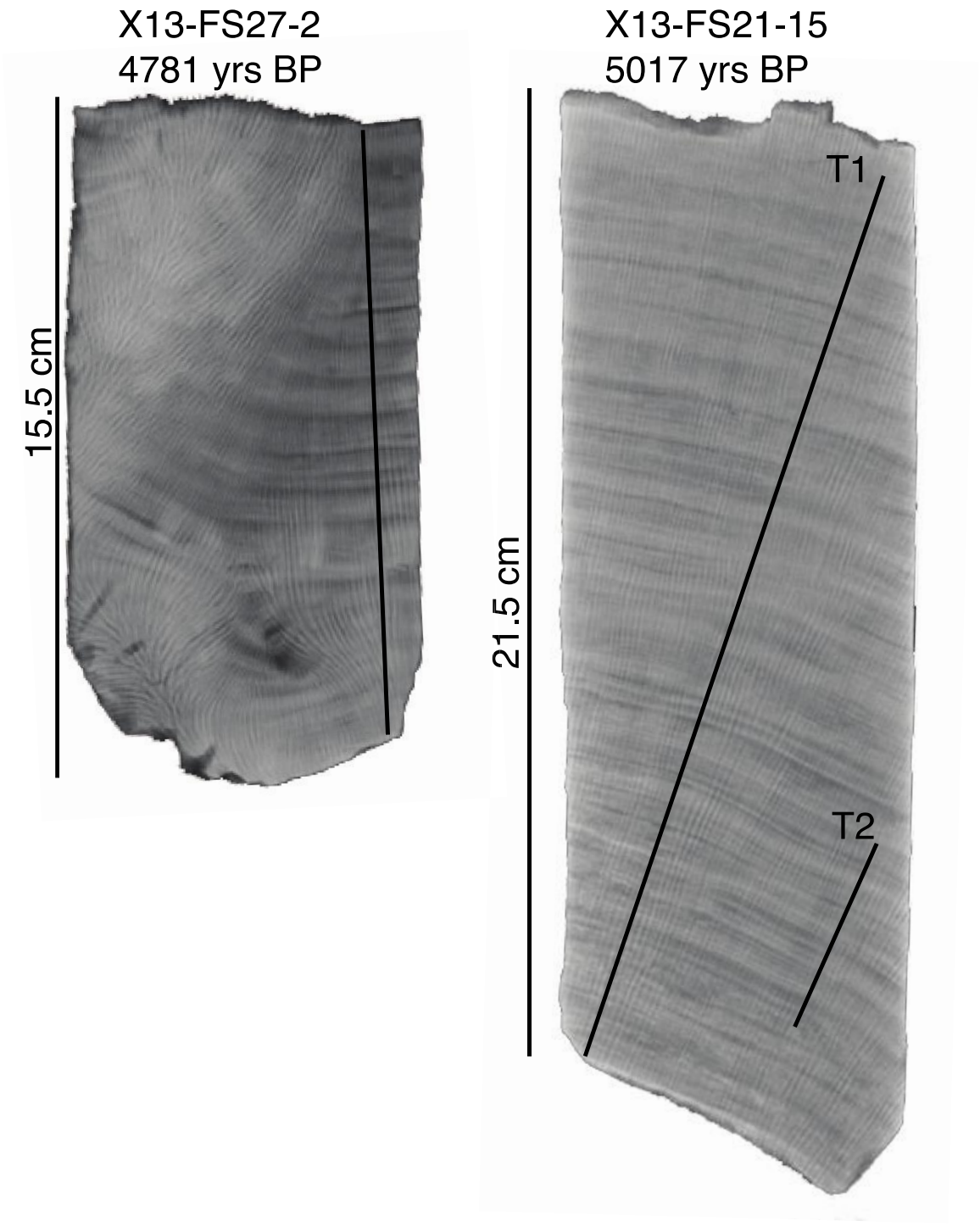

Figure B-S2, Plate 6 X-Ray images with sampling transects of Christmas Island coral. [Full caption under Plate 5.]

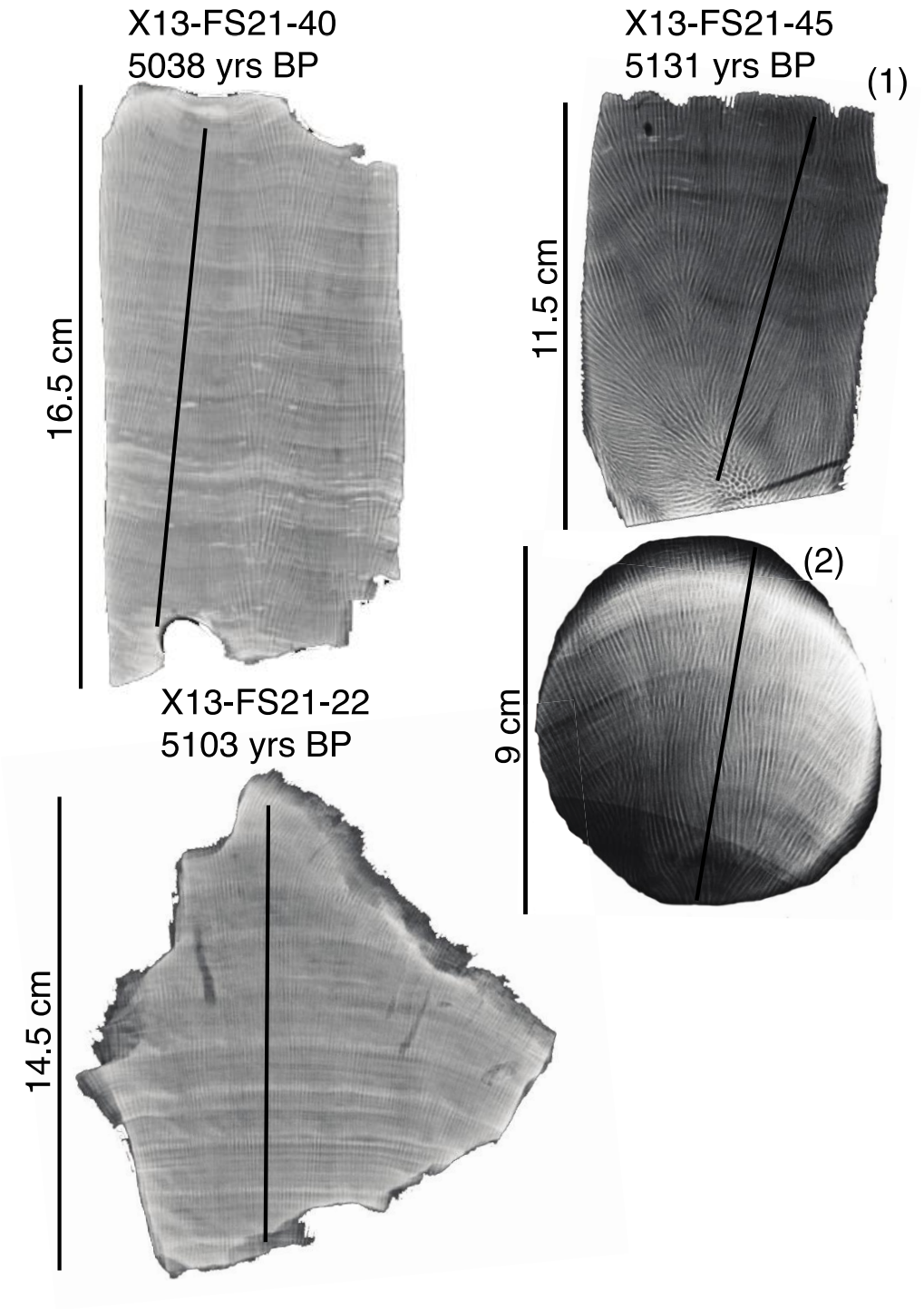

Figure B-S2, Plate 7 X-Ray images with sampling transects of Christmas Island coral. [Full caption under Plate 5.]

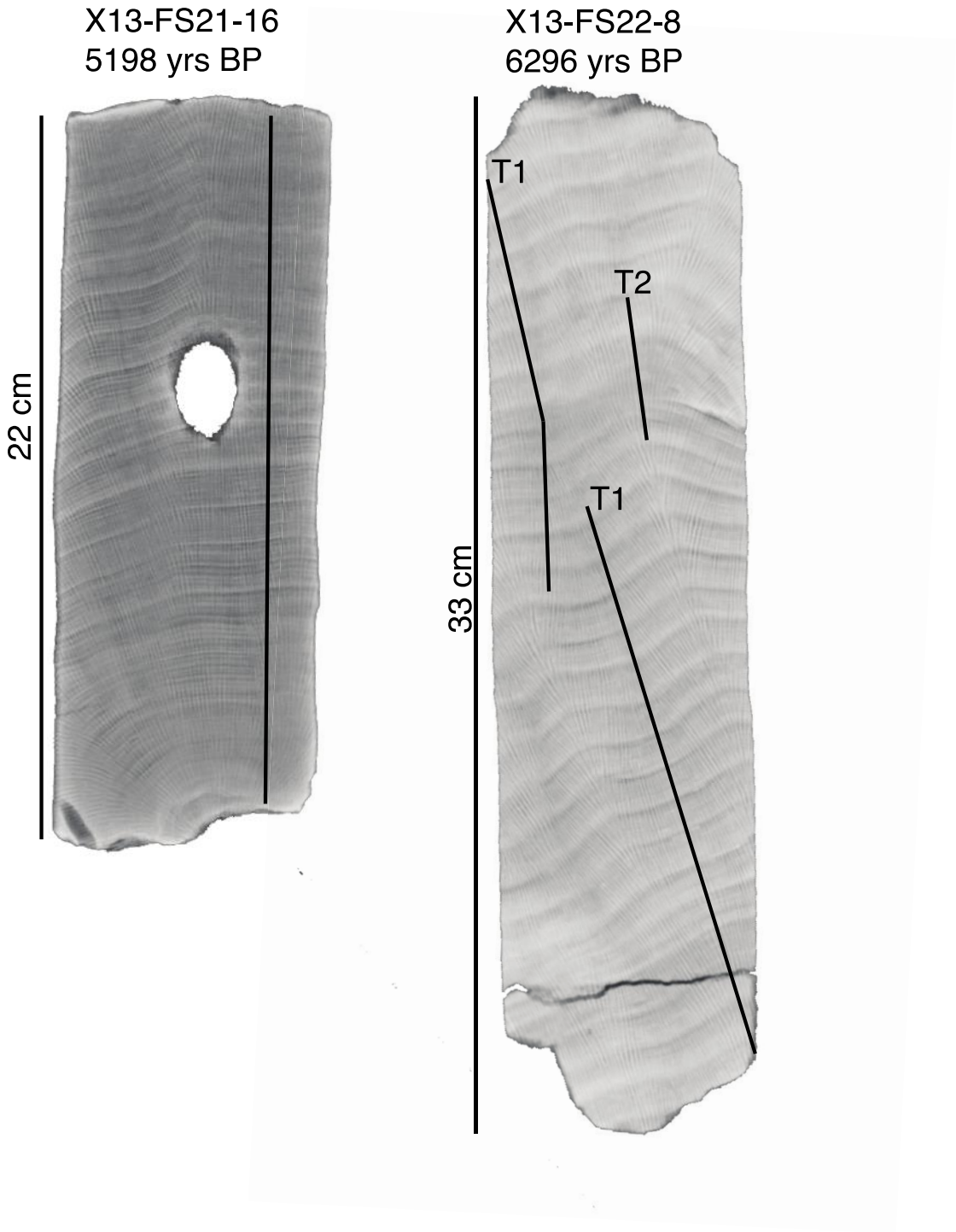

Figure B-S2, Plate 8 X-Ray images with sampling transects of Christmas Island coral. [Full caption under Plate 5.]

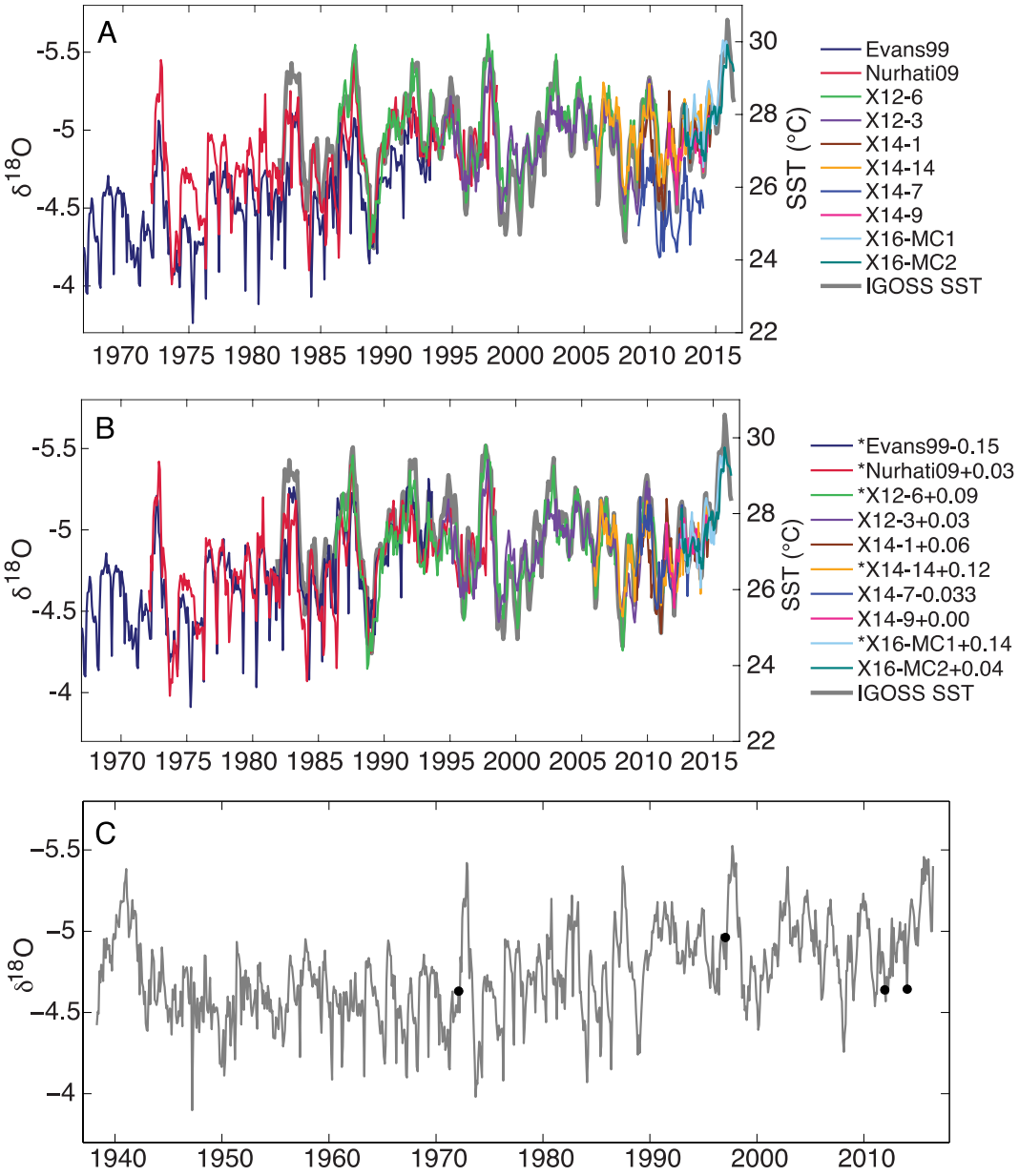

Figure B-S3 Construction of the Christmas Island modern coral $\delta^{18}O$ composite. (A) Plot of IGOSS SST with individual modern coral raw $\delta^{18}O$ records from *Evans et al.*, 1999, *Nurhati et al.*, 2009 and newly generated records for this study (X12-6 and X12-3), for *Chen et al.*, in prep (X14-1, X14-14, X12-7 and X14-9) and *O'Connor et al.*, in prep (X16-MC1 and X16-MC2). (B) Plot of all coral $\delta^{18}O$ records after applying offsets (in per mill; see legend) to match the mean $\delta^{18}O$ values in overlapping intervals of the records. The asterisks next to the coral name in the legend indicate the sections of coral that were combined to form the splice plotted in (C). (C) Plot of the composite Christmas Island coral $\delta^{18}O$ record, spanning from 1938 to 2016. Black circles indicate the tie points between corals.

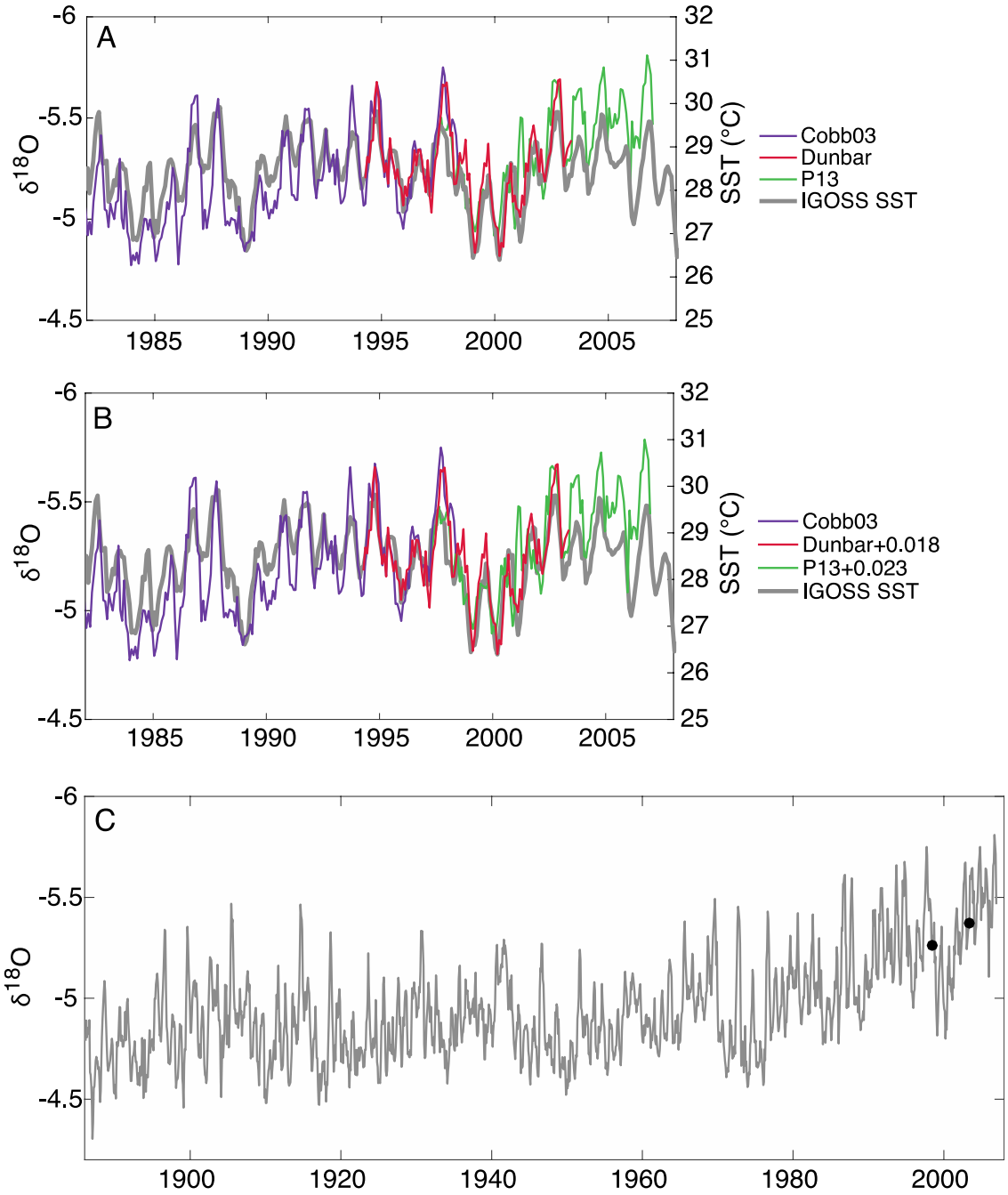

Figure B-S4 Construction of the Palmyra Island modern coral $\delta^{18}O$ composite. (A) Plot of IGOSS SST with individual modern coral raw $\delta^{18}O$ records from *Cobb et al.*, 2003 and newly generated records Dunbar and P13. (B) Plot of all coral $\delta^{18}O$ records after applying offsets (in per mill; see legend) to match the mean $\delta^{18}O$ of Cobb03. (C) Plot of the composite Palmyra Island coral $\delta^{18}O$ record, spanning from 1886 to 2007. Black circles indicate the tie points between corals. The P13 record was spliced into the Dunbar record, which was spliced into the Cobb03 record.

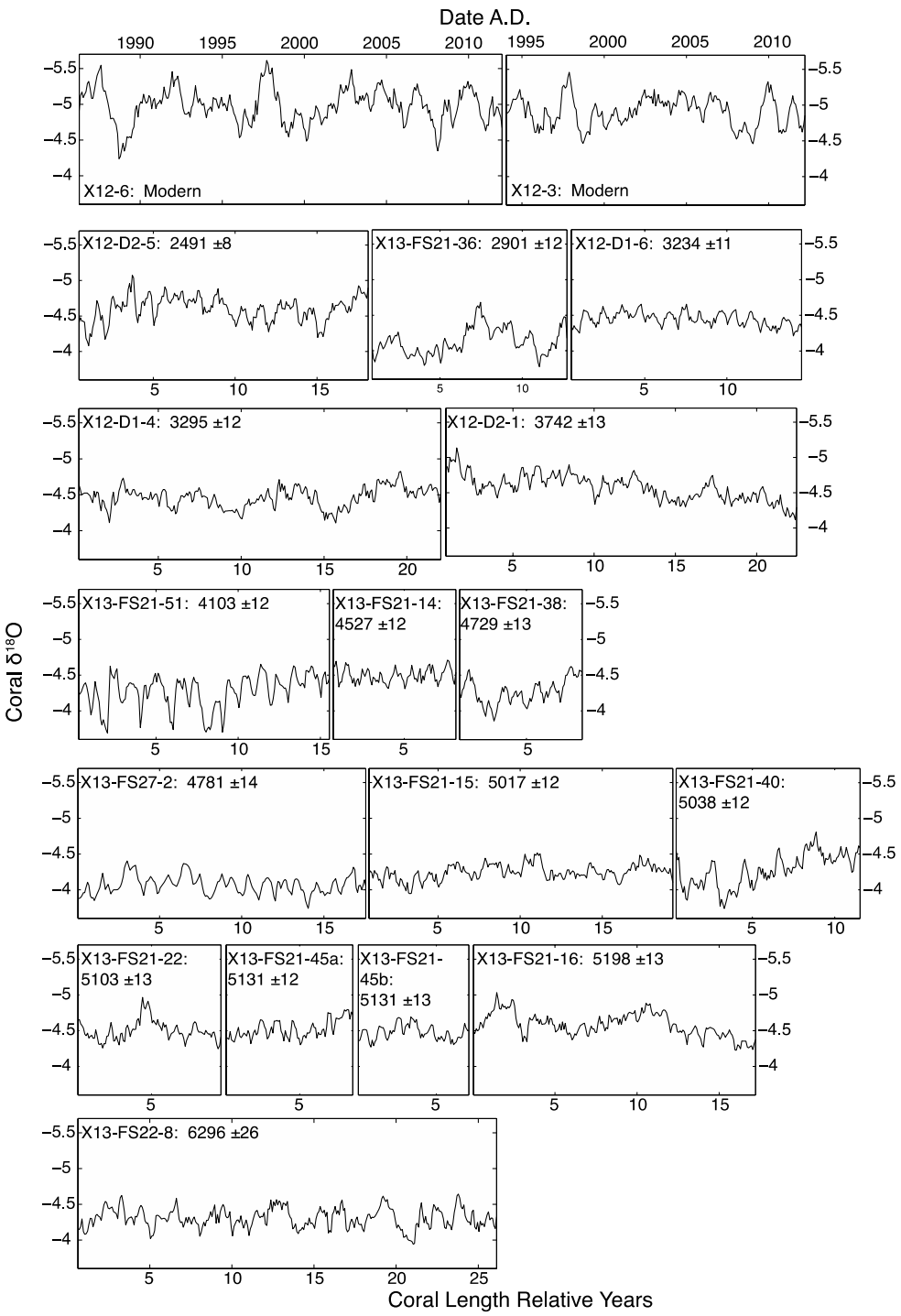

Figure B-S5 Plots of the new raw coral $\delta^{18}O$ sequences presented in this study, shown with their respective U-series dates [see Table B-S3].

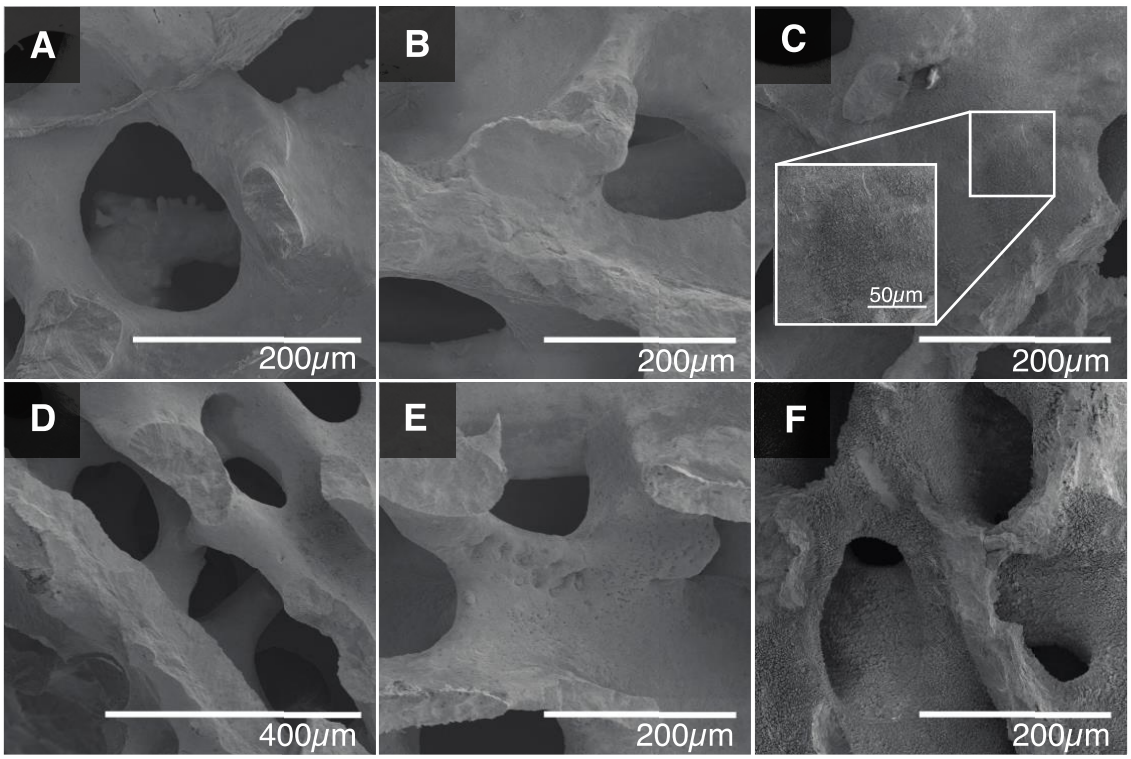

Figure B-S6, Plate 1 A collection of representative SEM images from modern and fossil Christmas Island corals.
Plate 1. Christmas Island modern corals: A-C) X12-3; D-F) X12-6

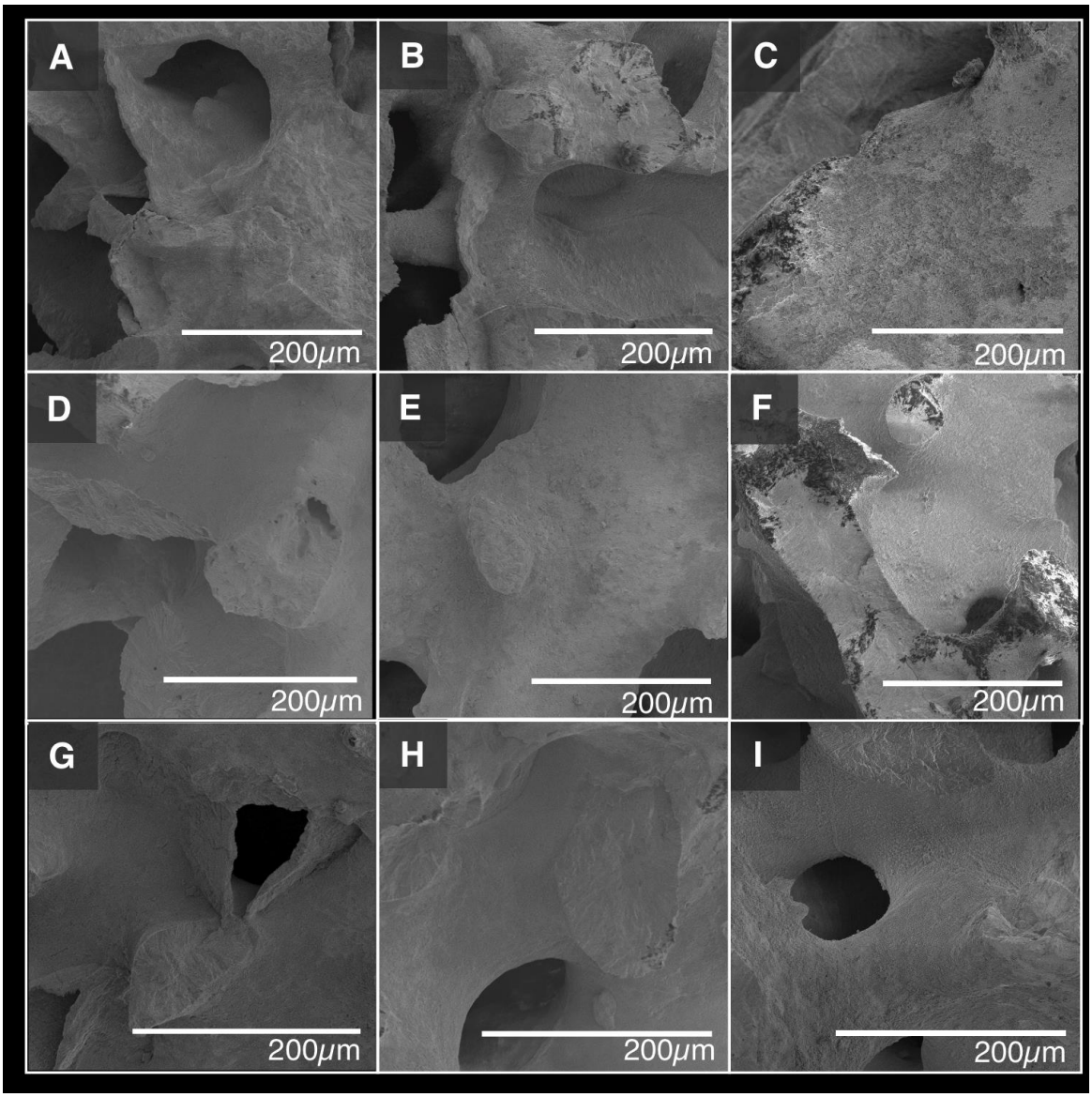

Figure BS-6, Plate 2 Christmas Island fossil corals: A-B) X12-D2-5 (2.5kyBP); C) X12-D1-6 (3.2kyBP); D) X12-D1-4 (3.3kyBP); E) X13-FS21-14 (4.5kyBP); F) X13-FS21-15 (5.0kyBP); G) X13-FS21-22 (5.1kyBP); H-I) X13-FS22-8 (6.3kyBP)

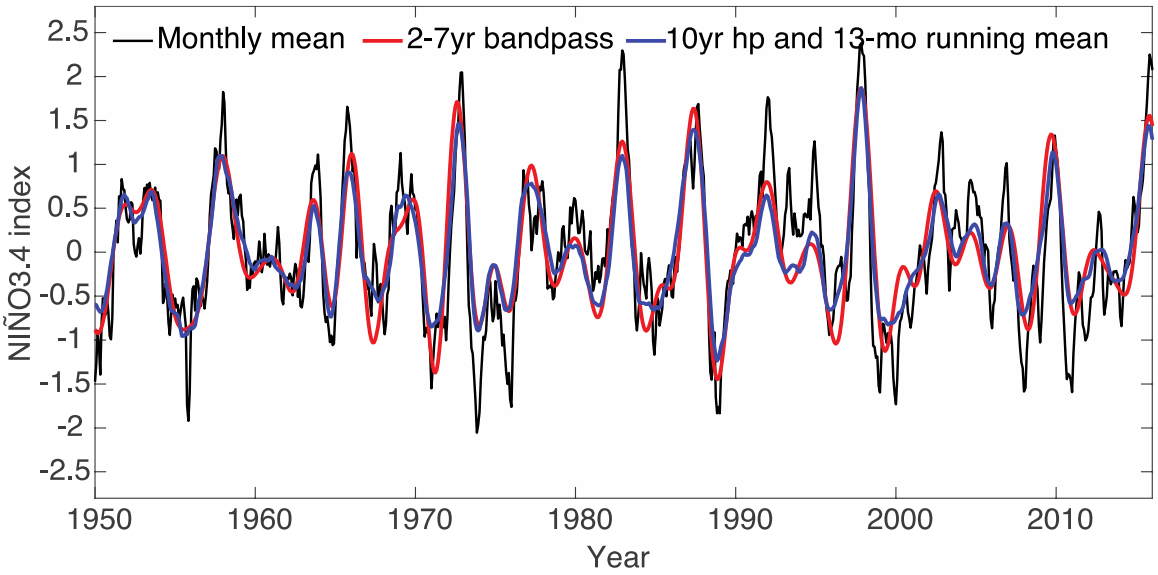

Figure B-S7 Plot of the NIÑO3.4 monthly mean [black] with our chosen filter of 10-yr high pass and 13-month running mean [blue] against the universal filter of a 2-7-year bandpass [red]. The correlation coefficient between the two filters is 0.92.

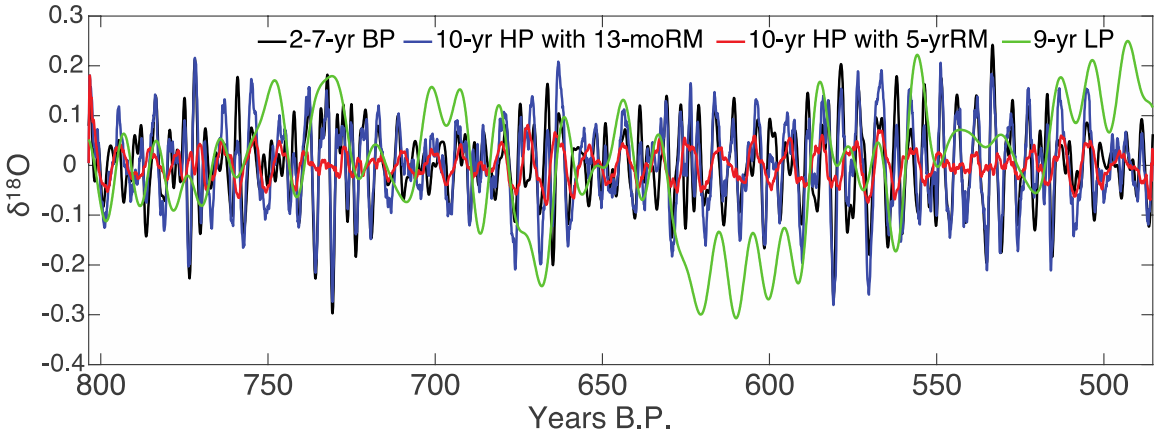

Figure B-S8 Comparison of different filters applied to the longest fossil coral sequence, spl13. Plotted are the 2-7-year bandpass [black], 10-yr high pass with 13-month running average [blue], 10-yr high pass with 5-year running average, [red], and 9-year low pass. Correlation coefficient between the 2-7-yr bandpass and 10 year high pass with 13-month running average is 0.81.

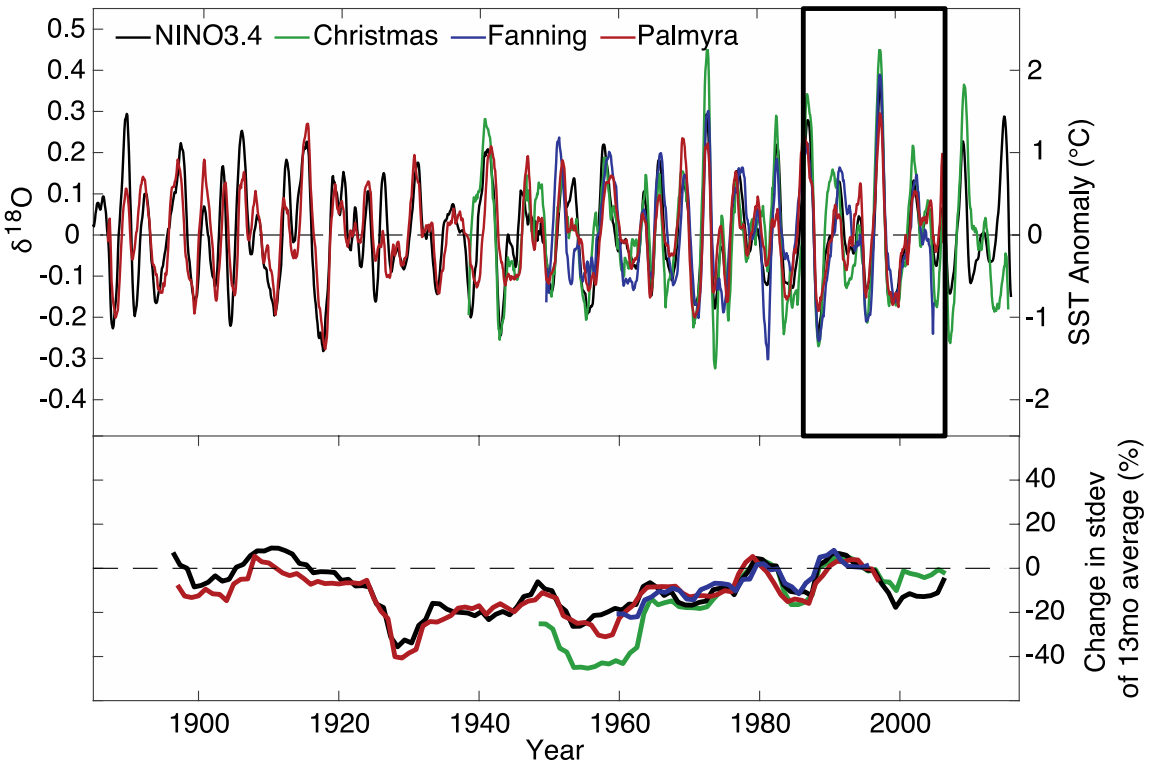

Figure B-S9 ENSO variability in the Line Islands modern coral $\delta^{18}O$ records and the NIÑO3.4 index [Extended Reconstruction Sea Surface Temperatures (ERSST v.4)]. Coral $\delta^{18}O$ are from Christmas [composite record constructed from data in *Evans et al.*, 1999, *Nurhati et al.*, 2009, and newly generated modern sequences); (fig. B-S2); Fanning [composite record from *Cobb et al.*, 2013]; and Palmyra [composite record from *Cobb et al.*, 2003 and newly generated modern sequences; (fig. B-S3)]. (Top) Each monthly resolved time series has been filtered using a 10-year high-pass followed by a 13-month moving average to highlight ENSO-related variability. Correlation coefficients computed between the NIÑO3.4 index and the filtered coral records are -0.79, -.082, and -.80 for Christmas, Fanning and Palmyra, respectively. The black box denotes the 20-year benchmark period [1987-2007], which we compare all coral sequences with. (Bottom) The difference in the standard deviation from the benchmark period to 20-year moving windows in each of the modern coral records and the NIÑO3.4 index, plotted as a percent change from the 20-year benchmark period.

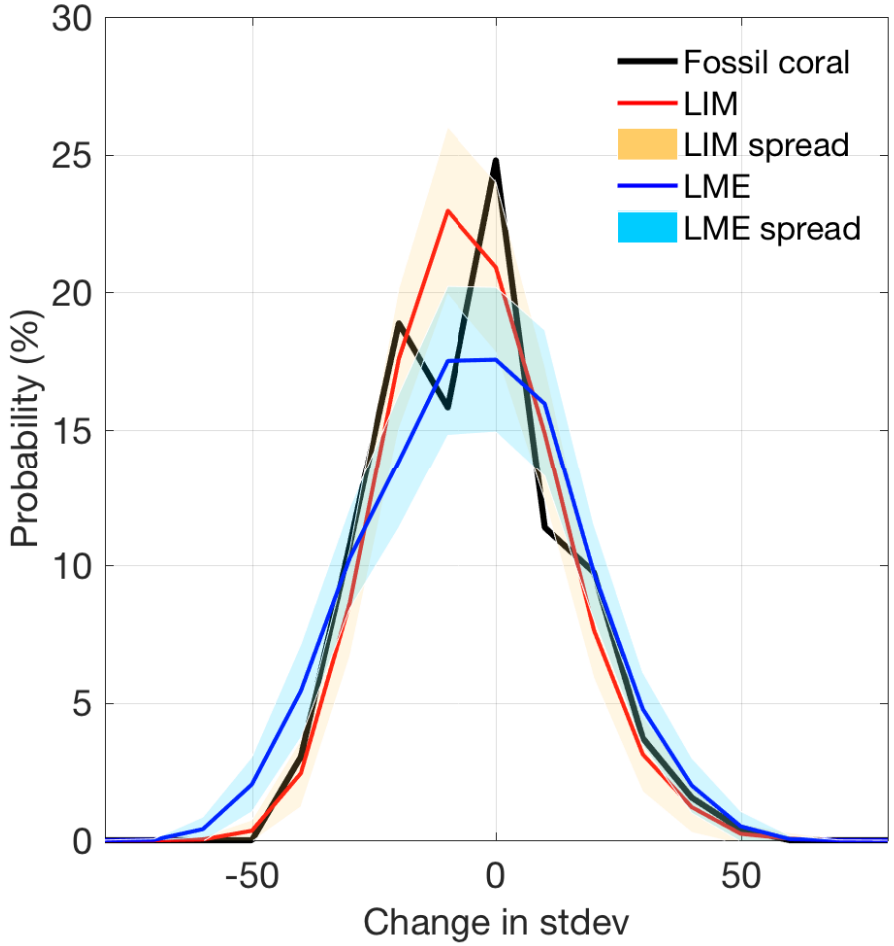

Figure B-S10 Plot of distribution of relative changes of the distribution of 10,000 "pseudo fossil coral" databases compiled by extracting 1,631 years of both LIM [red] and LME [blue] model output data in segment lengths corresponding to the actual fossil coral lengths [red and blue envelope represent individual pseudocoral ensemble distributions], and the distribution of relative changes of ENSO variance from Line Island fossil coral archive [black].

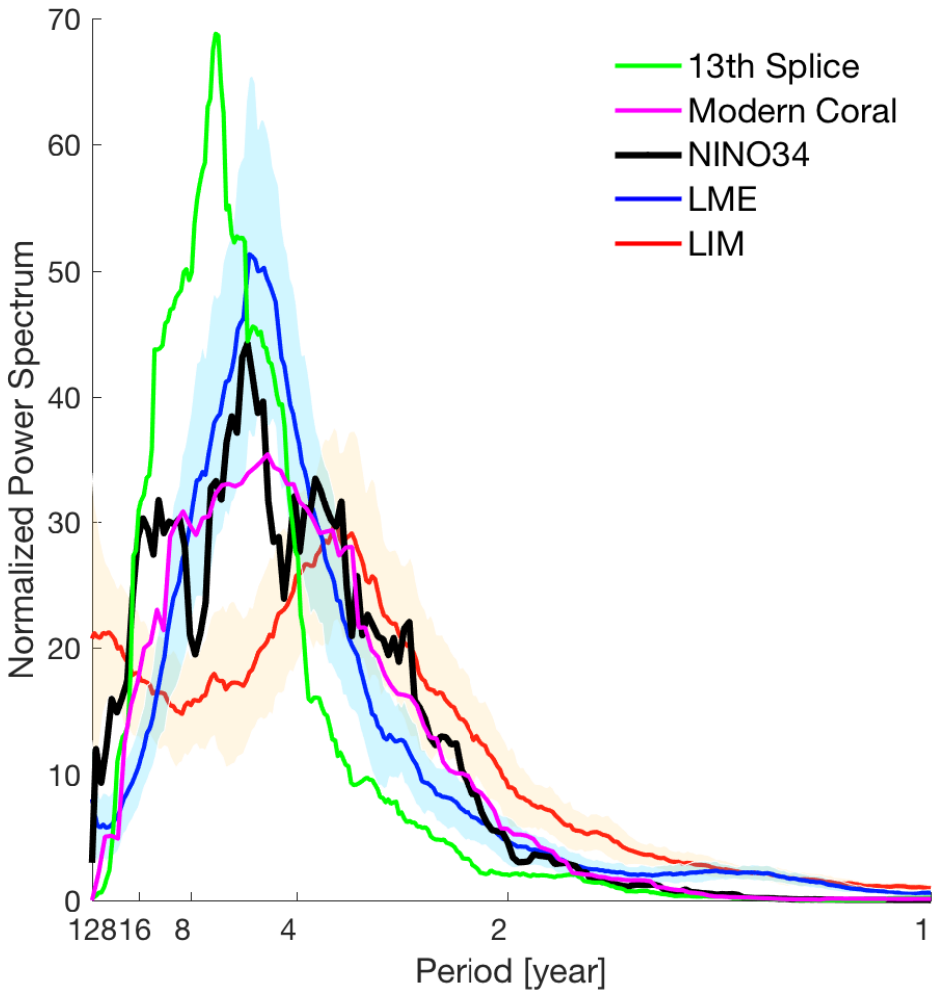

Figure B-S11 Power spectrum for the 320-yr long 13th century splice from Palmyra [green], the Line Island's modern coral composite record [magenta], the NINO 3.4 index [black], and the 10,000 realizations of "psuedo fossil coral" from both the LIM [red] and LME [blue], where the line represents the mean and the envelope the spread from the different realizations.

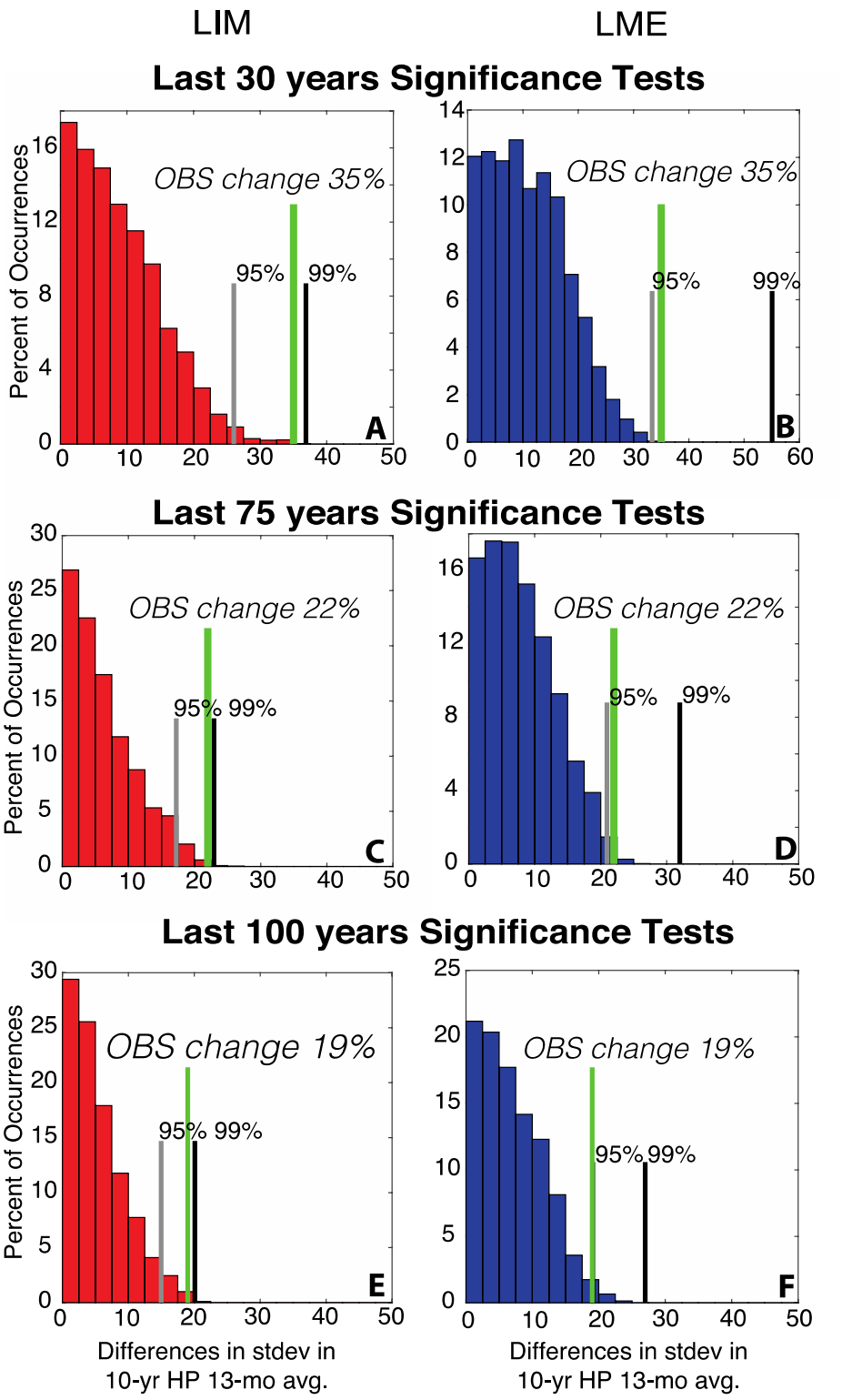

[caption on following page]

Figure B-S12 Results of significance testing for the observed differences in interannual variability of coral $\delta^{18}O$ over last 7,000yrs. A) Probability density function and significance levels (95%, 99%; gray and black lines, respectively) of differences between interannual variance in 10,000 pseudocoral datasets designed to replicate the segment lengths of the last 50 years of modern coral data and all the fossil coral data, generated from NIÑO3.4 time series from a linear inverse model (LIM) of ENSO [*Capotondi and Sardeshmukh*, 2017]. The observed difference in interannual variance is denoted by the green line. B) Same as (A) but psuedocoral data are generated from NIÑO3.4 time series from the Last Millennium Ensemble (LME) [*Otto-Bliesner et al.*, 2016]. C) Same as (A) but targeted at the last 75 years of coral data (1941-2016). D) Same as (C) but pseudocoral data generated from the LME. E) Same as (C) but targeted at the last 100 years of coral data (1916-2016). F) Same as E but pseudocoral data generated from the LME.

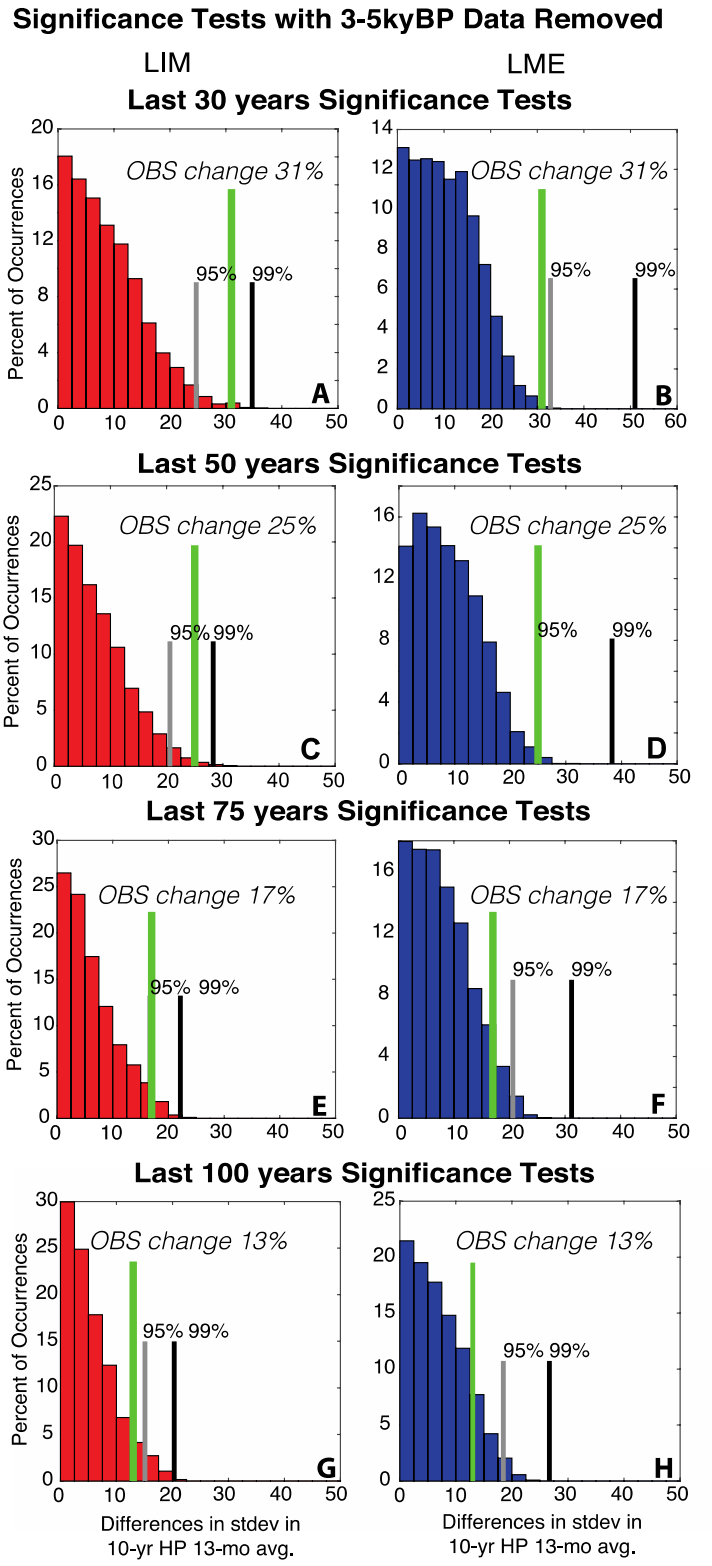

[Caption on following page]

Figure B-S13 Results of significance testing for the observed differences in interannual variability of coral $\delta^{18}O$ over last 7,000yrs but with sequences 3-5kyBP removed. Caption same as Fig. B-S12, but for the last 30 (A-B), 50 (C-D), 75 (E-F) and 100 (G-H) years.

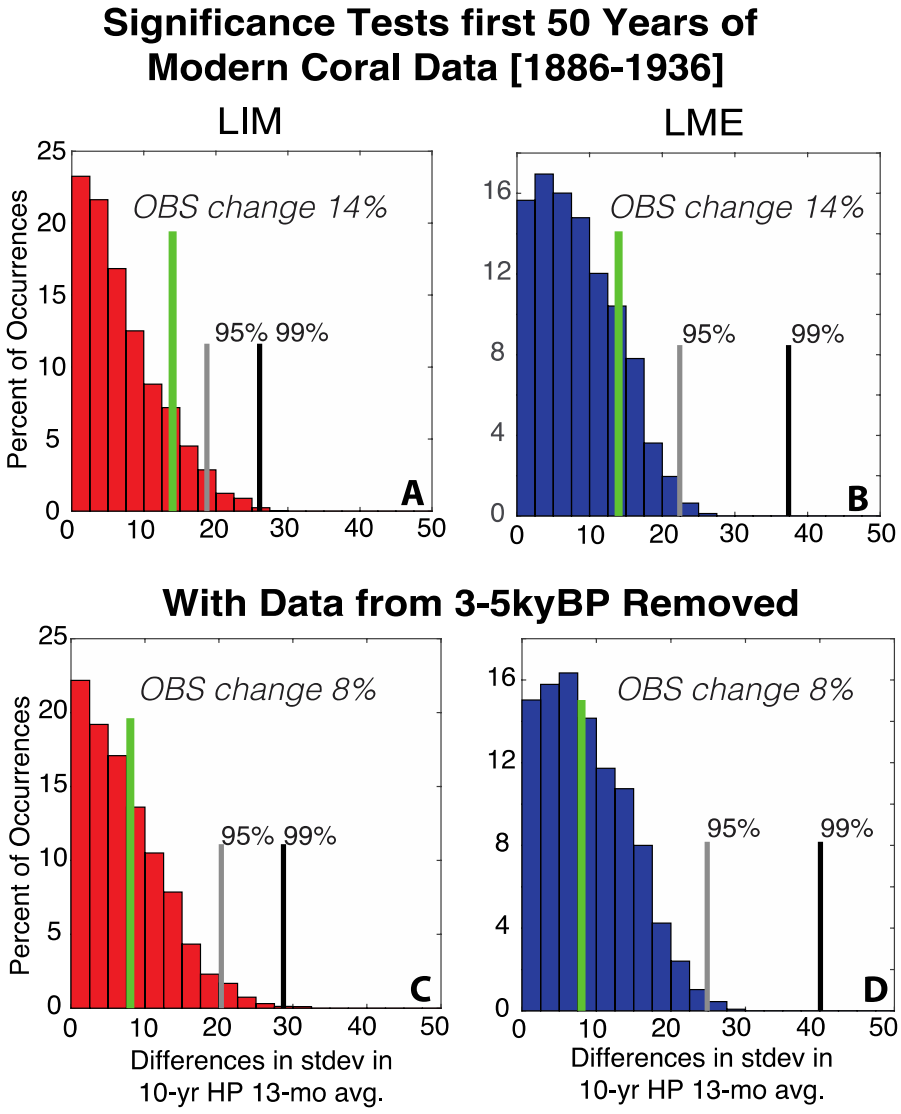

Figure B-S14 Results of significance testing for the observed differences in interannual variability of coral $\delta^{18}O$ over last 7,000yrs with the first 50 years of modern coral data (1886-1936). Caption same as Fig. B-S12. (C) and (D) are with sequences between 3-5kyBP removed.

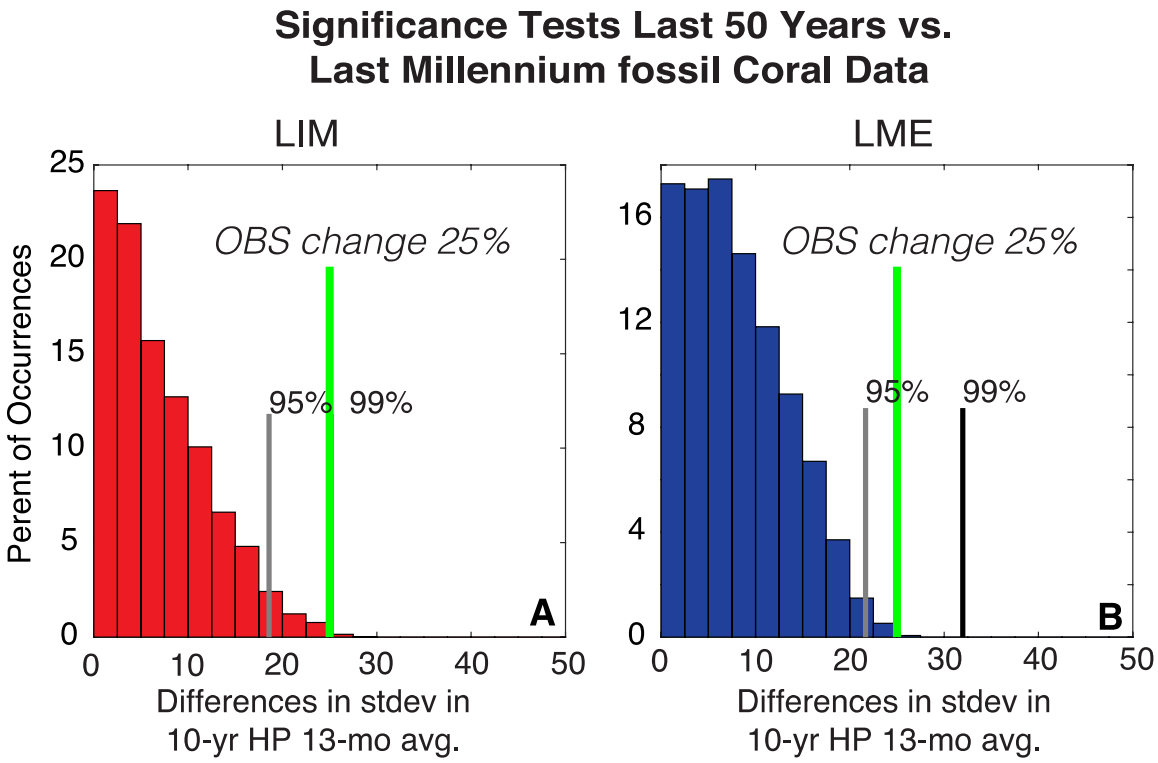

Figure B-S15 Results of significance testing for the observed differences in interannual variability of coral $\delta^{18}O$ over last 1,000yrs with the last 50 years of modern coral data (1966-2016). Caption same as Fig. B-S12.

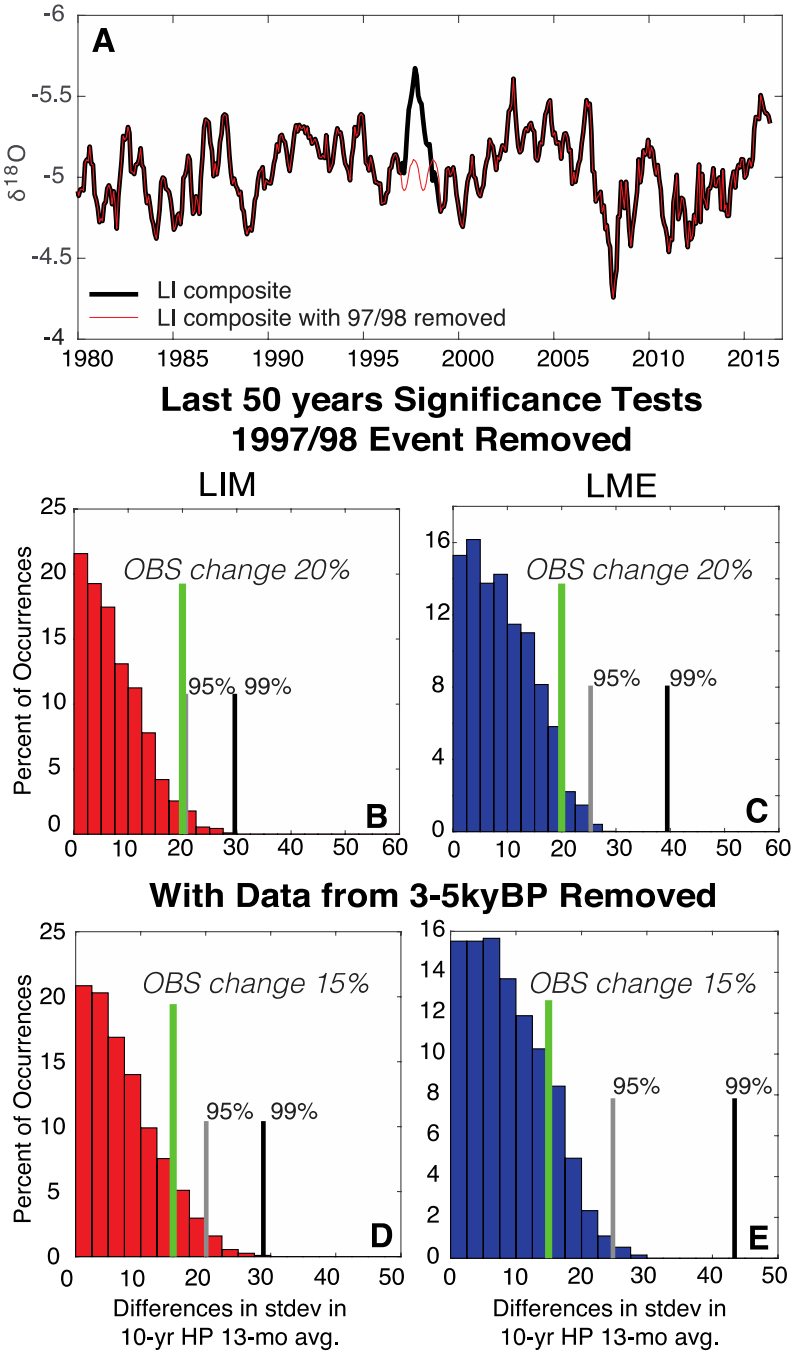

Figure B-S16 Sensitivity test of the significance of the 1997/98 El Niño event on the Monte Carlo statistical testing. A) Plot of the Line Islands composite (black) with the Line Islands composite with the 1997/98 event removed (red). The 97/98 event was removed from the Line Islands modern composite record and replaced with climatology based on the average $\delta^{18}O$ values for each month for the last 50 years. Panels B-E same as Fig. B-S12 but with the 1997-98 event removed from the modern coral sequence (B&C) and again but with the sequences from 3-5kyBP removed from the fossil coral dataset (D&E).

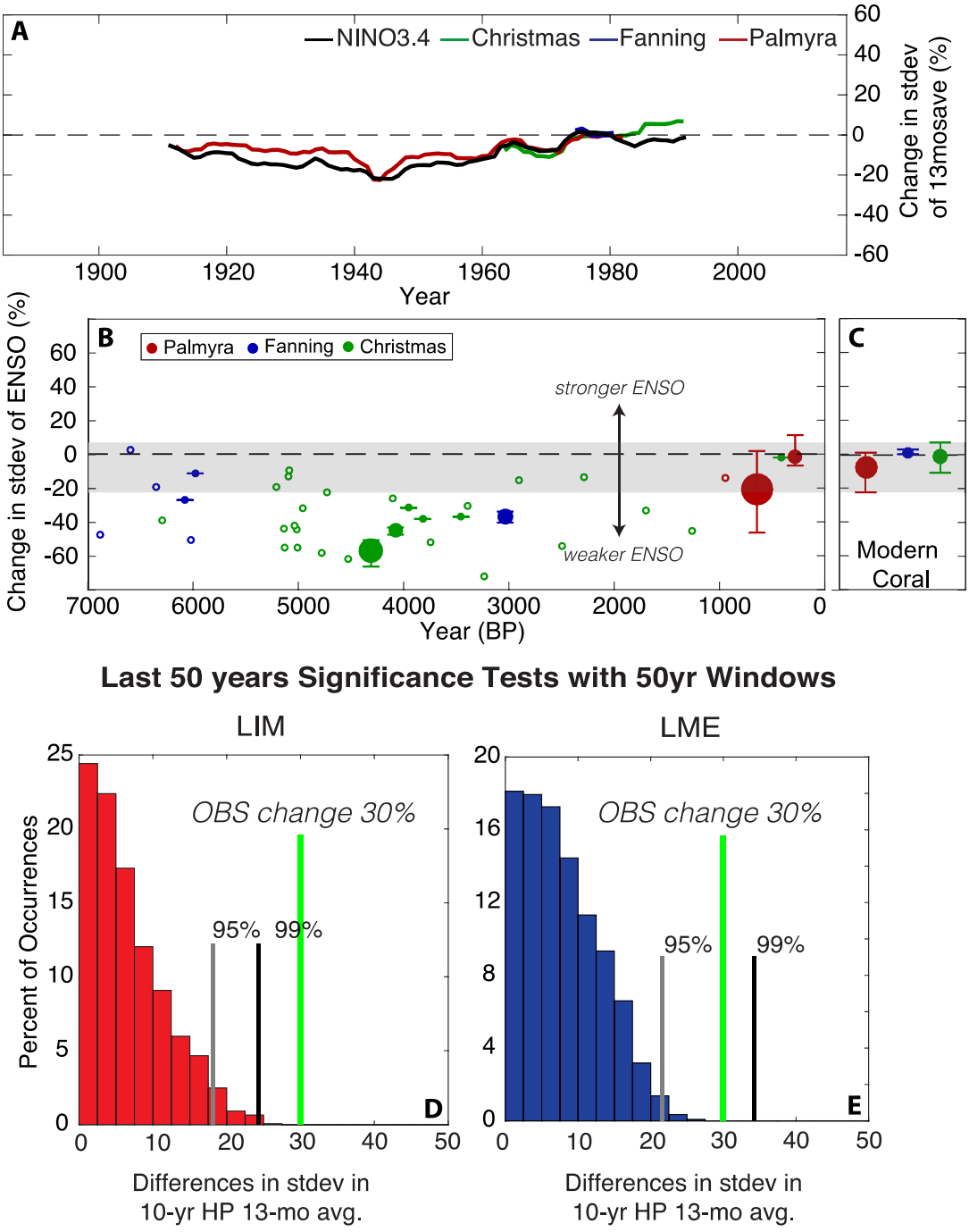

Figure B-S17 Reanalysis using 50-yr windows. A) Change in standard deviation from 1957-2007 in the NINO3.4 SST index [ERSSTv3b] (black), Palmyra (red), Christmas (green), and Fanning (blue) in 10-yr high passed 13-month running average with 50-yr sliding windows. B) Same as Fig. 3.3 but using 50-yr sliding windows with the reference period being 1957-2007. D) Same as Fig. 3.4 but using 50-yr windows. E) Same as (D) but using the LME.

Table B-S1 GPS coordinates for modern sample collection sites on Christmas Island

Site Number	Latitude	Longitude
X12-3	N1 56.087	W157 29.815
X12-6	N1 51.161	W157 30.171

Table B-S2 Summary of the new Christmas Island coral sequences presented in this study

Sample Name	IGSN	Date AD or Age (years BP)	Length (years)	Extension Rate (mm/year)	Maximum Angle of Coralites (degrees)	Diagenetic Condition[a]	Chronology Score[b]
X12-3	IEPRG000G	1994-2012 AD	18	18	0	Very Good	A
X12-6	IEPRG000H	1986-2012 AD	26	19	0	Excellent	A
X12-D2-5	IEPRG0001	2491	18	15	25	Very Good	B
X13-FS21-36	IEPRG0002	2901	12	11	0	Very Good	B
X12-D1-6	IEPRG0003	3234	14	13	0	Good	A
X12-D1-4	IEPRG0004	3295	22	11	35	Good	C
X12-D2-1	IEPRG0005	3742	22	17	15	Good	C
X13-FS21-51	IEPRG0006	4103	15	9	25	Good	A
X13-FS21-14	IEPRG0007	4527	8	20	0	Good	A
X13-FS21-38	IEPRG0008	4729	8	20	20	Good	B
X13-FS27-2	IEPRG0009	4781	17	8	10	Good	A
X13-FS21-15	IEPRG000A	5017	19	11	15	Fair	A
X13-FS21-40	IEPRG000B	5038	11	12	0	Fair	B
X13-FS21-22	IEPRG000C	5103	9	16	0	Good	A
X13-FS21-45(1)	IEPRG000D	5131	8	13	30	Fair	A
X13-FS21-45(2)	IEPRG000D	5131	7	13	10	Fair	A
X13-FS21-16	IEPRG000E	5198	17	12	0	Fair	A
X13-FS22-8	IEPRG000F	6296	26	11	20	Good	A

[a] Diagenetic condition assessed using SEM photos of fossil corals, according to the following guidelines from Cobb et al. (2013): excellent = little to no evidence of diagenetic alteration, very good = some evidence of minor diagenetic alteration, good = pervasive evidence of minor alteration (e.g. light surface coatings, fair = isolated evidence of major alteration (thick surface coatings), and poor = pervasive evidence of moderate alteration (thick surface coatings and/or dissolution)

[b] Chronologies are scored A-C where samples scored A have excelled seasonal cycle to control winter tie points and may have additional annual carbon spikes and/or banding in coral XRAY, B have slight noise in the seasonal cycle and may have few to no carbon spikes and/or banding in coral XRAY, and C have modernate noise in seasonal cycle and the carbon contains no annual spikes and there is no banding in the XRAYs.

Table B-S3 U/Th dates for Christmas Island fossil corals presented in this study

Sample [a]	$[^{238}U]$ [b] (ppm)		$(^{230}Th/^{238}U)$ [c] (activity) x10^3		$\delta^{234}U$ (i) [d] (‰)		^{232}Th (ppt)		^{230}Th Age [e] (uncorrected) (years B.P.)		230Th Age [f] (corrected) (years B.P.)	
X12-D2-5*	2.306	±3	26.5	±0.07	144.1	±1.5	16	±2	2554	±8	2491	±8
X13-FS21-36	2.713	±3.2	30.9	±0.07	149.7	±3.6	94	±2	2967	±12	2901	±12
X12-D1-6*	2.244	±3	34.1	±0.11	144.5	±1.7	3	±2	3297	±11	3234	±11
X12-D1-4*	2.727	±5	34.7	±0.10	143.9	±1.9	28	±3	3358	±12	3295	±12
X12-D2-1*	2.384	±4	39.2	±0.12	141.3	±1.8	7	±2	3805	±13	3742	±13
X13-FS21-51	2.563	±2.2	43.0	±0.11	145.6	±1.3	2	±3	4168	±12	4103	±12
X13-FS21-14	2.655	±2.5	47.2	±0.11	143.5	±1.3	51	±2	4593	±12	4527	±12
X13-FS21-38	2.862	±2.7	49.2	±0.11	143.7	±1.3	112	±3	4795	±13	4729	±13
X13-FS27-2	2.823	±2.8	49.6	±0.12	139.7	±1.4	40	±2	4846	±14	4781	±14
X13-FS21-15	2.726	±2.4	52.2	±0.10	145.1	±1.3	5	±2	5082	±12	5017	±12
X13-FS21-40	2.872	±2.6	52.4	±0.11	144.3	±1.2	39	±2	5103	±12	5038	±12
X13-FS21-22	2.835	±2.1	53.1	±0.12	145.1	±1.1	30	±3	5168	±13	5103	±13
X13-FS21-45	2.496	±1.9	53.4	±0.11	145.9	±1.2	54	±2	5197	±12	5131	±12
X13-FS21-16	2.657	±2.5	54.0	±0.12	144.6	±1.3	25	±2	5263	±13	5198	±13
X13-FS22-8	2.407	±2.2	64.9	±0.15	144.3	±1.4	89	±3	6362	±17	6296	±17

[a] Asterick denotes U/Th dates initially published in Grothe et al., 2016.

[b] The errors reported in this table are quoted as 2σ; for $[^{238}U]$, error is for last significant figure.

[c] The measured, uncorrected $(^{230}Th/^{238}U)$activity ratio; 2σ error is for last significant figure.

[d] $\delta^{234}U = \{[(^{234}U/^{238}U)/(^{234}U/^{238}U)_{eq} - 1\} \times 10^3$, where $(^{234}U/^{238}U)_{eq}$ represents the atomic ratio at secular equilibrium; $\delta^{234}U$ (i) represents the initial value calculated using U/Th dating equations. Decay constants from Cheng et al., 2013.

[e] All dates are reported as years B.P. (before present), where "present" is defined as 1950 A.D.

[f] Date corrected with (230Th/232Th)atomic of 4.4 ± 2.2 x 10-6, which is the value for materials at secular equilibrium, assuming a bulk Earth crustal 232Th/238Th ratio of 3.8.

Table B-S4 Fossil corals presented in the analyses of this study

Island	Sample Name	Date AD or Age (years BP)	Length (years)	% Change in 13-month running mean Stdev wrt 1987-2007	Reference
Christmas	M2	1516-1561AD	45	-18	Cobb et al., 2013
	P49	1248	19	-52	Cobb et al., 2013
	P2	1684	21	-43	Cobb et al., 2013
	P37	2273	26	-19	Cobb et al., 2013
	X12-D2-5	2491	16	-60	This paper
	X13-FS21-36	2901	10	-25	This paper
	X12-D1-6	3234	14	-75	This paper
	X12-D1-4	3295	25	-37	This paper
	P26	3432	42	-45	Cobb et al., 2013
	X12-D2-1	3742	20	-59	This paper
	P43	3797	44	-42	Cobb et al., 2013
	P40	3926	48	-39	Cobb et al., 2013
	P34	4042	68	-51	Cobb et al., 2013
	X13-FS21-51	4103	15	-35	This paper
	X13-FS21-14	4527	8	-66	This paper
	X13-FS21-38	4729	8	-31	This paper
	X13-FS27-2	4781	17	-63	This paper
	P382	4941	36	-38	Cobb et al., 2013
	P381	4992	27	-60	Cobb et al., 2013
	X13-FS21-15	5017	19	-51	This paper
	X13-FS21-40	5038	11	-49	This paper
	P11	5075	22	-21	Cobb et al., 2013; Grothe et al., 2016
	X13-FS21-22	5103	9	-23	This paper
	X13-FS21-45(1)	5131	8	-60	This paper
	X13-FS21-45(2)	5131	7	-50	This paper
	X13-FS21-16	5198	17	-28	This paper
	X13-FS22-8	6296	26	-46	This paper
Fanning	V10	2994	81	-41	Cobb et al., 2013
	V30	5958	42	-16	Cobb et al., 2013
	V13	6007	27	-55	Cobb et al., 2013
	V8	6056	41	-40	Cobb et al., 2013
	V28	6340	21	-26	Cobb et al., 2013
	V33	6581	25	-2	Cobb et al., 2013
	V11	6860	37	-57	Cobb et al., 2013

	17th splice	1635-1703AD	68	-13	Cobb et al., 2003
Palmyra	13th splice	1147-1465AD	318	-30	This paper; Cobb et al., 2003
	NB12	928-961AD	32	-22	Cobb et al., 2003

Table B-S5 Observed differences between modern and fossil corals

Time Period	Years	Observed difference	Percent Significant		Observed difference without 3-5ky corals	Percent Significant	
			LIM	LME		LIM	LME
Last 30 years	1986-2016	-35	99	96	-31	98	95
Last 50 years	1966-2016	-30	99	97	-25	98	95
Last 75 years	1941-2016	-22	98	96	-17	95	90
Last 100 year	1916-2016	-19	99	95	-13	91	83

REFERENCES

Ashok, K., S. K. Behera, S. A. Rao, H. Y. Weng, and T. Yamagata (2007), El Nino Modoki and its possible teleconnection, *Journal of Geophysical Research-Oceans*, *112*(C11).

Bathurst, R. G. (1974), Marine diagenesis of shallow-water calcium-carbonate sediments, *Annual Review of Earth and Planetary Sciences*, *2*, 257-274, doi: 10.1146/annurev.ea.02.050174.001353.

Battisti, D. S., and A. C. Hirst (1989), Interannual variability in a tropical atmosphere ocean model – influences of the basic state, ocean geometry and nonlinearity, *Journal of the Atmospheric Sciences*, *46*(12), 1687-1712.

Beck, J. W., R. L. Edwards, E. Ito, F. W. Taylor, J. Recy, F. Rougerie, P. Joannot, and C. Henin (1992), Sea-surface temperature from coral skeletal strontium calcium ratios, *Science*, *257*(5070), 644-647.

Bellenger, H., E. Guilyardi, J. Leloup, M. Lengaigne, and J. Vialard (2014), ENSO representation in climate models: from CMIP3 to CMIP5, *Climate Dynamics*, *42*(7-8), 1999-2018.

Bender, M. L., R. G. Fairbanks, F. W. Taylor, R. K. Matthews, J. G. Goddard, and W. S. Broecker (1979), Uranium-series dating of the Pleistocene reef tracts of Barbados, West-Indies, *Geological Society of America Bulletin*, *90*(6), 577-594, 10.1130/0016-7606(1979)90<577:udotpr>2.0.co;2.

Beverly, R. K., W. Beaumont, D. Tauz, K. M. Ormsby, K. F. von Reden, G. M. Santos, and J. R. Southon (2010), The Keck Carbon Cycle AMS Laboratory, University of California, Irvine: Status Report, *Radiocarbon*, *52*(2), 301-309.

Bish, D. L., and J. E. Post (1993), Quantitative mineralogical analysis using the rietveld full-pattern fitting method, *American Mineralogist*, *78*(9-10), 932-940.

Bjerknes, J. (1969), Atmospheric teleconnections from equatorial Pacific, *Monthly Weather Review*, *97*(3), 163-&.

Braconnot, P., Y. Luan, S. Brewer, and W. Zheng (2012), Impact of Earth's orbit and freshwater fluxes on Holocene climate mean seasonal cycle and ENSO characteristics, *Climate Dynamics*, *38*(5-6), 1081-1092.

Broecker, W. S., D. L. Thurber, J. Goddard, T. L. Ku, R. K. Matthews, and Mesolell.Kj (1968), Milankovitch hypothesis supported by precise dating of coral reefs and deep-sea sediments, *Science*, *159*(3812), 297-300, doi: 10.1126/science.159.3812.297.

Broecker, W., A. Mix, M. Andree, and H. Oeschger (1984), Radiocarbon measurements on coexisting benthic and planktic foraminifera shells – potential for reconstructing ocean ventilation times over the last 20000 years, *Nuclear Instruments & Methods in Physics Research Section B-Beam Interactions with Materials and Atoms*, *5*(2), 331-339, 10.1016/0168-583x(84)90538-x.

Burke, A., L. F. Robinson, A. P. McNichol, W. J. Jenkins, K. M. Scanlon, and D. S. Gerlach (2010), Reconnaissance dating: A new radiocarbon method applied to assessing the temporal distribution of Southern Ocean deep-sea corals, *Deep-Sea Research Part I-Oceanographic Research Papers*, *57*(11), 1510-1520, 10.1016/j.dsr.2010.07.010.

Burr, G. S., R. L. Edwards, D. J. Donahue, E. R. M. Druffel, and F. W. Taylor (1992), Mass-Spectrometric C-14 and U-Th measurements in coral, *Radiocarbon*, *34*(3), 611-618.

Bush, S. L., G. M. Santos, X. Xu, J. R. Southon, N. Thiagarajan, S. K. Hines, and J. F. Adkins (2013), Simple, rapid, and cost effective: a screening method for 14C analysis of small carbonate samples, *Radiocarbon*, *55*.

Cai, W. J., A. Santoso, G. J. Wang, E. Weller, L. X. Wu, K. Ashok, Y. Masumoto, and T. Yamagata (2014), Increased frequency of extreme Indian Ocean Dipole events due to greenhouse warming, *Nature*, *510*(7504), 254-+.

Cai, W. J., et al. (2015), ENSO and greenhouse warming, *Nature Climate Change*, *5*(9), 849-859.

Cane, M. A., and S. E. Zebiak (1985), A theory for El-Nino and the southern oscillation, *Science*, *228*(4703), 1085-1087.

Capotondi, A., and P.D. Sardeshmukh (2017), Is El Nino really changing? *Geophysical Research Letters*.

Carré, M., J. P. Sachs, A. J. Schauer, W. E. Rodríguez, and F. C. Ramos (2013), Reconstructing El Niño-Southern Oscillation activity and ocean temperature seasonality from short-lived marine mollusk shells from Peru, *Palaeogeography, Palaeoclimatology, Palaeoecology*, *371*(0), 45-53.

Carré, M., J. P. Sachs, S. Purca, A. J. Schauer, P. Braconnot, R. A. Falcon, M. Julien, and D. Lavallee (2014), Holocene history of ENSO variance and asymmetry in the eastern tropical Pacific, *Science*, *345*(6200), 1045-1048.

Chen, J. H., R. L. Edwards, and G. J. Wasserburg (1986), U-238, U-234 AND Th-232 in seawater, *Earth and Planetary Science Letters*, *80*(3-4), 241-251, doi: 10.1016/0012-821x(86)90108-1.

Chen, J. H., H. A. Curran, B. White, and G. J. Wasserburg (1991), Precise chronology of the last interglacial period – ^{234}U-^{230}Th data from fossil coral reefs in the

Bahamas, *Geological Society of America Bulletin*, *103*(1), 82-97, doi: 10.1130/0016-7606(1991)103<0082:pcotli>2.3.co;2.

Chen, S., S. S. Hoffmann, D. C. Lund, K. M. Cobb, J. Emile-Geay, and J. F. Adkins (2016), A high-resolution speleothem record of western equatorial Pacific rainfall: Implications for Holocene ENSO evolution, *Earth and Planetary Science Letters*, *442*, 61-71.

Chen, T., K.M. Cobb, P.R. Grothe, and H.R. Sayani (in prep), Sr/Ca and $\delta^{18}O$ in Favia, Platygyra and Porites corals from the central tropical Pacific

Cheng, H., R. L. Edwards, M. T. Murrell, and T. M. Benjamin (1998), Uranium-thorium-protactinium dating systematics, *Geochimica Et Cosmochimica Acta*, *62*(21-22), 3437-3452, doi: 10.1016/s0016-7037(98)00255-5.

Cheng, H., R. L. Edwards, J. Hoff, C. D. Gallup, D. A. Richards, and Y. Asmerom (2000), The half-lives of uranium-234 and thorium-230, *Chemical Geology*, *169*(1-2), 17-33, doi: 10.1016/s0009-2541(99)00157-6.

Cheng, H., R.L. Edwards, C. Shen, V.J. Polyak, Y. Asmerom, J. Woodhead, J. Hellstrom, Y. Wang, X. Kong, C. Spotl, X. Wang, and E.C. Alexander Jr. (2013), Improvements in Th-230 dating, Th-230 and U-234 half-life values, and U-Th isotopic measurements by multi-collector inductively coupled plasma mass spectrometry, *Earth and Planetary Science Letters*, *371*, 82-91, doi: 10.1016/j.epsl.2013.04.006.

Cherchi, A., S. Masina, and A. Navarra (2008), Impact of extreme CO_2 levels on tropical climate: a CGCM study, *Climate Dynamics*, *31*(7-8), 743-758.

Clement, A. C., R. Seager, and M. A. Cane (2000), Suppression of El Nino during the mid-Holocene by changes in the Earth's orbit, *Paleoceanography*, *15*(6), 731-737.

Cobb, K. M., C. D. Charles, and D. E. Hunter (2001), A central tropical Pacific coral demonstrates Pacific, Indian, and Atlantic decadal climate connections, *Geophysical Research Letters*, *28*(11), 2209-2212.

Cobb, K. M., C. D. Charles, H. Cheng, M. Kastner, and R. L. Edwards (2003a), U/Th-dating living and young fossil corals from the central tropical Pacific, *Earth and Planetary Science Letters*, *210*(1-2), 91-103, doi: 10.1016/s0012-821x(03)00138-9.

Cobb, K. M., C. D. Charles, H. Cheng, and R. L. Edwards (2003b), El Nino/Southern Oscillation and tropical Pacific climate during the last millennium, *Nature*, *424*(6946), 271-276.

Cobb, K. M., N. Westphal, H. R. Sayani, J. T. Watson, E. Di Lorenzo, H. Cheng, R. L. Edwards, and C. D. Charles (2013), Highly Variable El Nino-Southern Oscillation Throughout the Holocene, *Science*, *339*(6115), 67-70, doi: 10.1038/nature01779.

Collins, M., et al. (2010), The impact of global warming on the tropical Pacific ocean and El Nino, *Nature Geoscience*, *3*(6), 391-397.

Conroy, J. L., J. T. Overpeck, J. E. Cole, T. M. Shanahan, and M. Steinitz-Kannan (2008), Holocene changes in eastern tropical Pacific climate inferred from a Galapagos lake sediment record, *Quaternary Science Reviews*, *27*(11-12), 1166-1180.

Correge, T. (2006), Sea surface temperature and salinity reconstruction from coral geochemical tracers, *Palaeogeography Palaeoclimatology Palaeoecology*, *232*(2-4), 408-428.

Cutler, K. B., R. L. Edwards, F. W. Taylor, H. Cheng, J. Adkins, C. D. Gallup, P. M. Cutler, G. S. Burr, and A. L. Bloom (2003), Rapid sea-level fall and deep-ocean temperature change since the last interglacial period, *Earth and Planetary Science Letters*, *206*(3-4), 253-271, doi: 10.1016/s0012-821x(02)01107-x.

Deser, C., and J. M. Wallace (1990), Large-scale atmospheric circulation features of warm and cold episodes in the tropical Pacific, *Journal of Climate*, *3*(11), 1254-1281.

Donguy, J. R., and A. Dessier (1983), El-Nino-like events observed in the tropical Pacific, *Monthly Weather Review*, *111*(10), 2136-2139.

Douville, E., E. Salle, N. Frank, M. Eisele, E. Pons-Branchu, and S. Ayrault (2010), Rapid and accurate U-Th dating of ancient carbonates using inductively coupled plasma-quadrupole mass spectrometry, *Chemical Geology*, *272*(1-4), 1-11, 10.1016/j.chemgeo.2010.01.007.

Dykoski, C. A., R. L. Edwards, H. Cheng, D. X. Yuan, Y. J. Cai, M. L. Zhang, Y. S. Lin, J. M. Qing, Z. S. An, and J. Revenaugh (2005), A high-resolution, absolute-dated Holocene and deglacial Asian monsoon record from Dongge Cave, China, *Earth and Planetary Science Letters*, *233*(1-2), 71-86.

Edwards, R. L., J. H. Chen, and G. J. Wasserburg (1987), U-238 U-234-Th-230-Th-232 systematics and the precise measurement of time over the past 500000 years, *Earth and Planetary Science Letters*, *81*(2-3), 175-192.

Edwards, R. L., F. W. Taylor, and G. J. Wasserburg (1988), Dating earthquakes with high-precision Th-230 ages of very young corals, *Earth and Planetary Science Letters*, *90*(4), 371-381, doi: 10.1016/0012-821x(88)90136-7.

Eggins, S. M., et al. (2005), In situ U-series dating by laser-ablation multi-collector ICPMS: new prospects for Quaternary geochronology, *Quaternary Science Reviews*, *24*(23-24), 2523-2538, 10.1016/j.quascirev.2005.07.006.

Eltgroth, S. F., J. F. Adkins, L. F. Robinson, J. Southon, and M. Kashgarian (2006), A deep-sea coral record of North Atlantic radiocarbon through the Younger Dryas:

Evidence for intermediate water/deepwater reorganization, *Paleoceanography*, *21*(4), 10.1029/2005pa001192.

Emile-Geay, J., et al. (2016), Links between tropical Pacific seasonal, interannual and orbital variability during the Holocene, *Nature Geoscience*, *9*(2), 168-+.

Emile-Geay, J., and M. Tingley (2016), Inferring climate variability from nonlinear proxies: application to palaeo-ENSO studies, *Climate of the Past*, *12*(1), 31-50.

Enmar, R., M. Stein, M. Bar-Matthews, E. Sass, A. Katz, and B. Lazar (2000), Diagenesis in live corals from the Gulf of Aqaba. I. The effect on paleo-oceanography tracers, *Geochimica Et Cosmochimica Acta*, *64*(18), 3123-3132, doi: 10.1016/s0016-7037(00)00417-8.

Esat, T. M., and Y. Yokoyama (2006), Variability in the uranium isotopic composition of the oceans over glacial-interglacial timescales, *Geochimica Et Cosmochimica Acta*, *70*(16), 4140-4150, 10.1016/j.gca.2006.06.013.

Evans, M. N., R. G. Fairbanks, and J. L. Rubenstone (1999), The thermal oceanographic signal of El Nino reconstructed from a Kiritimati Island coral, *Journal of Geophysical Research-Oceans*, *104*(C6), 13409-13421.

Fedorov, A. V., and S. G. Philander (2001), A stability analysis of tropical ocean-atmosphere interactions: Bridging measurements and theory for El Nino, *Journal of Climate*, *14*(14), 3086-3101.

Fu, R., W. T. Liu, and R. E. Dickinson (1996), Response of tropical clouds to the interannual variation of sea surface temperature, *Journal of Climate*, *9*(3), 616-634.

Gallup, C. D., R. L. Edwards, and R. G. Johnson (1994), The timing of high sea levels over the past 200,000 years, *Science*, *263*(5148), 796-800, doi: 10.1126/science.263.5148.796.

Gallup, C. D., H. Cheng, F. W. Taylor, and R. L. Edwards (2002), Direct determination of the timing of sea level change during termination II, *Science*, *295*(5553), 310-313, doi: 10.1126/science.1065494.

Grothe, P. R., K. M. Cobb, S. L. Bush, H. Cheng, G. M. Santos, J. R. Southon, R. L. Edwards, D. M. Deocampo, and H. R. Sayani (2016), A comparison of U/Th and rapid-screen C-14 dates from Line Island fossil corals, *Geochemistry Geophysics Geosystems*, *17*(3), 833-845.

Guilyardi, E., P. Braconnot, F. F. Jin, S. T. Kim, M. Kolasinski, T. Li, and I. Musat (2009), Atmosphere Feedbacks during ENSO in a Coupled GCM with a Modified Atmospheric Convection Scheme, *Journal of Climate*, *22*(21), 5698-5718.

Haug, G. H., K. A. Hughen, D. M. Sigman, L. C. Peterson, and U. Rohl (2001),

Southward migration of the intertropical convergence zone through the Holocene, *Science*, *293*(5533), 1304-1308.

Heberling, F., M. A. Denecke, and D. Bosbach (2008), Neptunium(V) coprecipitation with calcite, *Environmental Science & Technology*, *42*(2), 471-476, 10.1021/es071790g.

Henderson, G. M., A. S. Cohen, and R. K. Onions (1993), U-234/U-238 ratios and Th-230 ages for Hateruma Atoll corals – implications for coral diagenesis and seawater U-234/U-238 ratios, *Earth and Planetary Science Letters*, *115*(1-4), 65-73, 10.1016/0012-821x(93)90213-s.

Henderson, G. M. (2002), Seawater (U-234/U-238) during the last 800 thousand years, *Earth and Planetary Science Letters*, *199*(1-2), 97-110, doi: 10.1016/s0012-821x(02)00556-3.

Hendy, E. J., M. K. Gagan, J. M. Lough, M. McCulloch, and P. B. deMenocal (2007), Impact of skeletal dissolution and secondary aragonite on trace element and isotopic climate proxies in Porites corals, *Paleoceanography*, *22*(4), doi: 10.1029/2007pa001462.

Holland, H. A., B. R. Schone, C. Lipowsky, and J. Esper (2014), Decadal climate variability of the North Sea during the last millennium reconstructed from bivalve shells (Arctica islandica), *Holocene*, *24*(7), 771-786, doi: 10.1177/0959683614530438.

Hua, Q., G. E. Webb, J. X. Zhao, L. D. Nothdurft, M. Lybolt, G. J. Price, and B. N. Opdyke (2015), Large variations in the Holocene marine radiocarbon reservoir effect reflect ocean circulation and climatic changes, *Earth and Planetary Science Letters*, *422*, 33-44, 10.1016/j.epsl.2015.03.049.

Jaffey, A. H., K. F. Flynn, Glendeni.Le, W. C. Bentley, and A. M. Essling (1971), Precision measurements of half-lives and specific activities of U-235 and U-238, *Physical Review C*, *4*(5), 1889-1906, doi: 10.1103/PhysRevC.4.1889.

James, N. P. (1974), Diagenesis of scleractinian corals in subaerial vadose environment, *Journal of Paleontology*, *48*(4), 785-799.

Jin, F. F., J. D. Neelin, and M. Ghil (1994), EL-NINO ON THE DEVILS STAIRCASE - ANNUAL SUBHARMONIC STEPS TO CHAOS, *Science*, *264*(5155), 70-72.

Jin, F. F. (1997a), An equatorial ocean recharge paradigm for ENSO .1. Conceptual model, *Journal of the Atmospheric Sciences*, *54*(7), 811-829.

Jin, F. F. (1997b), An equatorial ocean recharge paradigm for ENSO .2. A stripped-down coupled model, *Journal of the Atmospheric Sciences*, *54*(7), 830-847.

Jin, F. F., S. I. An, A. Timmermann, and J. X. Zhao (2003), Strong El Nino events and nonlinear dynamical heating, *Geophysical Research Letters*, *30*(3).

Kao, H. Y., and J. Y. Yu (2009), Contrasting Eastern-Pacific and Central-Pacific Types of ENSO, *Journal of Climate*, *22*(3), 615-632.

Karamperidou, C., P. N. Di Nezio, A. Timmermann, F. F. Jin, and K. M. Cobb (2015), The response of ENSO flavors to mid-Holocene climate: Implications for proxy interpretation, *Paleoceanography*, *30*(5), 527-547.

Kim, S. T., W. J. Cai, F. F. Jin, A. Santoso, L. X. Wu, E. Guilyardi, and S. I. An (2014), Response of El Nino sea surface temperature variability to greenhouse warming, *Nature Climate Change*, *4*(9), 786-790.

Kitano, Y., and T. Oomori (1972), The coprecipitation of uranium with calcium carbonate, *Journal of the Oceanographical Society of Japan*, 27, 34-42.

Koutavas, A., P. B. Demenocal, G. C. Olive, and J. Lynch-Stieglitz (2006), Mid-Holocene El Nino-Southern Oscillation (ENSO) attenuation revealed by individual foraminifera in eastern tropical Pacific sediments, *Geology*, *34*(12), 993-996.

Koutavas, A., and S. Joanides (2012), El Nino-Southern Oscillation extrema in the Holocene and Last Glacial Maximum, *Paleoceanography*, *27*.

Kug, J. S., F. F. Jin, and S. I. An (2009), Two Types of El Nino Events: Cold Tongue El Nino and Warm Pool El Nino, *Journal of Climate*, *22*(6), 1499-1515.

Kuhnert, H., J. Patzold, B. Schnetger, and G. Wefer (2002), Sea-surface temperature variability in the 16th century at Bermuda inferred from coral records, *Palaeogeography Palaeoclimatology Palaeoecology*, *179*(3-4), 159-171 doi: 10.1016/s0031-0182(01)00410-2.

Larkin, N. K., and D. E. Harrison (2005), On the definition of El Nino and associated seasonal average US weather anomalies, *Geophysical Research Letters*, *32*(13).

Lazar, B., R. Enmar, M. Schossberger, M. Bar-Matthews, L. Halicz, and M. Stein (2004), Diagenetic effects on the distribution of uranium in live and Holocene corals from the Gulf of Aqaba, *Geochimica Et Cosmochimica Acta*, *68*(22), 4583-4593, doi: 10.1016/j.gca.2004.03.029.

Linsley, B. K., Y. Rosenthal, and D. W. Oppo (2010), Holocene evolution of the Indonesian throughflow and the western Pacific warm pool, *Nature Geoscience*, *3*(8), 578-583.

Li, J. B., et al. (2013), El Nino modulations over the past seven centuries, *Nature Climate Change*, *3*(9), 822-826.

Liu, Z. Y., J. Kutzbach, and L. X. Wu (2000), Modeling climate shift of El Nino variability in the Holocene, *Geophysical Research Letters*, *27*(15), 2265-2268.

Liu, Z., E. Brady, and J. Lynch-Stieglitz (2003), Global ocean response to orbital forcing in the Holocene, *Paleoceanography*, *18*(2).

Liu, Z. Y., Z. Y. Lu, X. Y. Wen, B. L. Otto-Bliesner, A. Timmermann, and K. M. Cobb (2014), Evolution and forcing mechanisms of El Nino over the past 21,000 years, *Nature*, *515*(7528), 550-+.

Longworth, B. E., L. F. Robinson, M. L. Roberts, S. R. Beaupre, A. Burke, and W. J. Jenkins (2013), Carbonate as sputter target material for rapid C-14 AMS, *Nuclear Instruments & Methods in Physics Research Section B-Beam Interactions with Materials and Atoms*, *294*, 328-334, 10.1016/j.nimb.2012.05.014.

Maliva, R. G., and J. A. D. Dickson (1992), The mechanism of skeletal aragonite neomorphism – evidence from neomorphosed mollusks from the upper Purbeck formation (late Jurassic-early Cretaceous), Southern England, *Sedimentary Geology*, *76*(3-4), 221-232, doi: 10.1016/0037-0738(92)90085-6.

Mangerud, J. (1972), Radiocarbon dating of marine shells, including a discussion of apparent age of Recent shells from Norway. Boreas, 1: 143–172. doi: 10.1111/j.1502-3885.1972.tb00147.x

McGregor, H. V., and M. K. Gagan (2003), Diagenesis and geochemistry of Porites corals from Papua New Guinea: Implications for paleoclimate reconstruction, *Geochimica Et Cosmochimica Acta*, *67*(12), 2147-2156.

McGregor, H. V., and M. K. Gagan (2004), Western Pacific coral delta(18)O records of anomalous Holocene variability in the El Nino-Southern Oscillation, *Geophysical Research Letters*, *31*(11).

McGregor, H. V., M. K. Gagan, M. T. McCulloch, E. Hodge, and G. Mortimer (2008), Mid-Holocene variability in the marine C-14 reservoir age for northern coastal Papua New Guinea, *Quaternary Geochronology*, *3*(3), 213-225, 10.1016/j.quageo.2007.11.002.

McGregor, H. V., J. Hellstrom, D. Fink, Q. Hua, and C. D. Woodroffe (2011), Rapid U-series dating of young fossil corals by laser ablation MC-ICPMS, *Quaternary Geochronology*, *6*(2), 195-206, doi: http://dx.doi.org/10.1016/j.quageo.2010.10.002.

McGregor, H. V., M. J. Fischer, M. K. Gagan, D. Fink, S. J. Phipps, H. Wong, and C. D. Woodroffe (2013), A weak El Nino/Southern Oscillation with delayed seasonal growth around 4,300 years ago, *Nature Geoscience*, *6*(11), 949-953.

McGregor, S., A. Timmermann, M. H. England, O. Elison Timm, and A. T. Wittenberg (2013), Inferred changes in El Niño-Southern Oscillation variance over the past

six centuries, *Clim. Past Discuss.*, *9*(3), 2929-2966.

McIntyre, C. P., M. L. Roberts, J. R. Burton, A. P. McNichol, A. Burke, L. F. Robinson, K. F. von Reden, and W. J. Jenkins (2011), Rapid radiocarbon (C-14) analysis of coral and carbonate samples using a continuous-flow accelerator mass spectrometry (CFAMS) system, *Paleoceanography*, *26*, 10.1029/2011pa002174.

McPhaden, M. J., T. Lee, and D. McClurg (2011), El Nino and its relationship to changing background conditions in the tropical Pacific Ocean, *Geophysical Research Letters*, *38*.

Meece, D. E., and L. K. Benninger (1993), The coprecipitation of Pu and other radionuclides with $CaCO_3$, *Geochimica Et Cosmochimica Acta*, *57*(7), 1447-1458, 10.1016/0016-7037(93)90005-h.

Meyers, S. D., J. J. O'Brien, and E. Thelin (1999), Reconstruction of monthly SST in the tropical Pacific Ocean during 1868-1993 using adaptive climate basis functions, *Monthly Weather Review*, *127*(7), 1599-1612.

Moy, C. M., G. O. Seltzer, D. T. Rodbell, and D. M. Anderson (2002), Variability of El Nino/Southern Oscillation activity at millennial timescales during the Holocene epoch, *Nature*, *420*(6912), 162-165.

Newman, M., S. I. Shin, and M. A. Alexander (2011), Natural variation in ENSO flavors, *Geophysical Research Letters*, *38*.

Nothdurft, L. D., and G. E. Webb (2009), Earliest diagenesis in scleractinian coral skeletons: implications for palaeoclimate-sensitive geochemical archives, *Facies*, *55*(2), 161-201 doi: 10.1007/s10347-008-0167-z.

Nurhati, I. S., K. M. Cobb, C. D. Charles, and R. B. Dunbar (2009), Late 20th century warming and freshening in the central tropical Pacific, *Geophysical Research Letters*, *36*.

Nurhati, I. S., K. M. Cobb, and E. Di Lorenzo (2011), Decadal-Scale SST and Salinity Variations in the Central Tropical Pacific: Signatures of Natural and Anthropogenic Climate Change, *Journal of Climate*, *24*(13), 3294-3308.

O'Connor, G. K., K.M. Cobb, H.R. Sayani, P.R Grothe, A.R. Atwood (in prep), The 2015/16 El Niño Event as Recorded in Central Tropical Pacific Corals

Otto-Bliesner, B. L., E. C. Brady, S. I. Shin, Z. Y. Liu, and C. Shields (2003), Modeling El Nino and its tropical teleconnections during the last glacial-interglacial cycle, *Geophysical Research Letters*, *30*(23).

Park, W., N. Keenlyside, M. Latif, A. Stroh, R. Redler, E. Roeckner, and G. Madec (2009), Tropical Pacific Climate and Its Response to Global Warming in the Kiel Climate Model, *Journal of Climate*, *22*(1), 71-92.

Picaut, J., F. Masia, and Y. duPenhoat (1997), An advective-reflective conceptual model for the oscillatory nature of the ENSO, *Science*, *277*(5326), 663-666.

Pingitore, N. E. (1976), Vadose and phreatic diagenesis – processes, products, and their recognition in corals, *Journal of Sedimentary Petrology*, *46*(4), 985-1006.

Potter, E. K., C. H. Stirling, U. H. Wiechert, A. N. Halliday, and C. Spotl (2005), Uranium-series dating of corals in situ using laser-ablation MC-ICPMS, *International Journal of Mass Spectrometry*, *240*(1), 27-35, 10.1016/j.ijms.2004.10.007.

Power, S., F. Delage, C. Chung, G. Kociuba, and K. Keay (2013), Robust twenty-first-century projections of El Nino and related precipitation variability, *Nature*, *502*(7472), 541-+.

Rabier, C., Y. Anguy, G. Cabioch, and P. Genthon (2008), Characterization of various stages of calcitization in Porites sp corals from uplifted reefs - Case studies from New Caledonia, Vanuatu, and Futuna (South-West Pacific), *Sedimentary Geology*, *211*(3-4), 73-86, doi: 10.1016/j.sedgeo.2008.08.005.

Ramsey, C. B., P. Ditchfield, and M. Humm (2004), Using a gas ion source for radiocarbon AMS and GC-AMS, *Radiocarbon*, *46*(1), 25-32.

Rasmusson, E. M., and T. H. Carpenter (1982), Variations in tropical sea-surface temperature and surface wind fields associated with the southern oscillation El-Nino, *Monthly Weather Review*, *110*(5), 354-384.

Reeder, R. J., M. Nugent, C. D. Tait, D. E. Morris, S. M. Heald, K. M. Beck, W. P. Hess, and A. Lanzirotti (2001), Coprecipitation of uranium(VI) with calcite: XAFS, micro-XAS, and luminescence characterization, *Geochimica Et Cosmochimica Acta*, *65*(20), 3491-3503, doi: 10.1016/s0016-7037(01)00647-0.

Reimer, P. J., et al. (2013), Intcal13 and Marine13 radiocarbon age calibration curves, 0-50,000 years cal BP, *Radiocarbon*, *55*(4), 1869-1887.

Reynolds, R. W., N. A. Rayner, T. M. Smith, D. C. Stokes and W. Q. Wang, (2002) "An improved insitu and satellite SST analysis for climate." *Journal of Climate* 15(13): 1609-1625.

Richmond, B., and R. Morton (2007), Coral-Gravel Storm Ridges: Examples from the Tropical Pacific and Caribbean, in *Coastal Sediments '07*, edited, pp. 572-583.

Robinson, L. F., N. S. Belshaw, and G. M. Henderson (2004), U and Th concentrations and isotope ratios in modern carbonates and waters from the Bahamas, *Geochimica Et Cosmochimica Acta*, *68*(8), 1777-1789, doi: 10.1016/j.gca.2003.10.005.

Robinson, L. F., J. F. Adkins, D. P. Fernandez, D. S. Burnett, S. L. Wang, A. C. Gagnon,

and N. Krakauer (2006), Primary U distribution in scleractinian corals and its implications for U series dating, *Geochemistry, Geophysics, Geosystems, 7*(5), Q05022, doi: 10.1029/2005GC001138.

Rodbell, D. T. (1999), An similar to 15,000-year record of El Nino-driven alluviation in southwestern Ecuador (vol 283, pg 516, 1999), *Science*, *283*(5410), 2107-2107.

Rodbell, D. T., G. O. Seltzer, B. G. Mark, J. A. Smith, and M. B. Abbott (2008), Clastic sediment flux to tropical Andean lakes: records of glaciation and soil erosion, *Quaternary Science Reviews*, *27*(15-16), 1612-1626.

Rodgers, K. B., P. Friederichs, and M. Latif (2004), Tropical pacific decadal variability and its relation to decadal modulations of ENSO, *Journal of Climate*, *17*(19), 3761-3774.

Russell, A. D., S. Emerson, B. K. Nelson, J. Erez, and D. W. Lea (1994), Uranium in foraminiferal calcite as a recorder of seawater uranium concentrations, *Geochimica Et Cosmochimica Acta*, *58*(2), 671-681, 10.1016/0016-7037(94)90497-9.

Santos, G.M., J.R. Southon, K.C. Druffel-Rodriguez, S. Griffin, M. Mazon (2004), Magensium perchlorate as an alternative water trap in AMS graphite sample preparation: a report on sample preparation at KCCAMS at the University of California, Irvine, *Radiocarbon*, *46*(1), 165-173.

Santos, G. M., R. B. Moore, J. R. Southon, S. Griffin, E. Hinger, and D. Zhang (2007a), AMS C-14 sample preparation at the KCCAMS/UCI facility: Status report and performance of small samples, *Radiocarbon*, *49*(2), 255-269.

Santos, G. M., J. R. Southon, S. Griffin, S. R. Beaupre, and E. R. M. Druffel (2007b), Ultra small-mass AMS C-14 sample preparation and analyses at KCCAMS/UCI Facility, *Nuclear Instruments & Methods in Physics Research Section B-Beam Interactions with Materials and Atoms*, *259*(1), 293-302, doi: 10.1016/j.nimb.2007.01.172.

Sayani, H. R., K. M. Cobb, A. L. Cohen, W. C. Elliott, I. S. Nurhati, R. B. Dunbar, K. A. Rose, and L. K. Zaunbrecher (2011), Effects of diagenesis on paleoclimate reconstructions from modern and young fossil corals, *Geochimica et Cosmochimica Acta*, *75*(21), 6361-6373, doi: http://dx.doi.org/10.1016/j.gca.2011.08.026.

Sayani, H.R., K.M. Cobb, A. Khara, C.M. Stone, P.R. Grothe, T. Chen, H. Cheng, R.L. Edwards (in prep), Central tropical Pacific SST and Salinity variability over the Little Ice Age

Scholz, D., A. Mangini, and T. Felis (2004), U-series dating of diagenetically altered fossil reef corals, *Earth and Planetary Science Letters*, *218*(1-2), 163-178, 10.1016/s0012-821x(03)00647-2.

Scholz, D., and A. Mangini (2007), How precise are U-series coral ages?, *Geochimica Et Cosmochimica Acta*, *71*(8), 1935-1948 doi: 10.1016/j.gca.2007.01.016.

Schopf, P. S., and R. J. Burgman (2006), A simple mechanism for ENSO residuals and asymmetry, *Journal of Climate*, *19*(13), 3167-3179.

Shen, G. T., and R. B. Dunbar (1995), Environmental controls on uranium in reef corals, *Geochimica Et Cosmochimica Acta*, *59*(10), 2009-2024, 10.1016/0016-7037(95)00123-9.

Shen, C. C., R. L. Edwards, H. Cheng, J. A. Dorale, R. B. Thomas, S. B. Moran, S. E. Weinstein, and H. N. Edmonds (2002), Uranium and thorium isotopic and concentration measurements by magnetic sector inductively coupled plasma mass spectrometry, *Chemical Geology*, *185*(3-4), 165-178, doi: 10.1016/s0009-2541(01)00404-1.

Smith, S. V., R. W. Buddemeier, R. C. Redalje, and J. E. Houck (1979), Strontium-calcium thermometry in coral skeletons, *Science*, *204*(4391), 404-407.

Spooner, P. T., T. Chen, L. F. Robinson, and C. D. Coath (2016), Rapid uranium-series age screening of carbonates by laser ablation mass spectrometry, *Quaternary Geochronology*, *31*, 28-39, http://dx.doi.org/10.1016/j.quageo.2015.10.004.

Stott, L., K. Cannariato, R. Thunell, G. H. Haug, A. Koutavas, and S. Lund (2004), Decline of surface temperature and salinity in the western tropical Pacific Ocean in the Holocene epoch, *Nature*, *431*(7004), 56-59.

Stuiver, M., and H. A. Polach (1977), Reporting of ^{14}C data - discussion, *Radiocarbon*, *19*(3), 355-363.

Stuiver, M., P. J. Reimer, E. Bard, J. W. Beck, G. S. Burr, K. A. Hughen, B. Kromer, G. McCormac, J. Van der Plicht, and M. Spurk (1998), INTCAL98 radiocarbon age calibration, 24,000-0 cal BP, *Radiocarbon*, *40*(3), 1041-1083.

Stuiver, M., P.J. Reimer, and R.W. Reimer, (2005), CALIB 6.0.

Suarez, M. J., and P. S. Schopf (1988), A delayed action oscillator for ENSO, *Journal of the Atmospheric Sciences*, *45*(21), 3283-3287.

Taylor, R.E., and O. Bar-Yosef (2014), "Radiocarbon Dating, Second Edition: An Archaeological Perspective", Left Coast Inc., Walnut Creek, CA.

Thompson, W. G., M. W. Spiegelman, S. L. Goldstein, and R. C. Speed (2003), An open-system model for U-series age determinations of fossil corals, *Earth and Planetary Science Letters*, *210*(1-2), 365-381, 10.1016/s0012-821x(03)00121-3.

Timmermann, A., S. J. Lorenz, S. I. An, A. Clement, and S. P. Xie (2007), The effect of orbital forcing on the mean climate and variability of the tropical Pacific, *Journal*

of Climate, *20*(16), 4147-4159.

Tudhope, A. W., C. P. Chilcott, M. T. McCulloch, E. R. Cook, J. Chappell, R. M. Ellam, D. W. Lea, J. M. Lough, and G. B. Shimmield (2001), Variability in the El Nino - Southern oscillation through a glacial-interglacial cycle, *Science*, *291*(5508), 1511-1517.

van Oldenborgh, G. J., S. Y. Philip, and M. Collins (2005), El Nino in a changing climate: a multi-model study, *Ocean Science*, *1*(2), 81-95.

Villemant, B., and N. Feuillet (2003), Dating open systems by the U-238-U-234-Th-230 method: application to Quaternary reef terraces, *Earth and Planetary Science Letters*, *210*(1-2), 105-118, 10.1016/s0012-821x(03)00100-6.

Vecchi, G. A., B. J. Soden, A. T. Wittenberg, I. M. Held, A. Leetmaa, and M. J. Harrison (2006), Weakening of tropical Pacific atmospheric circulation due to anthropogenic forcing, *Nature*, *441*(7089), 73-76.

Wacker, L., J. Lippold, M. Molnar, and H. Schulz (2013), Towards radiocarbon dating of single foraminifera with a gas ion source, *Nuclear Instruments & Methods in Physics Research Section B-Beam Interactions with Materials and Atoms*, *294*, 307-310, 10.1016/j.nimb.2012.08.038.

Wake, B. (2016), SNAPSHOT Snow white coral, *Nature Climate Change*, *6*(5), 439-439.

Wang, C. Z., R. H. Weisberg, and J. I. Virmani (1999), Western Pacific interannual variability associated with the El Nino Southern oscillation, *Journal of Geophysical Research-Oceans*, *104*(C3), 5131-5149.

Wang, C. Z., and R. H. Weisberg (2000), The 1997-98 El Nino evolution relative to previous El Nino events, *Journal of Climate*, *13*(2), 488-501.

Wang, Y. J., H. Cheng, R. L. Edwards, Y. Q. He, X. G. Kong, Z. S. An, J. Y. Wu, M. J. Kelly, C. A. Dykoski, and X. D. Li (2005), The Holocene Asian monsoon: Links to solar changes and North Atlantic climate, *Science*, *308*(5723), 854-857, 10.1126/science.1106296.

Weare, B. C., A. R. Navato, and R. E. Newell (1976), Empirical orthogonal analysis of Pacific sea-surface temperatures, *Journal of Physical Oceanography*, *6*(5), 671-678.

Weber, J. N., and P. M. Woodhead (1972), Temperature dependence of oxygen-18 concentration in reef coral carbonates, *Journal of Geophysical Research*, *77*(3), 463-&.

Weisberg, R. H., and C. Z. Wang (1997), A western Pacific oscillator paradigm for the El Nino Southern Oscillation, *Geophysical Research Letters*, *24*(7), 779-782.

Wittenberg, A. T. (2009), Are historical records sufficient to constrain ENSO simulations?, *Geophysical Research Letters*, *36*.

Wood, R. (2015), From revolution to convention: the past, present and future of radiocarbon dating, *Journal of Archaeological Science*, *56*, 61-72, 10.1016/j.jas.2015.02.019.

Woodroffe, C. D., M. R. Beech, and M. K. Gagan (2003), Mid-late Holocene El Nino variability in the equatorial Pacific from coral microatolls, *Geophysical Research Letters*, *30*(7).

Wyrtki, K. (1975), El-Nino – dynamic-response of equatorial Pacific ocean to atmospheric forcing, *Journal of Physical Oceanography*, *5*(4), 572-584.

Wyrtki, K. (1985), Water displacements in the Pacific and the genesis of El-Nino cycles, *Journal of Geophysical Research-Oceans*, *90*(NC4), 7129-7132.

Xie, S. P., C. Deser, G. A. Vecchi, J. Ma, H. Y. Teng, and A. T. Wittenberg (2010), Global Warming Pattern Formation: Sea Surface Temperature and Rainfall, *Journal of Climate*, *23*(4), 966-986.

Yeh, S. W., Y. G. Park, and B. P. Kirtman (2006), ENSO amplitude changes in climate change commitment to atmospheric CO2 doubling, *Geophysical Research Letters*, *33*(13).

Yeh, S. W., and B. P. Kirtman (2007), ENSO amplitude changes due to climate change projections in different coupled models, *Journal of Climate*, *20*(2), 203-217.

Yeh, S. W., J. S. Kug, B. Dewitte, M. H. Kwon, B. P. Kirtman, and F. F. Jin (2009), El Nino in a changing climate (vol 461, pg 511, 2009), *Nature*, *462*(7273).

Yokoyama, Y. and T.M. Esat (2004), Long term variations of uranium isotopes and radiocarbon in the surface seawater recorded in corals, in Global Environmental Change in the Ocean and on Land, edited by M. Shiyomi et al., pp. 279-309, TERRAPUB, Tokyo, Japan.

Yu, K. F., Q. A. Hua, J. X. Zhao, E. Hodge, D. Fink, and M. Barbetti (2010), Holocene marine C-14 reservoir age variability: Evidence from Th-230-dated corals in the South China Sea, *Paleoceanography*, *25*, 10.1029/2009pa001831.

Zaunbrecher, L. K., K. M. Cobb, J. W. Beck, C. D. Charles, E. R. M. Druffel, R. G. Fairbanks, S. Griffin, and H. R. Sayani (2010), Coral records of central tropical Pacific radiocarbon variability during the last millennium, *Paleoceanography*, *25*, doi: 10.1029/2009pa001788.

Zebiak, S. E., and M. A. Cane (1987), A MODEL EL-NINO SOUTHERN OSCILLATION, *Monthly Weather Review*, *115*(10), 2262-2278.

Zebiak, S. E. (1990), Diagnostic studies of Pacific surface winds, *Journal of Climate*, *3*(9), 1016-1031.

Zelle, H., G. J. Van Oldenborgh, G. Burgers, and H. Dijkstra (2005), El Nino and Greenhouse warming: Results from ensemble simulations with the NCAR CCSM, *Journal of Climate*, *18*(22), 4669-4683.

Zhao, J. X., K. F. Yu, and Y. X. Feng (2009), High-precision U-238-U-234-Th-230 disequilibrium dating of the recent past: a review, *Quaternary Geochronology*, *4*(5), 423-433, 10.1016/j.quageo.2009.01.012.

Zheng, W., P. Braconnot, E. Guilyardi, U. Merkel, and Y. Yu (2008), ENSO at 6ka and 21ka from ocean-atmosphere coupled model simulations, *Climate Dynamics*, *30*(7-8), 745-762.